Scuola Internazionale Superiore di Studi Avanzati

International School of Advanced Studies

Astrophysics Sector

CORED DARK HALOS AROUND GALAXIES

The evidence of a turning point in the knowledge of our Universe

Thesis submitted for the degree of

Doctor Philosophiæ

Candidate:

Annamaria BORRIELLO

Supervisor:

Prof. Paolo SALUCCI

October 2002

Preface

This thesis reports the results of my Ph.D. research, under Prof. Paolo Salucci's supervision, at the International School of Advanced Studies, in Trieste, during the years $1998 - 2002$. It addresses to the issue of Dark Matter distribution in galaxies, by devising different strategies, according to their properties, even to test the Dark Matter gravitational effects, on galaxies scales, against the Cold Dark Matter predictions.

The plan of the thesis is the following. In Part I (§1) we introduce the DM issue and briefly outline the observational and theoretical framework. We report our work on disk galaxies in Part II: low–luminosity spirals (§2), the individual remarkable case of a dwarf galaxy (§3) and mass modeling of the spirals Universal Rotation Curve (§4). Part III deals with elliptical galaxies and our analysis of their Fundamental Plane, as a tool to derive DM properties in spheroids (§5). Finally, in Part IV (§6) we report our conclusions and perspectives for future work.

Chapters from 2 to 5 correspond, with slight modifications, to published or submitted papers (see List of Publications for references) and each of them can be read as a separate entity.

INDEX

Part I

INTRODUCTION

Chapter 1

Dark Matter in the Universe: What, Where, How Much?

1.1 The Concept of Dark Matter

Dynamical modeling of gravitationally bound systems in the Universe, at all scales from galaxies upwards, has led to the conclusion that most of the mass they are composed of (up to 90%) does not emit or reflect electromagnetic radiation, but reveals itself only through its gravitational effect on other, luminous, matter. Yet, formation, evolution and dynamics of astrophysical systems like galaxies and clusters are *driven* and *dominated* by this "dark" matter (DM), whose nature and distribution are only surmised, by now. Moreover, modern cosmology shows that DM nature and total amount have fundamental implications for the evolution of the Universe.

Since pioneering studies in early 70's, the discrepancy, observed in virialized systems, between the dynamically inferred mass and the visible (in the whole electromagnetic spectrum) baryonic content has been ascribed to the existence of some form of dark matter. However, it was only in late 70's, with new kinematic measures in spirals (Bosma, 1979; Rubin et al., 1980), that the overall presence of DM around galaxies was finally accepted. Since then, many different objects have been used in literature as test particles, to derive the gravitational potential exceeding that of the visible mass: stars, gas, globular clusters and galaxies themselves (in case of clusters potential). This kind of analysis has been, for a long time, the only tool to infer, by subtraction, the DM presence.

Moreover, a crucial mass discrepancy occurs *on cosmological scale*: the total mass density in the Universe ($\rho_c \cdot \Omega_m$, with ρ_c the critical density for closure) is much greater than the maximum value allowed for baryonic matter by standard Big Bang Nucleosynthesis (BBN). Indeed, a number of independent methods have been used to derive the mean matter density Ω_m in the Universe (Fig.1.1): hot gas in clusters of galaxies, X–Rays emitting, whose temperature and luminosity are linked to the overall density (e.g. White et al., 1993; Evrard, 1997; Krauss, 1998; Krauss, 2001), dynamical mass–to–luminosity ratios of groups and clusters (e.g. Bahcall, 1997; Einasto et al., 1999), gravitational lensing (e.g. Schindler et al., 1995) and, most recently, studies of

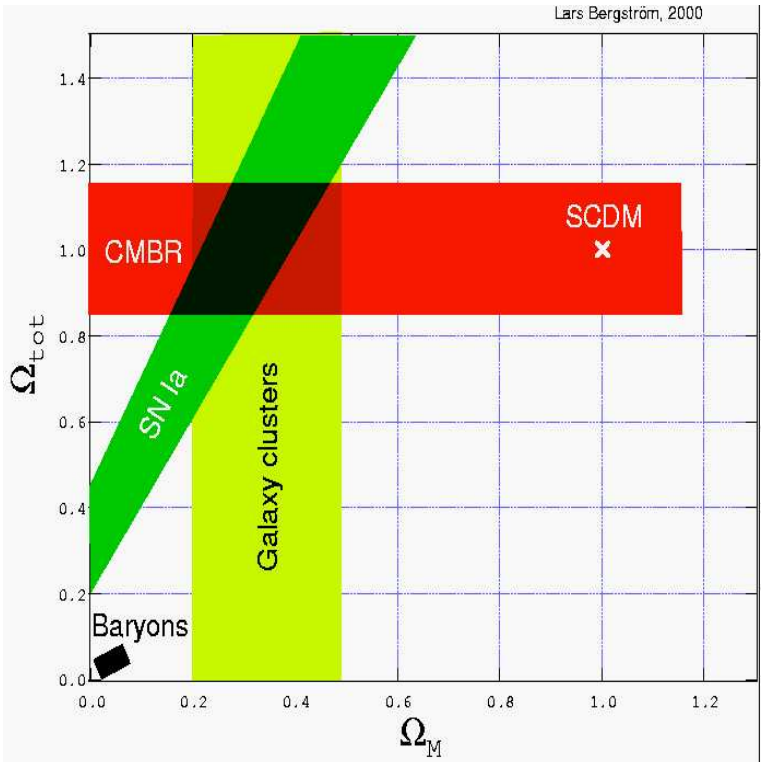

Figure 1.1: Approximate best–fit coincidence regions in the $\Omega_m - \Omega_{tot}$ plane, from the joint analysis of different investigation methods. A region at very small Ω_m is also shown, which bounds the baryons–only contribution according to BBN (from Bergström, 2000).

Cosmic Microwave Background (CMB) anisotropies (de Bernardis et al., 2000; Hanany et al., 2000) and distant supernovae (Perlmutter et al., 1998, 1999; Riess et al., 1998). The weighed mean of all these independent measurements is about $\Omega_m \simeq 0.30$ with a 20% uncertainty (Einasto & Einasto, 2000).

On the other hand, BBN predictions of the aboundances of the light elements produced during the first three minutes after the Big Bang strongly constraint the total baryonic mass fraction to a much lower value: $0.008h^{-2} < \Omega_b < 0.024h^{-2}$ (Burles et al., 2001; Pryke et al., 2002). Therefore, cosmological and astrophysical arguments leave no doubt that baryonic matter only accounts for between 5 and 20 percent of the total matter. Furthermore, luminous matter is known to provide just a small fraction

of all the baryons: $\Omega_{lum} \lesssim 0.004$ (Persic & Salucci, 1992; Salucci & Persic, 1999a). It is plausible that some baryons, though not strictly dark, are enclosed in the galaxies and not detectable at large distances (e.g. planets, brown dwarfs, cold white dwarfs); yet, it is generally believed that $\sim 75\%$ of baryons has somehow avoided the process of (luminous) galaxy formation and may be survived as cold/warm intergalactic gas, associated with the Lyman$-\alpha$ absorbing clouds detected at low redshift.

Last, but not least, the idea of Dark Matter probably would not have gained its importance, had it not assumed a primary role in the context of the structures formation and evolution. This was realized in the 80's, when large scale (~ 100 Mpc) observations (e.g. Huchra et al., 1988) and theories of structures formation (e.g. Davies et al., 1989) triggered each other. Indeed, we can follow the cosmic evolution rather well at the redshifts $10^{10} < z < 10$, i.e. from temperature about $T \sim 1$ MeV until cosmic structures become non–linear, and, thus, to integrate the equations of linear density perturbations in the early Universe, responsible for the CMB anisotropies and for large scale structure. These density fluctuations must have an amplitude of $\sim 10^{-3}$ at the time of recombination, in order to originate the large scale structures we observe today (e.g. de Lapparent, 1986; Efstathiou, 1991; Efstathiou et al., 1992). This is possible only if density perturbations start growing already during the radiation–dominated era, which is impossible for baryons, whose clumping is damped by radiation. Baryons just flow, after recombination, into non–baryonic DM gravitational wells. Therefore, the whole Universe as we observe it, with its highly organized mass hierarchy and very large scale (~ 100 Mpc) structures, would have not even formed in the absence of non–baryonic DM.

Almost 30 years of investigations allowed us to gain a knowledge about DM in galaxies. Pioneering studies in late 70's–early 80's (Bosma, 1979; Rubin et al., 1980; Bosma, 1981; Faber & Lin, 1983) were especially concentrated to unveil the *presence* of DM in galaxies, through the evidence that $M_{grav} > M_{lum}$, i.e. that the luminous mass could not account for the whole gravitational potential. In the last ~ 15 years, however, studies have concentrated on the idea that DM is revealed when $dM_{grav}/dr \gg$

dM_{lum}/dr (e.g. Persic & Salucci, 1990b). Summarizing, we know the answers to the "first order" questions: does DM exist in galaxies? How much DM lies therein? In this introduction, as a first step, we will briefly review what we know about DM in galaxies, spanning their morphology and luminosity ranges, and presenting evidence that all of them bear the kinematical signature of a mass component distributed differently from the luminous one.

1.2 What We Know: DM Ubiquitous Presence

It is remarkable that the $\sim 10^{11}$ galaxies we observe within the Hubble radius can be classified in a small number of basic types: spiral, elliptical and dwarf (spheroidal and irregular) galaxies, with the add of the class of low-surface-brightness (LSB) galaxies (e.g. Davies et al., 1989; Impey et al., 1993; Mc Gaugh et al., 1995). These families are clearly characterized by their position in the plane (μ_0, M), i.e. central surface brightness and magnitude, both in B–band (Fig.1.2). In this plane, spiral galaxies lie at the center and show a very small range ($\sim$ 0.5 mag) in μ_0; ellipticals are very bright systems and span only a factor 10 in luminosity, that however well correlates with central brightness; dwarfs are very low–luminosity (spheroidal, disk or irregular) systems, which barely join the faintest normal systems and span the largest interval in μ_0. Finally, LSB galaxies are the counterpart of spirals at low surface brightness. These different observational properties correspond to different *physical* configurations, essentially driven by the angular momentum content and the stellar populations, which are intimately related to the process of galaxy formation. Finally, there is a general trend for lower luminosity systems to be much more numerous, thus storing, altogether, a significant amount of baryons.

Observational evidence of the ubiquitous presence of DM in galaxies have come from a variety of inquiry strategies; indeed, according to the galaxies geometrical structure, dynamics, light distribution and stellar populations, different methods of investigations have been employed, with different reliability degrees in deriving galaxies

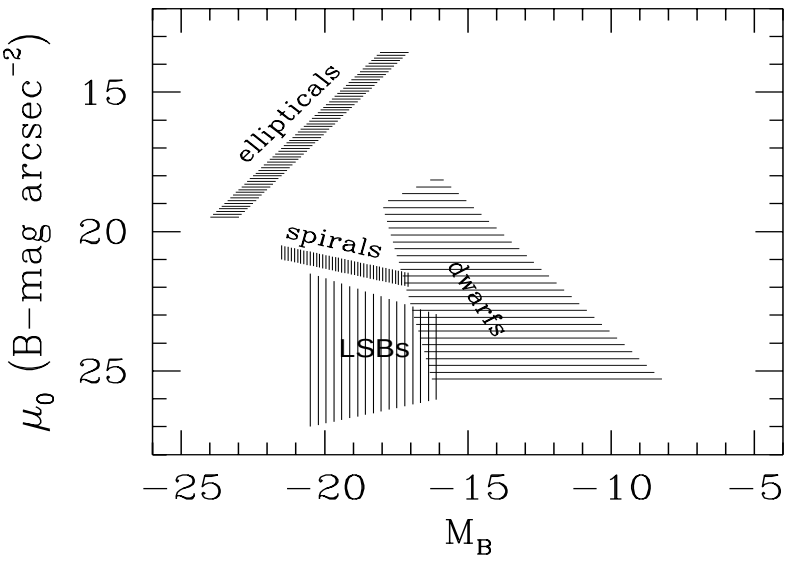

Figure 1.2: The loci populated by the various families of galaxies in the central brightness *vs.* luminosity plane (from Salucci & Persic, 1997).

mass–to–light ratios and mass decomposition. From a theoretical point of view, this evidence is natural within the hierarchical (bottom–up) cosmological scenario (White & Rees, 1978; Davis et al., 1985; Frenk et al., 1988), according to which DM halos have driven the dissipative infall of baryons and, modulo a variety of initial conditions, have built the bulge/disk/spheroid galaxies we observe today. Within this framework, we expect to detect DM within and surrounding any galaxy, regardless of its luminosity and morphological type.

1.2.1 DM in spiral galaxies

The first and most convincing evidence for DM in galaxies was found in spiral galaxies, due to their intrinsic simple geometry and to the existence of good kinematical tracers of the gravitational potential. The luminous matter in spiral galaxies is distributed in two components: a concentrated, spheroidal bulge, with projected density distribution approximately described by the de Vaucouleurs law:

$$I(R) = I_0 \; e^{-7.67\,(R/r_e)^{1/4}} \tag{1.1}$$

where R is the projected radius and r_e the half–light radius, and a thin disk with surface luminosity distribution described by:

$$I(R) = I_0 \; e^{-R/r_D} \tag{1.2}$$

with r_D being the exponential disk length scale (Freeman, 1970). Let the optical radius R_{opt} be the radius encircling 83% of the integrated light, which corresponds to $R_{opt} \simeq 3.2 \; r_D$ for a Freeman disk. The relative importance of the two luminous components defines the Hubble sequence of spirals, going from the bulge–dominated Sa galaxies to the progressively more disk–dominated Sb/Sc/Sd galaxies. We recall that the spiral arms are non–axisymmetric density perturbations, traced by newly–formed bright stars or HII regions, which are conspicuous in the light distribution and perturb the circular velocity field through small–amplitude sinusoidal disturbances (i.e. wiggles in the rotation curves), but they are immaterial to the axisymmetric gravitational potential and must not be fitted by the overall mass model.

The circular velocity as a function of galactic radius is known as the rotation curve (RC), which, along with the virial theorem, provides a measure of the total gravitating mass within the last measured point. Let V be the circular rotation velocity at radius R and M the enclosed mass, rotation curves $V(R)$ have been measured, since early 80's, by using the Doppler shift of the optical Hα line (e.g. Rubin et al. 1980; Faber & Lin, 1983) or the radio 21–cm line of hydrogen (e.g. Bosma, 1979).

It was soon recognized that RC's of spirals did not show any keplerian fall–off at outer radii (Rubin et al. 1980; Bosma, 1981), as would be expected if the visible stars provided all the mass. In fact, their shapes at $R \gtrsim 1 - 2 \; r_D$ are inconsistent with the light distribution, for which $L(R) \propto [1 - (1 + R/r_D) \exp(-R/r_D)]$, so that the "local" dynamical mass–to–light ratio strongly increases outwards, unveiling the presence of a dark mass component. Moreover, HI rotation curves can extensively

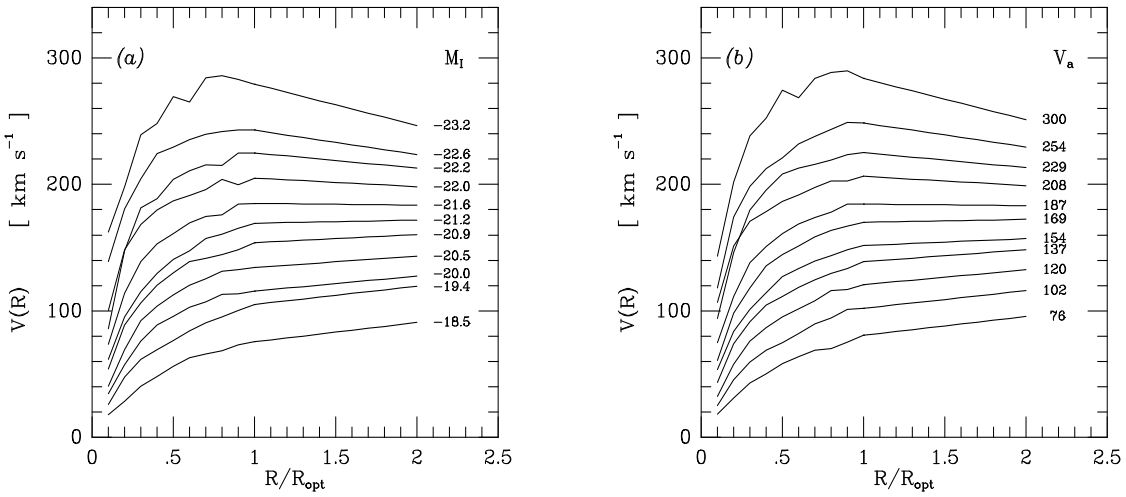

Figure 1.3: Coadded spirals rotation curves per luminosity bin (*left*) and velocity bin (*right*) (from Persic, Salucci & Stel, 1996).

probe the gravitational potential, much further than the optical disk (e.g. Broeils, 1992), thus making more difficult to contrive ways to make DM unnecessary.

It was long believed that spiral galaxies RC's were all flat almost at any radius and this had led to the concept of a *disk/halo conspiracy*, which maintains the total circular velocity featureless, irrespective of the relative strength of the disk and halo contributions (van Albada et al., 1985; Bahcall & Casertano, 1985). Later investigations, anyway, superseded the paradigms of "flat rotation curves" and "conspiracy", showing that the existence of significant features in the outer RC and the analysis of the velocity derivative $dV(r)/dr$ could solve the mass structure and separate the disk/halo gravitational contributions (Salucci & Frenk, 1989; Persic & Salucci, 1990b, 1992).

Rotation curves features and properties were fully characterized by Persic, Salucci & Stel (1996, hereafter PSS96), through the analysis of ~ 1100 RC's, extracted from a large survey of Hα velocities in southern spirals (Mathewson et al., 1992), about 100 of which extended out to $\lesssim 2\ R_{opt}$. They found that the entire range of RC's properties (both coadded and individual ones) can be very well reproduced by mass modeling

spirals with a standard exponential thin disk plus a spherical halo, characterized by two free parameters: β, the visible mass fraction at R_{opt} (also inclusive of the gas content), and a, the radius (in units of R_{opt}) of the halo central region (core), where dark matter density roughly stays constant. The circular velocity for such a mass model writes:

$$V(x) = V(R_{opt}) \left[\beta \frac{1.97\ x^{1.22}}{(x^2+0.78^2)^{1.43}} + (1-\beta)\ (1+a^2)\ \frac{x^2}{x^2+a^2} \right]^{1/2} \quad \text{km s}^{-1} \quad (1.3)$$

where the two terms of the sum are, respectively, the disk and the halo contribution to the total circular velocity profile. The disk+halo fits to the coadded RC's (in luminosity bins) yield (with fitting errors within 1% on average):

$$\beta = 0.72 + 0.44\ \log\left(\frac{L}{L_*}\right) \quad (1.4)$$

$$a = 1.5\ \left(\frac{L}{L_*}\right)^{0.2} \quad (1.5)$$

where $\log(L_*/L_\odot) = 10.4$ in the I–band. As a result, the RC shape and amplitude of spiral galaxies and, therefore, their axisymmetric gravitational potential, are fully specified by just one parameter: the luminosity (or, equivalently, the disk mass). Coadded RC's per luminosity bin (Fig.1.3) show a continuity of properties with increasing galaxy luminosity: at any chosen normalized radius $x \equiv R/R_{opt}$, both the RC amplitude and the local slope strongly correlate with the luminosity, with a *rms* scatter much smaller than the variations among galaxies. In Fig.1.4 we show these correlations at R_{opt}.

Eq.(1.4) reveals a correlation between the disk mass fraction within the optical radius and the galaxy luminosity, which has also been confirmed by direct mass modeling (e.g.: Broeils, 1992; Broeils & Courteau, 1997). This luminosity dependence can be interpreted in terms of a mass–dependent efficiency in transforming the primordial

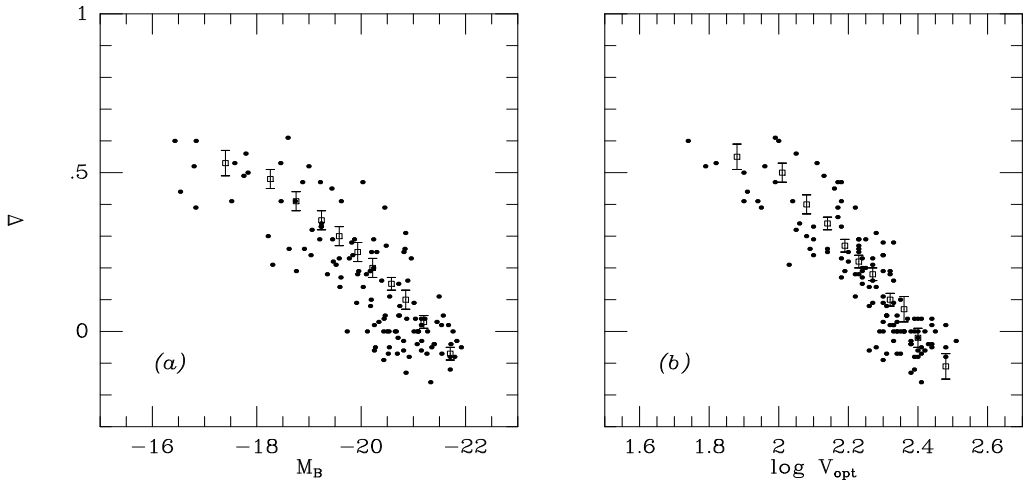

Figure 1.4: The spirals RC's slope at R_{opt} *vs.* luminosity (*left*) and V_{opt} (*right*); from Persic & Salucci (1995) and PSS96.

gas fraction into stars. In fact, from eq.(1.3), the dark–to–luminous mass fraction of a galaxy, computed at the border of the halo virialized region (the "total" $M/M_\star$) is estimated to be (PSS96):

$$\frac{M}{M_\star} \simeq 10 \left(\frac{L}{L_*}\right)^{-0.8} \tag{1.6}$$

This suggests that only the brightest objects reach a value comparable with the BBN value $\simeq 10$, while in low–L galaxies only a small fraction of their original baryon content has been turned into stars.

On the other hand, eq.(1.5) shows that the DM component has a central constant–density region of size comparable to R_{opt}, slightly increasing with luminosity. In Fig.1.3 we can also see that the transition between the inner, disk–dominated regime, and the outer, DM-dominated one, occurs well inside the optical radius (typically at $R \ll R_{opt}$) in low–luminosity galaxies, and farther out, closer to $\sim R_{opt}$, at high luminosities.

All these results led to the definition of an *Universal Rotation Curve* (URC) for

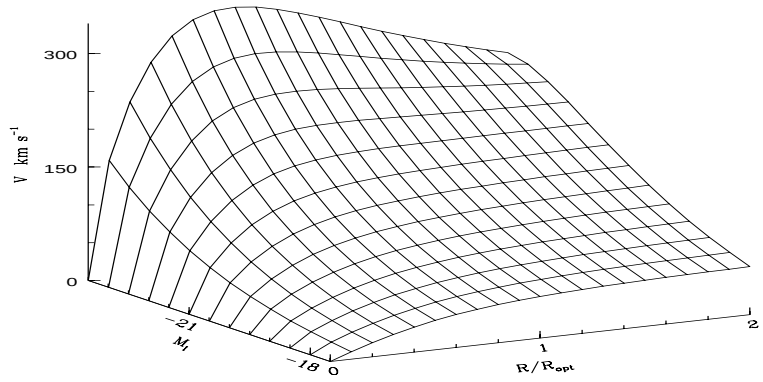

Figure 1.5: The Universal Rotation Curve surface of spiral galaxies.

spiral galaxies (Persic & Salucci 1991, PSS96), which is given by the combination of eq.(1.3), (1.4) and (1.5) and is shown in Fig.1.5. Remarkably, spirals show a very small cosmic variance around the URC. In 80% of the cases the difference between the individual RC's and the URC is smaller than the observational errors. This result has been confirmed by a Principal Component Analysis study of URC (Rhee, 1996; Rhee & van Albada, 1996): they found that the two first components alone account for $\sim 90\%$ of the total variance of the RC shapes.

The luminosity dependence of the URC strongly contrasts with the self–similarity of the luminous distribution of stellar disks. This reflects the discrepancy between the distribution of light and that of the gravitating mass, a discrepancy which increases with radius and with decreasing galaxy luminosity, pointing to a dark mass component with specific characteristics.

Concluding, the main dark matter features in spiral galaxies can be summarized as follows:

- DM has been detected within the luminous regions of all spirals, where dark and luminous matter are already well mixed;
- the transition between the inner, star–dominated region of spirals and the outer, halo–dominated one, moves progressively inwards with decreasing luminosity. As

a consequence, the dark–to–luminous mass ratio at any (normalized) radius increses with decreasing luminosity and DM starts dominating the spirals dynamics at smaller normalized radii for lower luminosities. Moreover, the total $M/M_\star$ spans the range between the BBN predition ~ 10 at very high luminosities and $\sim 10^4$ at $L \ll L_*$;

- the DM halo structure seems to involve a core radius comparable in size with the optical one, slightly increasing with the galaxy luminosity.

DM in LSB galaxies

The central surface luminosity of normal spirals is about constant: $\mu_0 = 21.65 \pm 0.30$ in B-band. In the early 90's, however, a large population of disk systems, with a significantly lower surface brigthness ($\mu_{0;B} \simeq 24 - 25$), was detected (Schombert et al., 1992; Driver et al., 1994; Morshidi et al., 1997). In these systems the light distribution follows that of an exponential thin disk (McGaugh & Bothun, 1994), with total magnitude ~ 1.5 mag fainter than that of normal (HSB) spirals. They show maximum circular velocities similar to HSB's ones, but their optical sizes are ~ 3 times larger (de Blok et al., 1996). Moreover, faint LSB galaxies ($M_B \sim -16$), have very extended HI disks, whose kinematics allows a good estimate of their mass structure (de Blok et al., 1996).

Neverthless, no difference can be detected between the LSB and HSB rotation curves (PSS96; Swaters et al., 2000), which coincide within the observational uncertainties, when the radial coordinate is normalized to the disk length scale (Fig.1.6). By adopting, for LSB galaxies, a similar mass model as for spirals, PSS96 found that they stay on the "spiral" β–L and a–L relationships, which describe the dark–luminous matter coupling: HSB's and LSB's are indistinguishable in the $(\beta,\ a)$ space. In other words, LSB's strongly deviate with respect to the spirals' luminosity–disk lengthscale relation, but follow the same Universal Rotation Curve.

Anyway, LSB's are significantly less dense than normal spirals, for both the dark

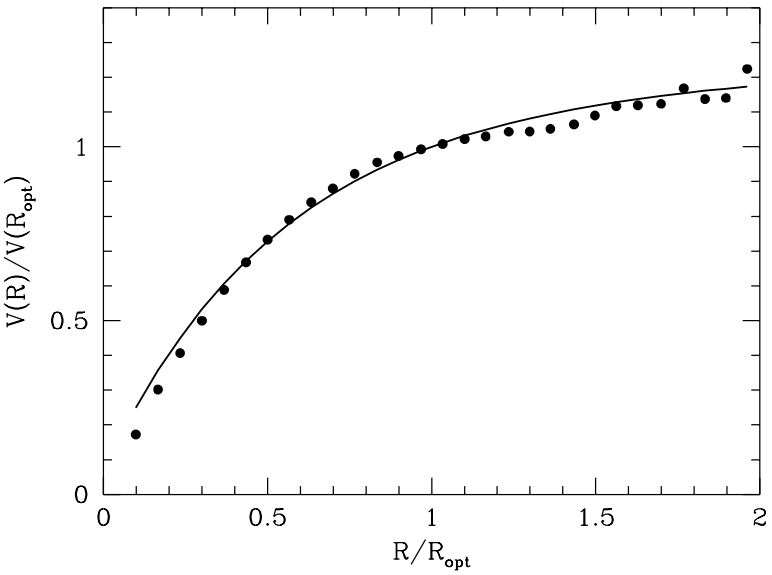

Figure 1.6: Coadded rotation curves of LSB galaxies with $V_{opt} \sim (70 \pm 30)$ km s^{-1}. The solid line represents the V_{URC} of spirals of similar V_{opt}.

and luminous components, and have lower stellar mass–to–light ratios. This suggests that the differentiation between HSB and LSB galaxies is due to different initial conditions (e.g., content of angular momentum, epoch of formation) rather than to later stages of formation.

Let us stress that, to mass modeling this type of galaxies, HI data are always needed, due to the overwhelming gravitational contribution of gas with respect to the stellar one. Early results from the analysis of HI rotation curves (e.g. van der Hulst et al., 1993; de Blok et al., 1996), claiming cores in dark halos of LSB's, have been questioned because of the modest angular resolution of the observations (e.g. Swaters et al., 2000) . Anyway, later works, using both supplementary data in the optical emission lines (e.g. de Blok et al., 2001a) and high–resolution RC's (de Blok & Bosma, 2002) strongly confirm that the halos density profiles are characterized by an almost flat inner region, with core radii of a few kpc.

1.2.2 DM in dwarf galaxies

Dwarf irregulars

The stellar component in dwarf irregular systems (dIrr's) is distributed according to an exponential thin disk as in spirals (Carignan & Freeman, 1988). At high luminosities, dIrr's barely join the low–L tail of spirals; at low luminosities, they reach down to $\sim 10^{-3} L_*$ in B–band. They have very extended HI disks, so that high–quality RC's can be measured out to 2 R_{opt} (e.g. Côté et al., 1997; Swaters, 1997), which allow reliable determinations of the DM properties.

By working out the mass model that best reproduces the RC's shapes of a dIrr's sample, Salucci & Persic (1997, hereafter SP97) found the following main results: *1)* the contribution of the baryonic disk (stars + gas) to the circular velocity is roughly constant with radius (e.g., Carignan & Freeman, 1988), as the decrease of the stellar contribution outwards is counterbalanced by the increase of the gas contribution (see also Corbelli & Salucci, 2000); *2)* These objects are the darkest in the Universe: β continues to decrease at lower luminosities down to $\sim 10^{-2}$. Therefore, the DM fraction in these systems is overwhelming, continuing, at smaller V_{opt}, the trend of low–luminosity spirals. *3)* dwarf galaxies have the densest halos, with high values of the central DM density, continuing the same inverse trend with luminosity as spirals. However, dIrr's halos may have "larger" core radii, in units of R_{opt}, inverting the trend with luminosity detected in spirals.

Similar results are found through best–fit mass models of individual RC's (Puche & Carignan, 1991; Broeils, 1992; Côté et al., 1997; Swaters, 1997). They, in fact, show that DM halos, with large core radii ($\gtrsim r_D$), completely dominate the mass distribution of dIrr's. In greater detail, Côté (1995) and Côté et al. (1997), compiling previous work, find that, at $r \simeq 2\ R_{opt}$, $M_{dark}/M_{baryons} = 1 - (M_B + 20)$ and that central densities increase by a factor ~ 10 from $\mathrm{M}_B = -20$ to $\mathrm{M}_B = -14$.

A direct and important consequence of these results is that dwarf irregulars, although having a negligible amount of light, do have a non–negligible total mass: $\sim 8 \times 10^{10} (L/L_{max})^{1/3}\ M_\odot$ with $L_{max} = 0.04\ L_*$ being the maximum luminosity observed in this family.

Dwarf spheroidals

Dwarf ellipticals/spheroidals (dSph's) are the faintest galaxies we observe; yet, they represent the most common morphological type in the nearby universe (e.g., Ferguson & Binggeli, 1994). In their case, the main kinematical quantity tracing the gravitational potential is the velocity dispersion, which can be determined by measuring redshifts of individual stars.

Ever since early measurements of dSph's velocity dispersions, very high tidal M/L ratios were derived, implying large amounts of DM (Faber & Lin, 1983). Kormendy (1988) and Pryor (1992) showed that dSph's are DM dominated at all radii; core fitting methods (Richstone & Tremaine, 1986) yielded central DM densities of $0.1 M_\odot \mathrm{pc}^{-3}$ (i.e., overdensities of 10^7), a factor 10–100 larger than the stellar ones. Later kinematical studies (e.g. Mateo, 1994; Armandroff et al., 1995; Ibata et al., 1997) have gathered a suitable number of galaxies with central velocity dispersions derived by measurements of stellar motions. Mateo (1997) showed that the central M/L increases with decreasing galaxy luminosity, implying, even in the innermost regions, the presence of a dark component whose importance is greater at low luminosity.

Fitting their M/L–L relationship through a mass model composed of a luminous spheroid with $M_\star = 5\ L_V$ (as in Mateo, 1997) plus a cored dark halo, SP97 obtain a striking agreement between observed and predicted *central* mass–to–light ratios (Fig.1.7). They find $M_{dark} \propto L_V^{1/4}$, indistinguishable from Mateo's best fit, $M_{dark} \sim 2 \times 10^7 M_\odot$ independent of luminosity, and in qualitative agreement with pioneering studies of the dSph's Fundamental Plane (Ferguson & Binggeli, 1994).

Summarizing, dwarf galaxies are the densest galaxies in the Universe and are

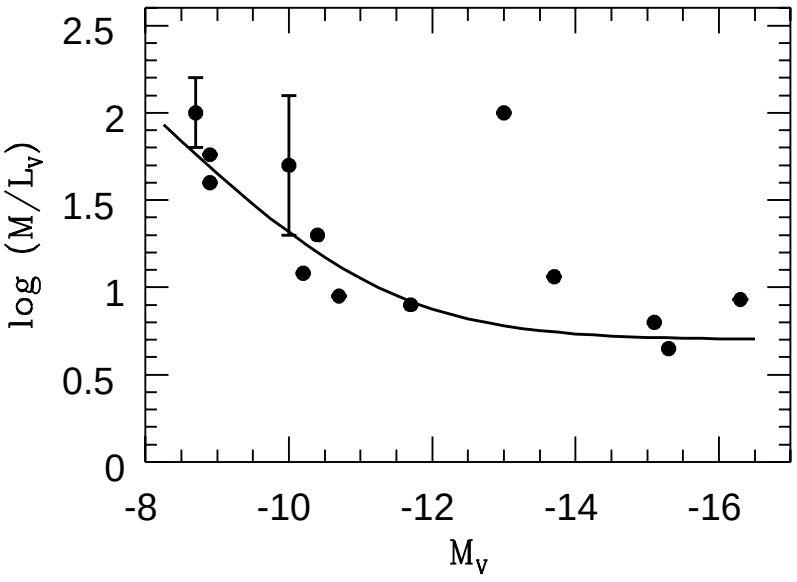

Figure 1.7: The M/L ratios of dSph's: the observational data *vs.* prediction from the "spiral" mass model (line).

also completely DM–dominated. Their low baryon content just smoothly continues downwards the dependence with galaxy mass followed by larger galaxies, and this continuity seems to extends even to all other structural properties.

1.2.3 DM in elliptical galaxies

Compared to spirals, whose geometry and kinematics are well known, elliptical galaxies (E's) are much more complicated systems, as, for many reasons, we do not even know the distribution and the properties of the luminous matter itself. The story of modern studies about E's began when Binney (1978) and Davies et al. (1983) demonstrated that luminous ellipticals are not flattened by rotation. Their correlation between the ratio of the maximum rotation velocity to the central dispersion velocity and the ellipticity clearly reveals that luminous ellipticals are not totally rotationally supported; however, stability with respect to gravitational collapse is ensured by the

anisotropy of their velocity dispersion, rather than by global rotation. Therefore, the intrinsic 3–dimensional shape of ellipticals is, generally, triaxial (indeed, isophote twists and minor–axis rotation have been observed, interpreted as evidence for triaxiality), even though their mean triaxiality is supposed not to be very great. Moreover, their stellar orbital structure is not univocal, in that it depends on the angular momentum content, on the degree of triaxiality and on velocity dispersion anisotropy (radial and/or tangential). As a consequence, inferring their mass distribution from observations is not straigthforward, due to the lack of an ideal, dynamically cold, tracer (like RC's in spirals) and the interpretation of observational data has often been ambiguous (e.g. the issue of the mass–anisotropy degeneracy).

Much of our knowledge has been derived from the analysis of the stellar absorption spectra, integrated along the line of sight: the classical quantitiE's so derived are the stellar luminosity density distribution, the mean velocity profile and the mean velocity dispersion profile, along the line of sight. In principle, these should allow the stellar dynamical modeling by means of the Jeans equations and provide the Distribution Function (DF) of the integrals of the motions and the gravitational potential of the system. In practice, due to degeneracy problems, good results only came with the analysis of the *line of sight velocity distributions* (LOSVD's), measuring the deviations of line profiles from Gaussian functions in terms of h_3 and h_4, the third and fourth order Hermite polynomial terms (Gerhard, 1993; Merritt, 1993). Absorption lines profiles data make now possible (even though quite hard) to determine both the mass distribution and anisotropy out to $2 - 3r_e$ (Kronawitter et al., 2000; Gerhard et al., 2001). Unfortunately, this method involves quite a complicated analysis and can not be applied to a great number of galaxies. Furthermore, observations can not extend further than to $\sim 3\ r_e$, because of the rapid decreasing of surface brightness with radius.

Other mass tracers have been used to probe the gravitational potential out to external radii, involving different observational techniques: *a)* X–Ray emission from hot gas (10^7 K), which gives constraints on M/L at large radii, provided the gas

temperature profile is known; *b)* warm gas (10^4 K) in gaseous disks and HII regions, often confined inside $\sim 2\ r_e$; *c)* 21–cm emission of cold (10^2 K) neutral hydrogen, from HI rings (unfortunately, they are rather rare); *d)* "test particles" of the galaxy gravitational potential, such as Globular Clusters and individual stars in dwarf E's of the Local Group; *e)* gravitational lensing, a successful technique in last years, due to the improvement of observations quality.

All these methods have complemented each other in revealing the presence of DM even in in early–type galaxies, with large value of the total $M/L \simeq 80 - 100$ (Saglia et al., 1993; Bertola et al., 1991, 1993). Notice that extended velocity dispersion profiles up to $1 - 2\ r_e$ indicate no evidence of large amounts of DM in the internal regions: M/L is found to be constant inside $0.5 - 1\ r_e$, which is the typical extent of the ionized gas emission, with a mean value of $3 - 4\ M/L_{B\odot}$ (e.g. van der Marel, 1991; Bertola et al., 1991, 1993). In particular, DM density profile in the inner region of the galaxies is found to be much flatter than the baryons profile, the two profiles intersecting at about the effective radius.

It is worth recalling that much work has also been done, from a theorical point of view, to construct two–components models for ellipticals and to study the corresponding phase–space properties. Large survey of two–components, spherically symmetric, collisionless and self–consistent models have been employed to study ellipticals embedded in massive dark halos (e.g. Bertin et al., 1991, 1993; Ciotti et al., 1996; Ciotti 1999). One important result is that numerical investigations (Ciotti & Pellegrini, 1992; Ciotti, 2000) reveal the difficulty of superimposing, in a consistent way, a centrally peaked profile to a centrally flat one. For instance, a de Vaucouleurs model (peaked in the center) cannot be coupled to a King (quasi–isothermal) density profiles (flat in the center), because their DF's run into negative values near the model center (Ciotti & Pellegrini, 1992).

1.2.4 Summary

Summarizing, the claim for the ubiquitous presence of dark halos around galaxies is observationally supported. From the kinematics of a very large number of systems, there unquestionably emerges a one–to–one relation between a luminous galaxy and a massive dark halo; a hypothetical galaxy found with no dark halo should be considered as a peculiar exception. More specifically, SP97 claim that a stellar system of size R_{opt} and mass $M_\star$, should be actually seen as embedded in a dark halo of radius $\sim 15\ R_{opt}$ and mass $M \simeq 3 \times 10^{12} (\frac{M_\star}{2 \times 10^{11} M_\odot})^{0.4} M_\odot$.

Thus, all galaxies lie within large self–gravitating dark halos; the luminous matter, not surprisingly considering the dissipational collapse it has experienced, is more concentrated than the dark one, by a factor $\sim 10 - 15$. This explains why the former nearly always dominates the inner regions of galaxies. From the galaxy center out to R_{opt}, the DM fraction goes from 0% up to $30\% - 70\%$. Thus, all across the region where the baryonic matter resides, the dark and luminous components are well mixed, except in very–low–luminosity galaxies, which are DM–dominated at all radii. An important consequence is that the two common (and competing) ideas, according to which either *i)* DM is the main component inside R_{opt} or *ii)* DM is important only where the stellar distribution ends, are both ruled out by observational evidence.

As regards halos properties, results from spirals and dwarfs suggest that the DM density should remains approximately constant in the galaxies inner region. This "core" seems to be slightly larger in more luminous galaxies, both in physical and in normalized units. To investigate the existence of halo cores, that would imply that DM halos, arising from scale–free perturbations, have developed a scale related to the luminous matter scale, is a main aim of this thesis.

1.3 What We *Do Not* Know: Open Problems

1.3.1 Collisionless CDM crisis on galactic scale

According to the collisionless Cold Dark Matter (CDM) scenario (Blumenthal et al., 1982; Peebles, 1982), darm matter halos formed out of small, Gaussian and adiabatic density fluctuations, via dissipationless hierarchical merging. They are the main virialised systems within which the primordial gas cools and subsequent star formation occurs, leading, after some possible merging episodes, to the present–day galaxies (White & Rees, 1978; Frenk et al., 1988; Davies et al., 1989; Cole & Lacey, 1996). Collisionless CDM theories with a cosmological constant (or quintessence) give a fine description of large–scale structure in the Universe and have been confirmed by a number of crucial observations, from the abundances of clusters nearby and at $z \lesssim 1$ to CMB anisotropies (see Bahcall et al., 1999; Primack, 2002). However, this success does not extend down to *galactic and subgalactic scales*: a worrying discrepancy exists between observations and theoretical predictions of CDM models concerning: *a)* the central mass distribution in galaxies, *b)* the shapes of the dark halos, *c)* the halos substructure and *d)* the angular momentum of galaxies disks (for a review, see Tasitsiomi, 2002). Here, we focus on the issue of the *DM distribution* within and surrounding galaxies, which is the guideline of our work.

In the following, it will be useful, in order to represent generic dark halos, to refer to the following broad family of density profiles (Zhao, 1996):

$$\rho(r) = \frac{\rho_s}{[k + (r/r_s)^\gamma]\,[1 + (r/r_s)^\alpha]^{(\delta-\gamma)/\alpha}} \tag{1.7}$$

where γ and δ are, respectively, the inner and the outer slope and α marks the turnover point between the two regimes. The parameter k is related to the presence of a central core: if $k \neq 0$, there exists an inner region where the density roughly stays constant and r_s is connected to its extent; otherwise, i.e. for $k = 0$, DM density diverges for $r \to 0$.

Since early 80's, several studies have investigated the detailed structure of collisionless CDM halos, mainly by means of N-body simulations at a progressively higher resolution. Neverthless, it was only in the second half of 90's that spatial/mass resolution of simulations became high enough ($\sim 10\%\ r_{vir}$) to yield predictions of dark halos properties on galactic scale $\sim$ 10 kpc (Navarro, Frenk & White, 1995, 1996, 1997, hereafter NFW; Cole & Lacey, 1996; Fukushige & Makino, 1997; Klypin et al., 1999; Bullock et al., 2001). On the other hand, observational data (especially RC's of DM–dominated galaxies) have increased, in the meantime, in quantity and quality, and substantial improvement occurred in mass modeling tecniques (e.g. PSS96); therefore, it is now possible to test, with high reliability, the above theorical predictions.

The univocal outcome of recent N–body simulations, across a wide range of cosmologies, is well known: CDM halos, with masses in the range $10^{11} M_{\odot} - 10^{15} M_{\odot}$, have an "universal" density profile whose properties are: *a)* a divergent behaviour for $r \to 0$ ($k = 0$, $\gamma \gtrsim 1$); *b)* an outer slope $\delta = 3$ and *c)* a characteristic lenght scale, r_s, marking the separation between inner and outer regime and weakly depending on the halo mass and cosmological parameters. For example, the NFW density profile corresponds to (k, α, δ, γ)= (0, 1, 3, 1) in eq.(1.7). However, a number of simulations with higher mass/spatial resolution (Moore et al., 1998–1999; Ghigna et al., 2000; Jing & Suto, 2000; Fukushige & Makino, 2001) found profiles somewhat steeper in the inner region: for example, Moore and collaborators (1998, 1999) resolved the density profiles down to $\sim 1\%$ of the virial radius, with 10^6 particles and force softening $\sim 0.2\%\ r_{vir}$, finding (k, α, δ, γ)= (0, 1.5, 3, 1.5), thus a density profile steeper, in the center, than the classical NFW.

As a matter of fact, it is well established that the central cusp in halos density profile is not an artifact due to poor numerical resolution, but a specific feature of collisionless CDM halos. Indeed, as cold particles are by definition moving slowly, there are no primordial phase space constraints that could impose a scale (Tremain & Gunn, 1979; Moore, 1994), so that the resulting core radius is negligible. Dynamically, since in the context of hierarchical merging lower–mass halos have higher densities,

DM falls into the center of the more diffuse merger remnant, generating high–density cusps (Syer & White, 1998).

On the observational point of view, since the dark component in galaxies can be better traced when the stellar contribution to the dynamics is negligible, it has been customary to investigate DM–dominated objects, such as dwarfs and LSB galaxies, neglecting their stellar and gaseous components and approximating them as spheres of dark matter. A number of studies claimed that, in these objects, the rotation curves rise more slowly and mass is much less concentrated than predicted by CDM (Moore, 1994; Flores & Primack, 1994; Burkert, 1995; de Blok & McGaugh, 1997; Klypin et al., 1998; Firmani et al., 2000; de Blok et al., 2001a; Moore, 2001; de Blok & Bosma, 2002). The behaviour of the observed RC's requires a constant DM density in the central regions, implying core–dominated halos.

The origin of these flat density cores is quite difficult to understand in the framework of CDM theory. Recent N–body simulations have enough resolution to determine the DM density distribution within 0.5 r_e (e.g. Moore et al., 1998); therefore, any flattening should have emerged. This serious discrepancy led to questioning about the reality of flat cores in DM halos. Indeed, it has been argued that: *a*) the crucial HI rotation curves are of insufficient spatial resolution and beam smearing effects are likely to alter the intrinsic density profile (van den Bosch et al., 2000); *b)* there are several degeneracy problems (van den Bosch & Swaters, 2001) in decomposing the circular velocity in its separate dark and visible components and, therefore, in inferring the dark halo density.

By this point, it is clear that we have a lack of knowledge of halos features in the region where DM and baryons cohabit. This ignorance makes much difficult to give a detailed picture of the process of galaxies formation and, since we do not know the final configuration, this prevents us also by answering another question, perhaps the basic one: which particles non–baryonic DM is composed of? how they interact (if interact) with baryons?

1.3.2 Dark matter nature

Non–baryonic particles candidates to make up the dark matter are usually classified as either "hot" or "cold" (Bond and Szalay, 1983), according to their energy. In the early Universe, when structure starts to form, hot particles, which are very light and relativistics, can free–stream out of galaxy–sized overdense regions, so that only very large structures form. However, cold DM particles, massive (GeV or heavier) and non–relativistic, can clump on smaller scales. This leads to the two main scenarios for structure formation: in the hot DM model, very large structures form first; then, the fragmentation of cluster– or supercluster–sized sheets of collapsed matter ("pancakes") lead to galaxies. In the CDM model, however, galaxy formation and clustering proceeds hierarchically, with small objects merging to form larger ones.

It is well known that pure hot DM models are strongly disfavoured, in view of observations of the distribution of galaxies at very high redshift. There is general consensus on the idea that non–baryonic dark matter consists of cold collisionless elementary particles, without electromagnetic and, obviously, strong interactions (for otherwise they should have been detected). Particle physics offers several candidates with suitable properties. As a matter of fact, this is an exciting research field, in which cosmology and particle physics can strongly interact and contribution each other. We will come back on this important issue in Chapter 6, where we will also discuss the contraints from recent astrophysical findings to the DM particle nature.

1.4 Scope of the Thesis

Within this framework, our research addresses to the issue of DM distribution in galaxies, by devising an adequate strategy to test the DM gravitational effects in galaxies against the CDM predictions. Much work has been done about the "first order" properties of DM in galaxies, its amount and variations with galaxies types and luminosities. Here, we want to investigate the "second order" properties, such as

the DM *distribution*, which, neverthless, are linked to "zero order" physical properties: the nature and the interaction mechanisms of DM particles. To our aim, high quality kinematical data are essential, with high spatial resolution, small observational errors and extending to large radii. Thus, our inquiry strategy focuses on two classes of suitable galaxies:

- **low–luminosity spiral and dwarf galaxies**, with high quality RC's. They have a large DM amount, even in the internal regions and recent findings on the gas distribution in these systems (Corbelli & Salucci, 2000), so as on the amount of stellar matter inside the innermost kiloparsec (Ratnam & Salucci, 2000), will help solving the main problems related to their mass structure.

- **luminous elliptical galaxies**: they are galactic systems showing a variety of scaling laws and correlations between observables, well studied in literature. The most known of these is the Fundamental Plane, an empirical correlation between dynamical and photometrical quantities, with small scatter. There exists a considerable amount of data from large surveys of E's and, remarkably, very high quality observations are available for a number of individual galaxies.

Besides, other recent achievements favour us in our research: for example, we are able now to give better constraints, by means of synthetic spectral energy distribution (SED's), to the mass–to–light ratios of the baryonic component (e.g.. Silva et al., 2001). Moreover, weak (galaxy–galaxy) gravitational lensing is now mapping the distribution of DM in halos over large scales with unprecedented precision, giving very good constraints on the total dark–to–luminous mass ratio (e.g. McKay et al., 2002).

Furthermore, the actual formulation of CDM halos collapse, in the framework of a flat Λ–dominated Universe, turns to have no free parameter in the halos predicted structure but the total mass, which is sufficient to determine (even though with rather a great scatter) the remaining properties: the formation epoch, the concentration and the scale radius. This, of course, strongly limits the possibility of CDM halos to suitably

fit the observations. It is clear, however, that without a clear picture of DM/baryons physics and their present configuration, it is quite impossible (and makes little sense) to develop new theoretical scenarios.

The outline of this thesis is the following. In Part 1 we report our work on disk galaxies: low–luminosity spirals (§2), the case for a single dwarf galaxy (§3) and results from mass modeling the spirals Universal Rotation Curve (§4). Part 2 deals with ellipticals and reports our analysis of the Fundamental Plane as a tool to derive DM properties in spheroids (§5). Finally, in §6 we report our conclusions and perspectives for future work. Chapters from 2 to 5 correspond, with slight modifications, to published or submitted papers (see List of Publications for references) and each of them can be read as a separate entity.

Part II

DISK GALAXIES

Chapter 2

The Dark Matter Distribution in Spiral Galaxies

2.1 Introduction

Rotation curves of disk galaxies are the best probe for dark matter on galactic scale. Notwithstanding the impressive amount of knowledge gathered in the past 20 years, some crucial aspects of the mass *distribution* remain unclear. In fact, the actual density profile of dark halos is still matter of debate; we do not even know whether it is universal or related to some galaxy property, such as the total mass. This is partly because such issues are intrinsically crucial and partly because it is often believed that a RC leads to a quite ambiguous information on the dark halo density distribution (e.g. van Albada et al., 1985). Although deriving halo densities from individual RC's is certainly complicated, this belief is incorrect. In fact, the above argument is true only for rotation curves of low spatial resolution, i.e. with less than ~ 3 measures per exponential disk length scale r_D, as is the case of the great majority of HI RC's. Indeed, since the galaxy structure parameters are very sensitive to both the *amplitude* and the *shape* of the RC in the region $0 < r < r_D$ (the region of the RC steepest rise), HI RC's generally do not have sufficient data to constrain models. No reliable mass model can be derived if such a region is poorly sampled and/or radio beam–biased. However, in case of high–quality *optical* RC's with tens of independent measurements in the critical region, the kinematics can probe the halo mass distribution and resolve their structure.

Since the dark component can be better traced when the disk contributions to the dynamics in a modest way, a convenient strategy leads to investigate DM–dominated objects, like dwarf and low surface brightness (LSB) galaxies. It is well known that, for the latter, there are claims of dark matter distributions with cores of constant density, in disagreement with the steeply cusped density distributions of the Cold Dark Matter Scenario (Flores & Primack, 1994; Moore, 1994; Burkert, 1995; Burkert & Silk, 1997; Kravtsov et al., 1998; McGaugh & de Blok, 1998; Stil, 1999). However, these findings are far from being definitive in that they are: *1)* under the *caveat* that the low spatial resolution of the analysed RC's does not affect the mass modeling and *2)* uncertain,

due to the limited amount of available kinematical data (see van den Bosch et al., 2000).

In this framework, we will investigate the above–discussed issue by analysing a number of high–quality *optical* rotation curves of *low luminosity* late–type spirals, taken from Persic & Salucci (1995, hereafter PS95). They have I–band absolute magnitudes $-21.4 < M_I < -20.0$, that, in terms of rotational velocities, translate into $100 < V_{opt} < 170$ km s^{-1}. Objects in this luminosity/velocity range are DM dominated (e.g. Persic, Salucci & Stel, 1996; hereafter PSS96), but their RC's, measured at the PS95 angular resolution of $2''$, still have a spatial resolution of $w \sim 100(D/10$ Mpc) pc and $n_{data} \sim R_{opt}/w$ independent measurements. For nearby galaxies, this means: $w << r_D$ and $n_{data} > 25$. Moreover, we select rotation curves of bulge–less systems, so that the stellar disk is the only baryonic component for $r \lesssim r_D$.

Since most of the properties of cosmological halos are claimed universal, it is worth to concentrate on a small and particular sample of RC's, that, anyway, can provide crucial information on the dark halo density distribution. The systematics and the cosmic variance of the DM halos are investigated elsewhere (Salucci & Burkert, 2000; Salucci, 2001). We describe the RC's sample in §2.2 and present our mass modeling technique in §2.3. The results of the RC's fitting and the inferred halo profiles and properties are shown in §2.4. A disk–halo model assuming a CDM density profile for the dark halo is discussed in §2.5. We summarize our results in §2.6.

2.2 The Sample of Rotation Curves

The rotation curves of the PS95 'excellent' subsample of 80 galaxies are all suitable for an accurate mass modeling. In fact, these RC's properly trace the gravitational potential, in that: *1)* data extend at least to the optical radius, *2)* they are smooth and symmetric, *3)* they have small *rms* (a few percent), *4)* they have high spatial resolution and a homogeneous radial data coverage, i.e. about $30 - 100$ data points homogeneously distributed with radius and between the two spiral arms.

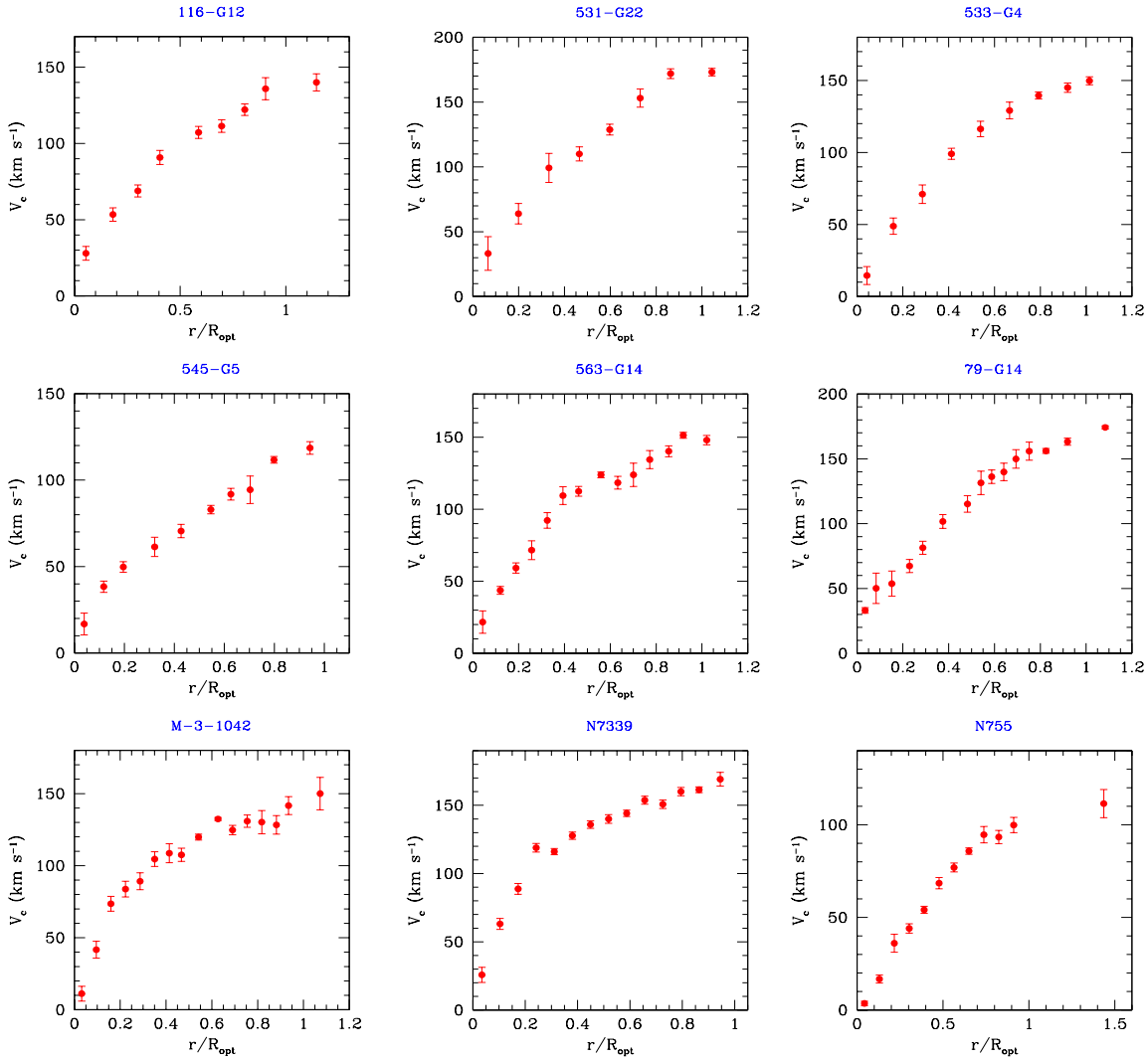

Figure 2.1: Rotation curves of the sample galaxies.

From this subsample, we extract 9 rotation curves (see Tab.2.1, at the end of this chapter) of low–luminosity galaxies ($5 \times 10^9 L_\odot < L_I < 2 \times 10^{10} L_\odot$; $100 < V_{opt} < 170$ km s^{-1}), with their I–band surface luminosity being an (almost) perfect radial exponential. These two last criteria, not indispensable to perform the *mass* decomposition, are however required to minimize the uncertainties of the resulting dark halo *density* distribution. The selected RC's are shown in Fig.2.1 (for all details we refer to PS95). They are still growing at R_{opt}, in that mostly tracing the dark halo component. Each RC has $7 - 15$ velocity points inside R_{opt}, each one being the average of $2 - 6$ independent data. The RC spatial resolution is better than $1/20$ R_{opt}, the velocity *rms* is about 3% and the RC's logarithmic derivative is generally known within about 0.05.

2.3 Mass Models

We model the mass distribution as the sum of two components: a stellar disk and a spherical dark halo. By assuming centrifugal equilibrium under the action of the gravitational potential, the observed circular velocity can be split into these two components:

$$V^2(r) = V_D^2(r) + V_H^2(r) \tag{2.1}$$

By selection, the objects are bulge–less and the stellar component is distributed like an exponential thin disk. Light traces the mass, via an assumed radially constant mass–to–light ratio.

In the r.h.s of eq.(2.1) we neglect the gas contribution $V_{gas}(r)$, since in normal spirals, it is usually modest within the optical region (e.g. Rhee, 1996): $\beta_{gas} \equiv (V_{gas}^2/V^2)_{R_{opt}} \sim 0.1$. Furthermore, high resolution HI observations show that in galaxies with RC's similar to those of the present sample (M33: Corbelli & Salucci, 2000; NGC300: Puche, Carignan & Bosma, 1990; N5585: Coté & Carignan, 1991; N3949

and N3917: Verheijen, 1997) $V_{gas}(r)$ is well represented by $V_{gas}(r) \simeq 0$ for $r < r_D$ and:

$$V_{gas}(r) \simeq (20 \pm 5)(r - r_D)/2r_D \qquad r_D \leq r \leq 3r_D \tag{2.2}$$

Thus, in the optical region: *i)* $V^2_{gas}(r) << V^2(r)$ and *ii)* $d(V^2(r) - V^2_{gas}(r))/dr \gtrsim 0$. This last condition implies that, by including V_{gas} in the r.h.s. of eq.(2.1), the halo velocity profiles would result *steeper* than we already find, and, then, the halo density core radius *larger*, thus strengthening our findings. Incidentally, this is not the case for dwarfs and LSBs: most of their kinematics is affected by the HI disk gravitational pull, in such a way that neglecting it could bias the determination of the DM density.

The circular velocity profile of the exponential thin disk writes (Freeman, 1970):

$$V^2_D(r) = V^2_{opt}\ \beta\ \frac{r^2}{R^2_{opt}}\ \frac{(I_0K_0 - I_1K_1)_{1.6r/R_{opt}}}{(I_0K_0 - I_1K_1)_{1.6}} \tag{2.3}$$

where I_n an K_n are the modified Bessel functions, V_{opt} is the measured circular velocity at R_{opt} and $\beta \equiv \left(\frac{V^2_D}{V^2}\right)_{R_{opt}}$. The parameter β quantifies the disk contribution to the total circular velocity at R_{opt} and ranges 0 to 1. On grounds of simplicity, we assumed β, rather than the disk mass–to–light ratio, as the disk free parameter.

For the DM halo we assume a spherical distribution, with an inner constant density region (CDR). Its contribution to the circular velocity $V_{CDR}(r)$ is given by (PSS96; Salucci & Persic, 1997):

$$V^2_{CDR}(r) = V^2_{opt}\ \gamma\ (1 + a^2)\frac{x^2}{(x^2 + a^2)} \tag{2.4}$$

where $x \equiv r/R_{opt}$ and a is the halo core radius measured in units of R_{opt}. From eq.(2.1): $\gamma = (1 - \beta)$. Since we normalize (at R_{opt}) the velocity model $(V^2_D + V^2_H)^{1/2}$ to the observed rotation velocity V_{opt}, β explicitly enters the halo velocity model and this reduces the free parameters of the mass model to two.

It is important to remark that, out to R_{opt}, the model proposed in eq.(2.4) is neutral with respect to the competing mass models. Indeed, by varying β and a, it approximately reproduces the maximum–disk, the solid–body, the no–halo, the all–halo, the CDM and the coreless–halo models. For instance, CDM halos with concentration parameter $c = 5$ and $r_s = R_{opt}$ are well fit by eq.(2.4) with $a \simeq 0.33$.

2.4 Fitting Rotation Curves

For each galaxy, we determine the values of the parameters β and a by means of a χ^2–minimization fit to the observed rotation curves of the model circular velocity:

$$V^2_{model}(r;\beta,a) = V^2_D(r;\beta) + V^2_{CDR}(r;\beta,a) \tag{2.5}$$

A central role in discriminating among the different mass decompositions is played by the derivative of the velocity field dV/dr. It has been shown (e.g. Persic & Salucci, 1990c; Persic & Salucci, 1992) that, by taking into account the logarithmic gradient of the circular velocity field, defined as:

$$\nabla(r) \equiv \frac{d\log V(r)}{d\log r} \tag{2.6}$$

one can significantly increase the amount of information available from kinematics and stored in the shape of the rotation curve. Then, we consider χ^2-s calculated on both velocities and logarithmic gradients:

$$\chi^2_V = \sum_{i=1}^{n_V} \frac{V_i - V_{model}(r_i;\ \beta,a)}{\delta V_i} \tag{2.7}$$

$$\chi^2_\nabla = \sum_{i=1}^{n_\nabla} \frac{\nabla(r_i) - \nabla_{model}(r_i;\ \beta,a)}{\delta \nabla_i} \tag{2.8}$$

where $\nabla_{model}(r_i;\ \beta, a)$ is computed from eq.(2.3), (2.4) and (2.6). As the linear combination of χ^2-s still follows the χ^2–statistics (Bevington & Robinson, 1992), we derived the mass models parameters by minimizing a *total* χ^2_{tot}, defined as:

$$\chi^2_{tot} \equiv \chi^2_V + \chi^2_\nabla \tag{2.9}$$

The above is the $\alpha = 1$ case of the general relation $\chi^2_{tot} \equiv \chi^2_V + \alpha \cdot \chi^2_\nabla$ we adopt in that the circular velocity at radius r_i and the corresponding log–gradient $\nabla(r_i)$ are statistically independent. Notice that the χ^2_{tot} best–fit solutions are not statistically different from those obtained with the usual χ^2 procedure; however, the ellipse uncertainty is now remarkably reduced.

2.4.1 Results

The parameters of the best–fit models are listed in Tab.2.2, at the end of this chapter, along with their 1σ uncertainties. The derived mass models are shown in Fig.2.2, alongside with the separate disk and halo contributions. The parameter β spans a range from about 0.1 to 0.5: within R_{opt} the disk mass is just 10% to 40% of the gravitating mass. The halo core radius a ranges from ~ 0.8 to ~ 2.5; thus, the halos have an inner region of approximately constant density, whose size is, remarkably, greater than the disk characteristic length scale r_D and it is comparable to (or greater than) the galaxy optical extension (i.e. the region investigated).

The mass models are well specified for each object: the allowed values for β and a span a small and continuous region of the (a, β) space. We get a "lowest" and a "highest" halo velocity curve by subtracting from $V(r)$ the maximum and the minimum disk contributions $V_D(r)$ obtained by substituting in eq.(2.3) the parameter β with $\beta_{best} + \delta\beta$ and $\beta_{best} - \delta\beta$, respectively. In each object, the uniqueness of the resulting halo velocity model can be realized by the fact that the lowest and the highest models mostly coincide. In Fig.2.3 we show the correlation between the halo parameters: halos

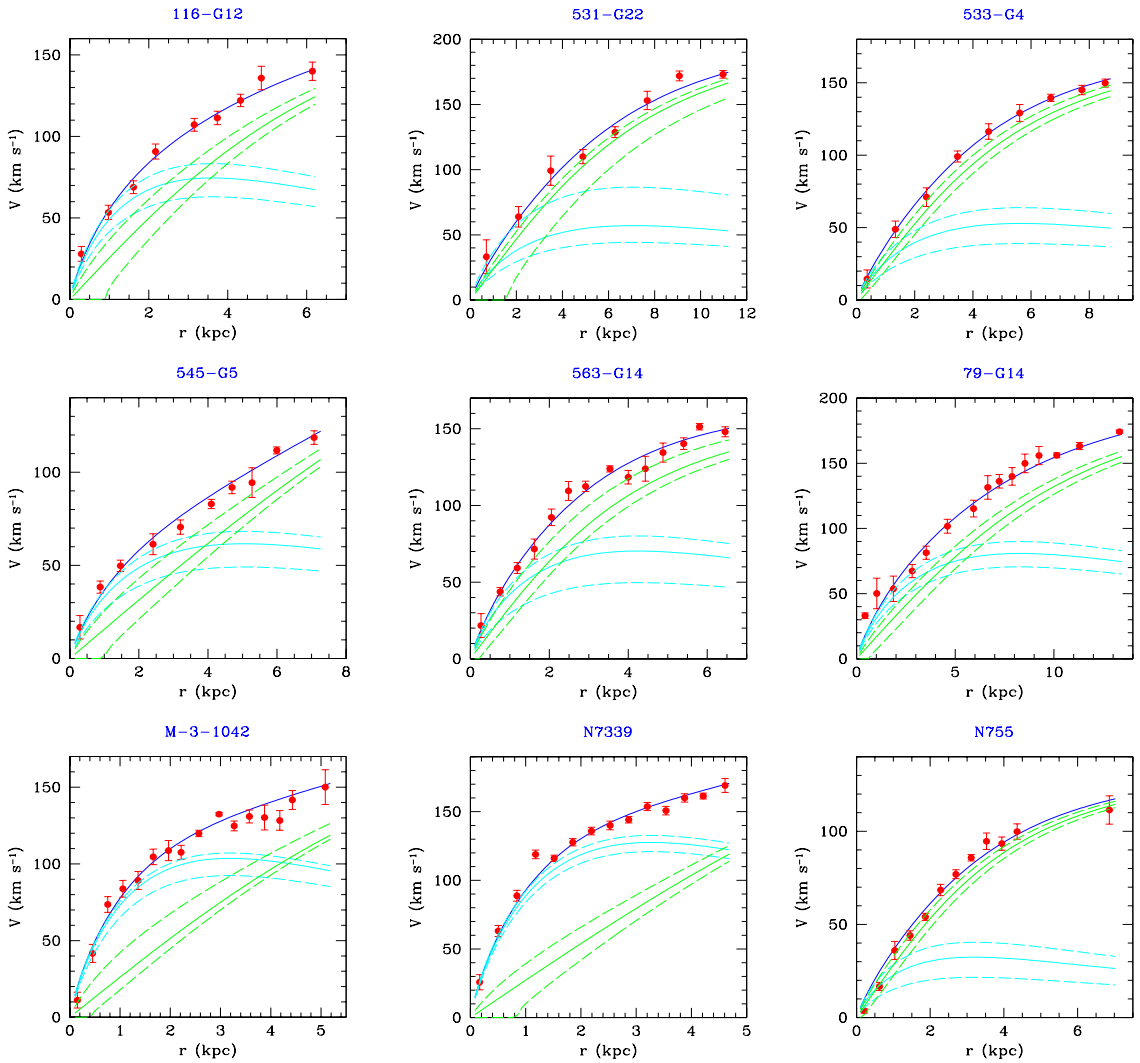

Figure 2.2: Fits (*thick solid line*) to the sample RC's (*points with errorbars*), obtained by assuming the mass model: disk + Constant Density Region (CDR) halo. Thin solid lines represent the separate disk and halo contributions. The maximum disk and the minimum disk solutions are also plotted (*dashed lines*).

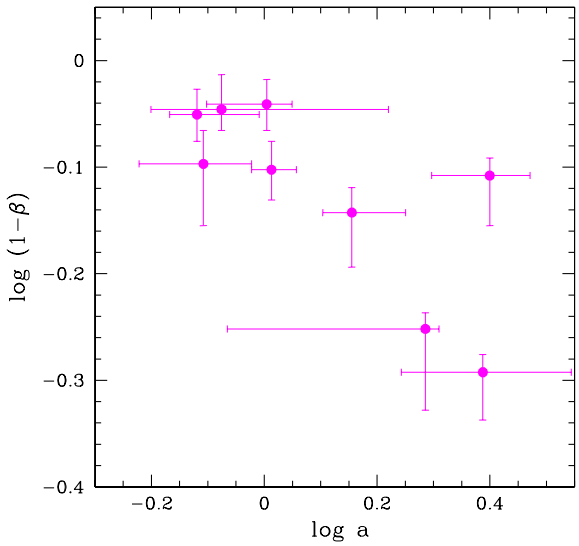

Figure 2.3: Relation between the halo parameters provided by the Constant Density Region (CDR) model fit to the RC's. The halo core radius a is in units of R_{opt}.

which are more dynamically important at R_{opt} (i.e. with higher $(1-\beta)$) tend to have smaller core radii. Part of the scatter of the relation may arise because the sample is limited in statistics and in luminosity range (see Salucci & Burkert, 2000).

As regards to the HI disk contribution, we also tested the reliability of our low–influence hypothesis. Its contribution to the circular velocity (see Corbelli & Salucci, 2000) has been computed and, then, actually subtracted from $V(r)$. As result of the RC's fitting, the values of the parameter β do not change, whereas we obtain slightly larger values of the core radius a, thus strengthening the above findings. We take the galaxy N755 as a typical example. By considering also the gas contribution to its RC, we get: $\beta = 0.05^{+0.07}_{-0.05}$ and $a = 1.1^{+0.2}_{-0.2}$, to be compared with the values in Tab.2.2.

Although the present sample is small for a thorough investigation of the stellar mass–to–light ratios, it is worth noticing that the disk mass–to–light ratios, we infer from the best–fit mass models, ($< M_D/L_I > \sim 0.8 M_\odot/L_{I\odot}$, see Tab.2.2) are typical of late–type spirals with young dominant stellar populations and ongoing star formation

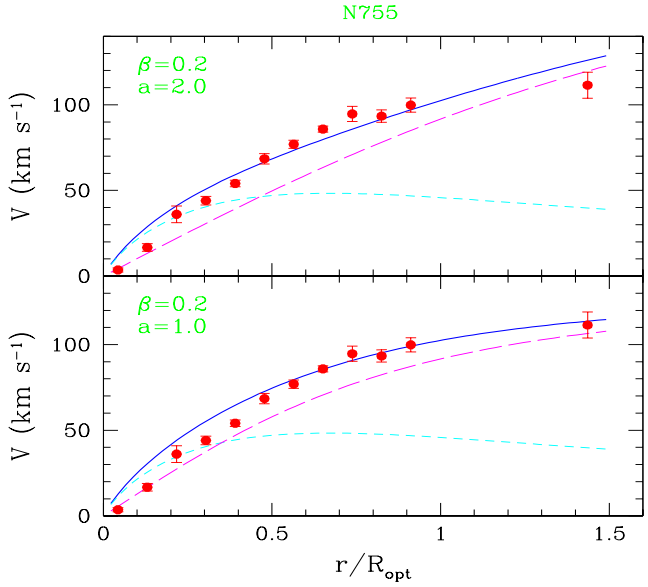

Figure 2.4: N755 rotation curve compared with over–maximum–disk models. Solid line represents the total circular velocity, short– and long–dashed lines represent the disk and halo contributions. The best–fit model for this galaxy is $\beta = 0.09^{+0.05}_{-0.05}$ and $a = 1.0^{+0.1}_{-0.2}$, corresponding to $M_D/L_I = 0.2\ M_\odot/L_{I\,\odot}$. We realize that models with significantly higher disk mass–to–light ratios are inconsistent with the inner rotation curve, regardless of the halo profile.

(e.g. de Jong, 1996), which adds to variations in stellar populations due to differences in age, metallicity, star formation history and to uncertainties in the estimate of distances and/or internal extinctions. In detail, we checked that, for the three galaxies with the lowest disk mass–to–light ratios, a significantly larger value of β is inconsistent with the (inner) rotation curve (see Fig.2.4). Finally, it is worth stressing that the present analysis computes the mass–to–light ratios from the model parameters as a secondary quantity; the uncertainties in Col.(4) of Tab.2.2 do not indicate the goodness of the *halo* mass models, but only specify how well we know this quantity.

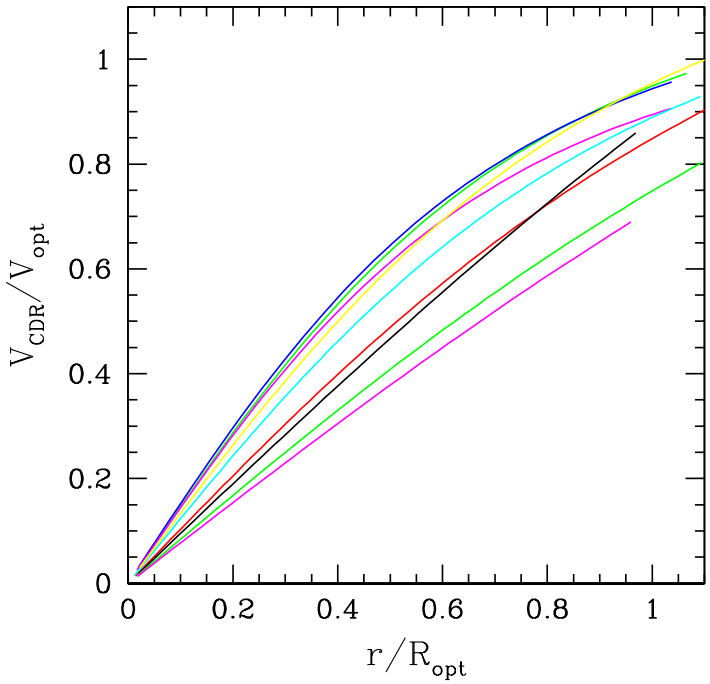

Figure 2.5: The halo velocity profiles of the sample galaxies, derived from the disk+CDR halo fit to the RC's. $V_{CDR}(r)$ rises almost linearly with radius: the DM halo density remains approximately constant.

2.4.2 Dark halos properties

In Fig.2.5 we show the halo velocity profiles for the nine galaxies, obtained from the disk + CDR halo model. The halo circular velocities are normalized to their values at R_{opt} and expressed as a function of the normalized radius r/R_{opt}. These normalizations allow a meaningful comparison between halos of different masses: the radius scaling removes the intrinsic dependence of size on mass (more massive halos are bigger), whereas the velocity scaling takes into account that more luminous galaxies have higher circular velocities.

It is evident that the halo circular velocity, in every galaxy, rises almost linearly with radius, at least out to the disk edge:

$$V_{CDR}(r) \propto r \qquad\qquad 0.05R_{opt} \lesssim r \lesssim R_{opt} \tag{2.10}$$

The halo density profile has a well defined core radius within which the density is approximately constant ($\rho_0 \simeq 1 - 4 \times 10^{-24}$ g/cm^3). This is inconsistent with the singular halo density distribution emerging in the Cold Dark Matter (CDM) scenario of halo formation: $\rho_{CDM} \propto r^{-1}$ (Navarro, Frenk & White (NFW) 1995, 1996, 1997; Cole & Lacey, 1996; Tormen et al., 1997; Tissera & Dominguez–Tenreiro, 1998; Nusser & Sheth, 1999). More precisely, since the CDM halos are, at small radii, likely more cuspy than the NFW profile: $\rho_{CDM} \propto r^{-1.5}$ (Fukushige & Makino, 1997; Moore et al., 1998; Jing, 1999; Jing & Suto, 2000; Ghigna et al., 2000) the steepest CDM halo velocity profile $\propto r^{1/4}$ results too shallow with respect to observations and, therefore, inconsistent with eq.(2.10).

2.4.3 The Burkert density profile

From the study of the density distribution of dark halos around dwarf galaxies, Burkert (1995) proposed the following phenomenological profile:

$$\rho_B(r) = \frac{\rho_0 r_0^3}{(r + r_0)(r^2 + r_0^2)} \tag{2.11}$$

where ρ_0 (the central density) and r_0 (the scale radius) are free parameters. This density law has a core radius of size r_0, and, at large radii, converges to the NFW profile; of course, for $r_0 \ll r_D$, we recover a cuspy profile. Within spherical symmetry, the mass distribution is given by:

$$M_B(r) = 4\ M_0\ \{\ln(1 + r/r_0) - \arctan(r/r_0) + 0.5 \ln[1 + (r/r_0)^2]\} \tag{2.12}$$

with M_0 the dark mass within the core:

$$M_0 \simeq 1.6\ \rho_0\ r_0^3 \tag{2.13}$$

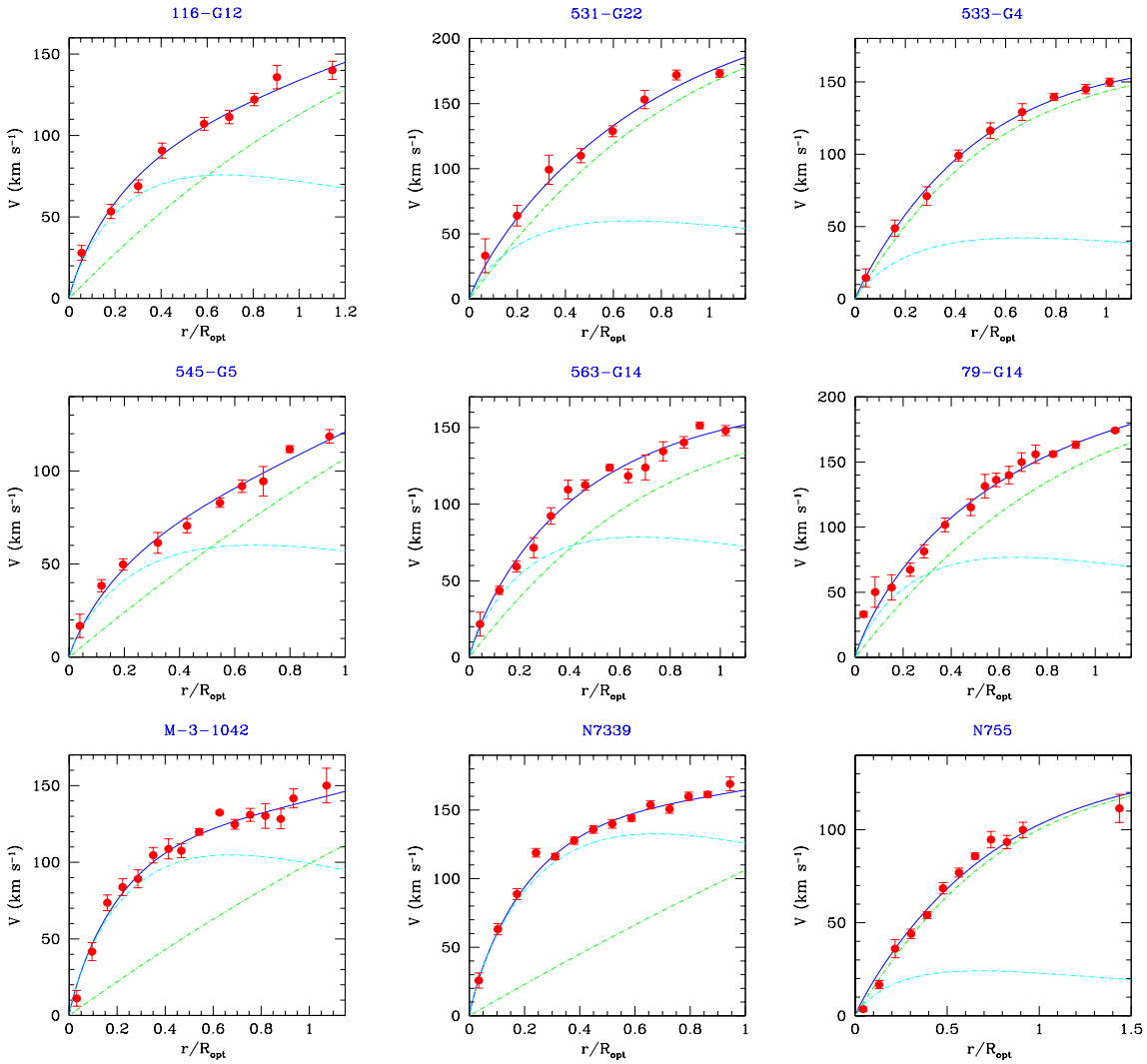

Figure 2.6: Fits (*thick solid line*) to the sample RC's (*points with errorbars*), obtained by assuming a mass model: disk + Burkert halo. Thin lines represent the separate disk and halo contributions.

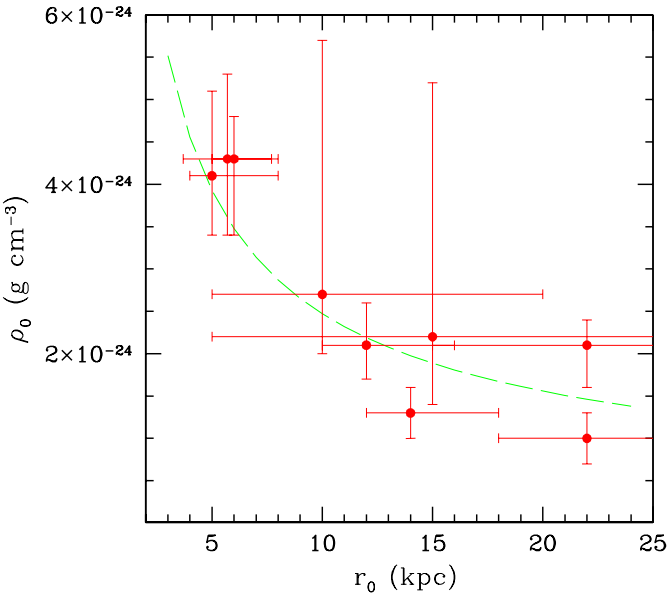

Figure 2.7: Halo central density ρ_0 *vs.* core radius r_0. The dashed line is the Burkert relationship for dwarf galaxies.

The halo contribution to the circular velocity is then: $V_B^2(r) = G\ M_B(r)/r$. Although the dark matter "core" parameters ρ_0 and r_0 are, in principle, independent, the observations reveal a strong correlation among them: $\rho_0 \sim r_0^{-2/3}$ (Burkert, 1995; Salucci & Burkert, 2000). Then, the halo profiles reduce to an 1–parameter family of curves.

For completeness, we also performed the fit to the RC's, by using a mass model composed by an exponential thin disk plus a Burkert halo profile, leaving as free parameters, besides β, both the halo core radius r_0 and the halo central density ρ_0. The results are shown in Tab.2.2 and Fig.2.6: we find that the disk+Burkert halo model can reproduce quite well the observed RC's, over the available radial range. Each of 9 halos has a central density ρ_0 of about $1 - 4 \times 10^{-24}$ g/cm^3, that keeps constant out the edge of the stellar distribution. Let us notice that the core radii are pretty large ($r_0 \gtrsim R_{opt}$); indeed, for three galaxies (545–G5, M–3–1042, N7339), the available spatial extent of the RC's is not sufficient to upper–limit their extension. Moreover, the best–fit values of r_0 and ρ_0, derived by this way, agree with the extrapolation at high masses of the scaling law $\rho \propto r_0^{-2/3}$, established for objects with much smaller

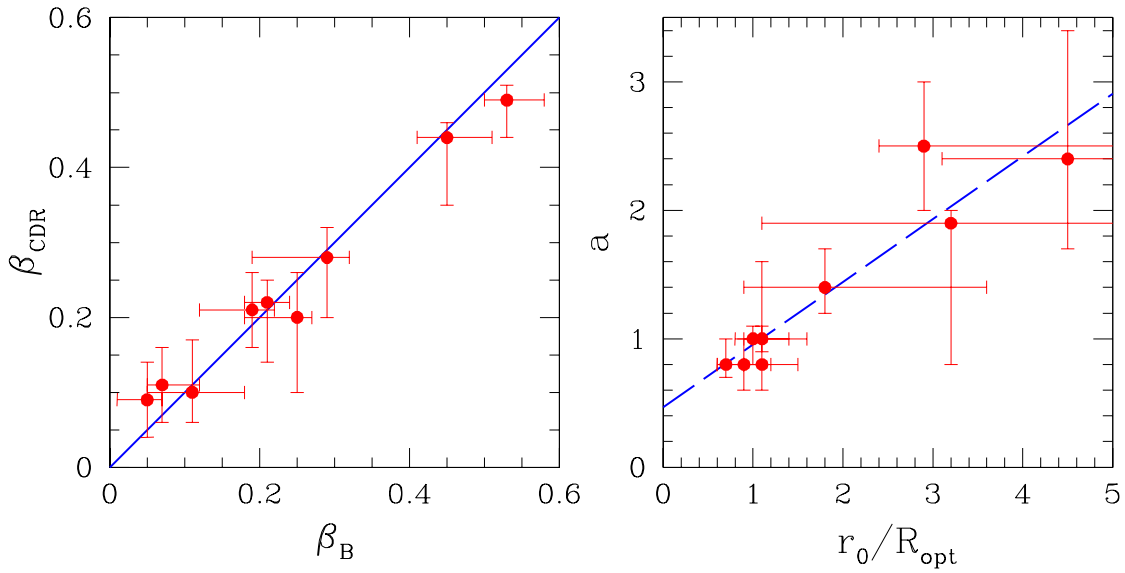

Figure 2.8: Comparison of the CDR and Burkert halo parameters, best–fitting the RC's: *left)* β, the disk contribution to the RC at the optical radius; *right)* the halo core radius of the two halo models; notice that a is in units of R_{opt}. Dashed line is the linear fit to the points.

core radii and stellar masses (Fig.2.7).

By comparing the best–fit models parameters provided from both the two mass models (disk+CDR halo and disk+Burkert halo), we find the following results: *i)* the two models provide consistent estimates of the disk contribution to the RC's at the optical radius (Fig.2.8, *left*). This ensures the reliability of our estimate of disk mass–to–light ratios; *ii)* as regards the halo core radii (Fig.2.8, *right*), however, we show the, remarkably linear, correlation between the two parameters connected to the central core: a (CDR profile) and r_0 (Burkert profile). Anyway, in most cases, the radial extension of our RC's is not sufficient to give reliable upper limits to the halo core size.

Finally, let us stress that the halo properties we find raise important issues by themselves and make quite irrelevant, in comparing theory and observations, arguments *per se* important, such as the CDM halos cosmic variance, the actual value of the concentration parameter or the effects of baryonic infalls or outflows (e.g. Martin, 1999; Gelato & Sommer–Larsen, 1999). We also want to remark that the above findings

imply that spiral galaxies are embedded (inside R_{opt}) in a *single* dark halo. Indeed, if more dark halos were relevantly present, then, in order to not violate the constraint given by eq.(2.10), all of them should have the same solid–body velocity profile.

2.5 The Inadequacy of CDM Mass Models

Although the mass model of eq.(2.4) converges to a distribution with an inner core, rather than with a central spike, i.e. to $a \gtrsim 1$ rather than to $a \simeq 1/3$, it is also worth, given the importance of such result, to check, in a direct way, the (in)compatibility of the CDM models with the observed kinematics. We assume the two–parameters density profile by Navarro, Frenk & White (NFW, 1995, 1996, 1997), resulting from N-body simulations of CDM halos :

$$\rho_{NFW}(r) = \frac{\rho_s}{(r/r_s)(1+r/r_s)^2} \tag{2.14}$$

where r_s is the inner characteristic length scale, corresponding to the radius where the effective logarithmic slope of the profile is -2, and $\rho_s = 4\ \rho_{NFW}(r_s)$. In order to translate the density profile into a circular velocity curve for the halo, we make use of the virial parameters: the halo virial radius r_{vir}, defined as the radius within which the mean density is Δ_{vir} times the background universal density ρ_{bkg} at that redshift, and the corresponding virial mass M_{vir} and velocity $V_{vir} \equiv GM_{vir}/r_{vir}$. By defining the concentration parameter as $c_{vir} \equiv r_{vir}/r_s$, the halo circular velocity $V_{NFW}(r)$ takes the form (Bullock et al., 2001):

$$V^2_{NFW}(r) = V^2_{vir}\frac{c_{vir}}{A(c_{vir})}\frac{A(x)}{x} \tag{2.15}$$

where $x \equiv r/r_s$ and $A(x) \equiv \ln(1+x) - \frac{x}{1+x}$. As the relation between V_{vir} and r_{vir} is fully specified by the background cosmology: we assume the standard ΛCDM cosmological

model, with $\Omega_m = 0.3$, $\Omega_\Lambda = 0.7$ and $h = 0.75$, and reduce from three to two (c_{vir} and r_s) the independent parameters characterizing the model. The choice is conservative: a high density $\Omega_m = 1$ model, with a concentration parameter $c_{vir} > 12$, is definitely unable to account for the observed galaxy kinematics (Moore, 1994). According to the assumed cosmological model, $\Delta_{vir} \simeq 340$ at $z \simeq 0$.

Though N–body simulations and semi–analytic investigations indicate that the two parameters c_{vir} and r_s correlate, we leave them independent to increase the chance of a good fit. Since the objects in our sample are of low luminosity, i.e. $L_*/12 \lesssim L_I \lesssim L_*/3$, we conservatively set for the halo mass M_{vir} an upper limit of $M_{up} = 2 \times 10^{12} M_\odot$, comparable to the total mass of the Milky Way (Wilkinson & Evans, 1999) and to the mass of bright spirals in pairs (e.g. Chengalur, Salpeter & Terzian, 1993). This value is further justified by considering that, if $M_{vir} > M_{up}$ in the above–specified luminosity range, then, the amount of dark matter locked in the only spiral galaxies $\Omega_S = \int_{L_*/12}^{L_*/3} M_{vir}\ \phi(L)\ dL$, with $\phi(L)$ the galaxy luminosity function, would much exceed 0.1, and would be unacceptable for the assumed $\Omega_m = 0.3$ cosmological model.

We performed the fit to the RC's by means of the χ^2_{tot} minimization technique described in §2.4; the results are reported in Tab.2.3. In Fig.2.9, we compare the NFW fits to the previous CDR ones: for 7 galaxies the NFW curve model is unacceptably worse than the CDR solution, whereas for 2 objects (M–3–1042 and N7339) the goodness level of the two fits is comparable, but let us recall that the associated virial mass is quite high: $M_{vir} \sim 2 \times 10^{12} M_\odot$. Taking at their face values, the residuals of the CDM model fits have a characteristic "S" shape, clearly indicating that this density profile is definitely too steep in the innermost region and too flat in the external part. Moreover, the NFW mass models have extremely low value of the disk mass–to–light ratios (see Tab.2.3): most of the objects have $M_D/L_I \leq 0.05$, in obvious disagreement with the spectro–photometric properties of spirals, that indicate mass–to–light ratios at least 10 times higher.

The inadequacy of the NFW model for our sample galaxies is even more evident if one performs the fit after removing any constraint on virial mass. Indeed, (see

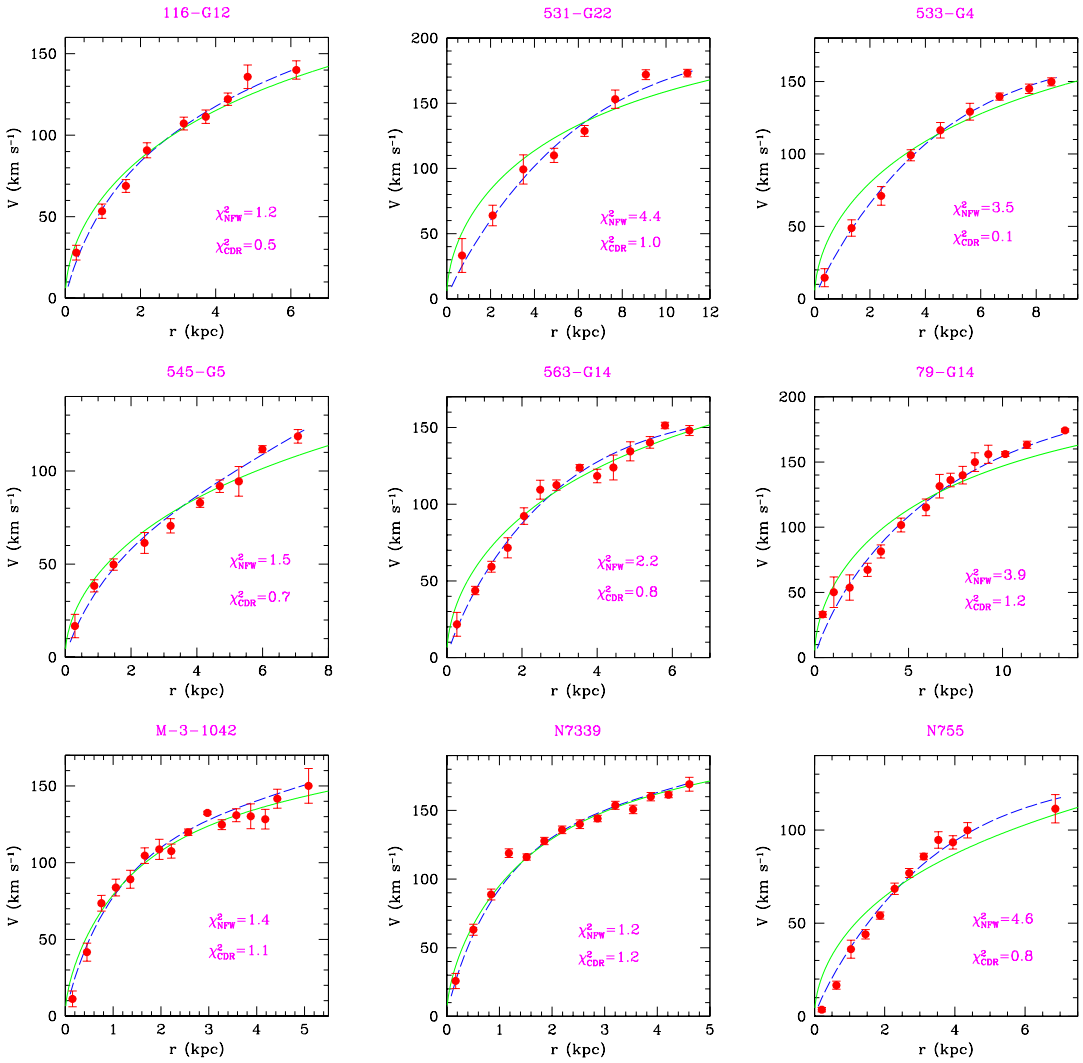

Figure 2.9: NFW best–fits (*solid lines*) to the rotation curves (*points with errorbars*), compared to the CDR fits (*dashed lines*). The χ^2 values are also indicated.

Tab.2.3), good fits are obtained only for uncomfortably large virial velocities and masses ($V_{vir} \simeq 600 - 800$ km s^{-1}; $M_{vir} \simeq 10^{13} - 10^{14} M_{\odot}$). These results can be explained as the attempt of the minimization routine to fit the $V(r) \propto r^{0.5}$ NFW velocity profile to data intrinsically linear in r.

2.6 Conclusions

Crucial insight has come from disk–halo mass decomposition of a well suited sample of 9 bulge–less disk galaxies, with $100 \leq V_{opt} \leq 170$ km s^{-1}. These galaxies have a relevant amount of dark matter: the contribution of the luminous matter to the dynamics is small and can be properly taken into account. Moreover, the high spatial resolution of the available rotation curves allows us to reliably obtain the separate dark and luminous density profiles. In fact, it is worth to notice that the claim of a so–called cosmic conspiracy (e.g. van den Bosch et al., 2000), i.e. the lack of a marker in the RC's of the transition from the inner (disk–dominated) region to the outer (halo–dominated) one, preventing an unique determination for $(1 - \beta)$ and r_0, does not hold, in that: *i)* the steepness of the 9 RC's makes sure that β is small and then well determined and *ii)* the transition, being at small radii, leaves the characteristic mark of a linear RC (see Persic & Salucci, 1992).

We find that dark matter halos have a central constant density region ($\rho_0 \simeq 1 - 4 \times 10^{-24}$ g/cm^3), whose size exceeds the stellar disk length scale r_D. These halo profiles disagree with the cuspy density distributions typical of CDM halos (e.g. Navarro, Frenk & White, 1997; Kravtsov et al., 1998), which, therefore, fail to account for the actual DM velocity data. On the other hand, these halo velocities are well described in terms of the Burkert density profile, an empirical functional form whose two structure parameters (central density and core radius) are related through: $\rho_0 \sim r_0^{-2/3}$.

To better stress our findings, we show in Fig.2.10 the actual dark halo profile around 116–G12 compared to the CDM prediction for the density profile of a dark halo of the same mass inside R_{opt}: the overall disagreement between the two profiles is

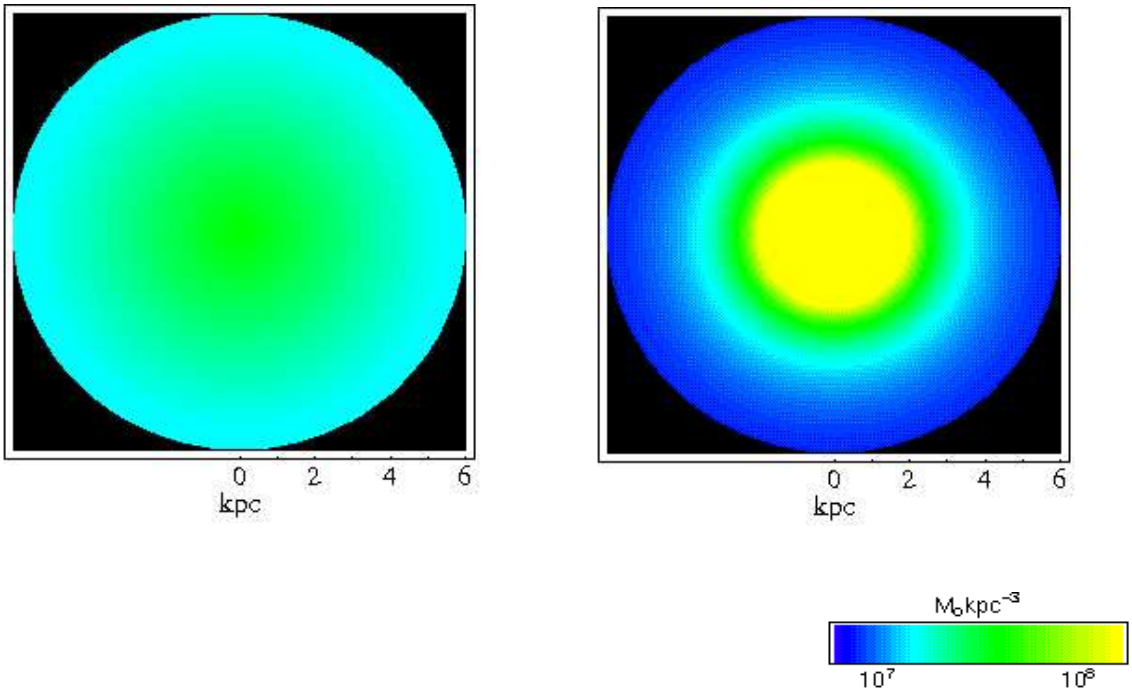

Figure 2.10: *Left)* actual dark halo profile around 116–G12; *right)* CDM prediction for the density profile of a dark halo of the same mass inside R_{opt}.

evident and excludes that this inconsistency could be a local feature.

The dark halo velocity linear rise, from 0.25 r_D to $\sim$ 3 r_D, sets a serious upper limit to the dynamical relevance of CDM–like dark halos in spirals. Indeed, once we rule out a CDM halo, also the claim by Burkert & Silk (1997) of *two* dark halos, a MACHO dark halo with a CDR profile and a standard CDM halo, meets a difficulty. Indeed, in this case, in order to satisfy eq.(2.10), the MACHO halo should account for $> 95\%$ of the dark mass inside R_{opt}. Then, it would dominate the dynamics out to well beyond 25 r_D. The CDM halo would, then, have dynamical importance in regions so external that its cosmological role itself would be in question.

Galaxy	r_D	V_{opt}	M_I
116-G12	1.7	133.5	-20.0
531-G22	3.3	171.1	-21.4
533-G4	2.7	151.1	-20.7
545-G5	2.4	124.4	-20.4
563-G14	2.0	148.9	-20.5
79-G14	3.9	167.1	-21.4
M-3-1042	1.5	148.0	-20.1
N7339	1.5	172.7	-20.6
N755	1.5	102.4	-20.1

Table 2.1: **Observational properties of the sample galaxies** – Col.(1): galaxy name; Col.(2): length scale of the exponential thin disk, in kpc (from Persic & Salucci, 1995). The optical radius R_{opt} is the radius encompassing 83% of the light: $R_{opt} = 3.2\, r_D$; Col.(3): circular velocity at R_{opt}, in km/s; Col.(4): total I–band absolute magnitude (Mathewson, Ford & Buchhorn, 1992).

	disk+CDR			**disk + Burkert**		
Galaxy	β_{CDR}	a	M_D/L_I	β_B	r_0/R_{opt}	$\rho_0 \cdot 10^{-24}$
116-G12	$0.28^{+0.04}_{-0.08}$	$1.4^{+0.3}_{-0.2}$	$1.0^{+0.1}_{-0.3}$	$0.29^{+0.03}_{-0.1}$	$1.8^{+1.8}_{-0.9}$	$2.7^{+3}_{-0.7}$
531-G22	$0.10^{+0.07}_{-0.04}$	$0.8^{+0.8}_{-0.2}$	$0.3^{+0.2}_{-0.1}$	$0.11^{+0.07}_{-0.06}$	$1.1^{+0.4}_{-0.2}$	$2.1^{+0.5}_{-0.4}$
533-G4	$0.11^{+0.05}_{-0.05}$	$0.8^{+0.2}_{-0.1}$	$0.4^{+0.2}_{-0.2}$	$0.07^{+0.05}_{-0.02}$	$0.7^{+0.2}_{-0.1}$	$4.3^{+0.5}_{-0.9}$
545-G5	$0.22^{+0.03}_{-0.08}$	$2.5^{+0.5}_{-0.5}$	$0.7^{+0.1}_{-0.2}$	$0.21^{+0.03}_{-0.03}$	$2.9^{+40}_{-0.5}$	$1.0^{+0.3}_{-0.3}$
563-G14	$0.20^{+0.06}_{-0.10}$	$0.8^{+0.2}_{-0.2}$	$0.7^{+0.2}_{-0.3}$	$0.25^{+0.02}_{-0.07}$	$0.9^{+0.3}_{-0.3}$	$4.3^{+1}_{-0.9}$
79-G14	$0.21^{+0.05}_{-0.05}$	$1.0^{+0.1}_{-0.1}$	$0.7^{+0.2}_{-0.2}$	$0.19^{+0.03}_{-0.07}$	$1.1^{+0.3}_{-0.2}$	$1.3^{+0.3}_{-0.3}$
M-3-1042	$0.44^{+0.02}_{-0.09}$	$1.9^{+0.1}_{-1.1}$	$1.6^{+0.1}_{-0.3}$	$0.45^{+0.06}_{-0.04}$	$3.2^{+60}_{-2.1}$	$2.2^{+3}_{-0.8}$
N7339	$0.49^{+0.02}_{-0.05}$	$2.4^{+1.0}_{-0.7}$	$1.6^{+0.1}_{-0.2}$	$0.53^{+0.05}_{-0.03}$	$4.5^{+60}_{-1.4}$	$2.1^{+0.3}_{-0.5}$
N755	$0.09^{+0.05}_{-0.05}$	$1.0^{+0.1}_{-0.2}$	$0.2^{+0.1}_{-0.1}$	$0.05^{+0.02}_{-0.04}$	$1.0^{+0.6}_{-0.2}$	$4.1^{+1}_{-0.7}$

Table 2.2: **Results of the RC's fits with "cored" halos** – Col.(1): galaxy name; Col. (2)-(3)-(4): parameters of the best–fit disk+CDR halo models with their 1σ uncertainties. Mass–to–light ratios in col.(4) are in $M_\odot/L_{I\odot}$). Col. (5)-(6)-(7): parameters of the best–fit disk+Burkert halo models with their 1σ uncertainties. Densities in col.(7) are in g cm^{-3}.

$M_{vir} \leq 2 \times 10^{12} M_\odot$				
Galaxy	β	c_{vir}	r_s (kpc)	M_D/L_I $(M_\odot/L_{I\odot})$
116-G12	$0.01^{+0.04}_{-0.01}$	$7.9^{+0.6}_{-0.4}$	26^{+4}_{-5}	$0.04^{+0.14}_{-0.04}$
531-G22	$0.01^{+0.03}_{-0.01}$	$7.5^{+0.5}_{-0.5}$	28^{+4}_{-3}	$0.03^{+0.10}_{-0.03}$
533-G4	$0.01^{+0.03}_{-0.01}$	$7.0^{+0.5}_{-0.5}$	30^{+5}_{-4}	$0.04^{+0.11}_{-0.04}$
545-G5	$0.01^{+0.04}_{-0.01}$	$4.7^{+0.3}_{-0.7}$	44^{+5}_{-4}	$0.03^{+0.12}_{-0.03}$
563-G14	$0.01^{+0.03}_{-0.01}$	$8.7^{+0.3}_{-0.7}$	24^{+4}_{-4}	$0.03^{+0.10}_{-0.03}$
79-G14	$0.01^{+0.04}_{-0.01}$	$6.5^{+0.5}_{-0.5}$	32^{+3}_{-4}	$0.03^{+0.14}_{-0.03}$
M-3-1042	$0.20^{+0.05}_{-0.10}$	$8.1^{+1.4}_{-0.6}$	26^{+3}_{-7}	$0.72^{+0.18}_{-0.36}$
N7339	$0.18^{+0.02}_{-0.08}$	$11.1^{+2.0}_{-0.6}$	19^{+2}_{-4}	$0.58^{+0.06}_{-0.26}$
N755	$0.03^{+0.02}_{-0.03}$	$4.8^{+0.2}_{-0.8}$	43^{+3}_{-4}	$0.05^{+0.04}_{-0.05}$

No limit on M_{vir}				
Galaxy	β	c_{vir}	r_s (kpc)	M_{vir} $(\cdot 10^{13} M_\odot)$
116-G12	$0.01^{+0.04}_{-0.01}$	$2.0^{+1.6}_{-0.2}$	456^{+50}_{-100}	20.0
531-G22	$0.01^{+0.01}_{-0.01}$	$1.8^{+0.8}_{-0.1}$	472^{+20}_{-90}	10.0
533-G4	$0.01^{+0.03}_{-0.01}$	$1.7^{+0.9}_{-0.2}$	500^{+20}_{-80}	7.9
545-G5	$0.01^{+0.02}_{-0.01}$	$1.4^{+0.7}_{-0.1}$	479^{+30}_{-90}	2.5
563-G14	$0.05^{+0.05}_{-0.05}$	$2.0^{+1.6}_{-0.2}$	472^{+30}_{-70}	20.0
79-G14	$0.01^{+0.02}_{-0.01}$	$1.6^{+0.4}_{-0.2}$	490^{+20}_{-110}	6.3
M-3-1042	$0.31^{+0.05}_{-0.06}$	$1.7^{+1.3}_{-0.2}$	493^{+30}_{-120}	10.0
N7339	$0.38^{+0.04}_{-0.08}$	$1.9^{+1.6}_{-0.3}$	497^{+20}_{-80}	15.8
N755	$0.01^{+0.02}_{-0.01}$	$1.5^{+0.9}_{-0.2}$	467^{+30}_{-110}	4.0

Table 2.3: **Results of the RC's fit with a disk+NFW halo mass model** – Col.(1): galaxy name; Col.(2)-(3)-(4): parameters of the best–fit models with their 1σ uncertainties. **Top**: an upper limit of $2 \times 10^{12} M_\odot$ is imposed on M_{vir}; in Col. (5) we show the corresponding disk mass–to–light ratio in the I–band. **Bottom**: best–fit models, obtained with no constraint on the virial mass; in Col. (5) we show the corresponding virial mass.

Chapter 3

Dark Matter in Dwarf Spiral DDO47

3.1 Introduction

Rotation curves (RC's) of disk galaxies have always been the best probes for dark matter (DM) on galactic scale. Although much progress has been made over the past 20 years, it is only very recently that we start to shed light on crucial aspects of the DM *distribution*. Indeed, the main focus was initially on *the presence* of a dark component; this later shifted to investigating the ratio of dark to visible matter (Salucci & Persic, 1997). Today, the focus is mainly on the actual density profile of dark halos.

Since Carignan & Freeman (1985), a "pseudo–isotermal" distribution for the dark matter halo has often been adopted, although the crucial implications of a cored DM distribution appeared only after cosmological N–body simulations found that the halos in Cold Dark Matter (CDM) simulations achieve a cuspy density profile (Navarro, Frenk & White, 1995, 1996, 1997; hereafter NFW):

$$\rho_{NFW}(r) = \frac{\rho_s}{(r/r_s)(1+r/r_s)^2} \tag{3.1}$$

where r_s and ρ_s are the characteristic inner radius and density. The halo virial radius r_{vir} is the radius within which the mean halo density is $\Delta_{vir} \simeq 200$ times the mean universal density at that redshift (see Bullock et al., 2001). The virial mass M_{vir} and the corresponding virial velocity are related by: $V_{vir} \equiv GM_{vir}/r_{vir}$. The concentration parameter is defined by $c_{vir} \equiv r_{vir}/r_s$. With the above definitions, the halo circular velocity V_{CDM} can be written as:

$$V^2_{NFW}(r) = V^2_{vir}\frac{c_{vir}}{A(c_{vir})}\frac{A(x)}{x} \tag{3.2}$$

where $x \equiv r/r_s$ and $A(x) = \ln(1+x) - x/(1+x)$. Numerical simulations give c_{vir} as a function of M_{vir} for a population of halos observed at any redshift, and particularly at $z = 0$ (see Wechsler et al., 2002: their Fig. 13) that, inserted in eq.(3.2), yields the

circular velocity as a function of radius for a halo of mass M_{vir}. Recent high–resolution CDM simulations have claimed central density cusps steeper than in eq.(3.1) (Moore et al., 1999; Ghigna et al., 2000), we conservatively will not consider here.

The discrepancy between the halos universal profile predicted by CDM theory and the halos mass distribution as inferred from the galaxies RC's emerged a few years ago, though the first claims were questioned in view of observational/modeling uncertainties. At the present, the phenomenon is widely accepted, but, with data of low spatial/velocity resolution, there are claims that some (but not all) RC's of DM–dominated galaxy can be equally well fitted by a NFW halo plus a stellar disk (e.g. van den Bosch et al., 2000).

In our work we approach the querelle "CDM halos *vs.* observed halos" in two different and complementary ways: *i)* to derive the *detailed* mass structure of halos around galaxies comparing the emerging picture to the CDM one (see §2) and *ii)* to test one or more *specific* CDM predictions by means of proper kinematical data. In the light of the latter approach, the dwarf galaxy DDO47 opens an unprecedented opportunity.

3.1.1 Data

Recent HI data (Walter & Brinks, 2001), in connection with I–band surface brightness photometry (Makarova et al., 2002), allow for the dwarf spiral galaxy DDO47 a very favourable scenario: *a)* its RC extends out to ~ 9 disk length scales, at a spatial resolution of $\sim 1/4\ r_D$, *b)* the HI disk has a surface density that strongly decreases for $r > 5\ r_D$; therefore, its contribution to the circular velocity cannot mimic that of a constant density halo, *c)* the galaxy is of very low luminosity; then, the luminous matter content is small with respect to the DM one (e.g. Persic & Salucci, 1988) and, following the ΛCDM scenario, its halo should be very concentrated ($r_s \ll 9\ r_D$). Therefore, we expect (see Salucci & Burkert, 2000) that a severe discrepancy between the CDM prediction and the actual DM distribution will emerge in this galaxy.

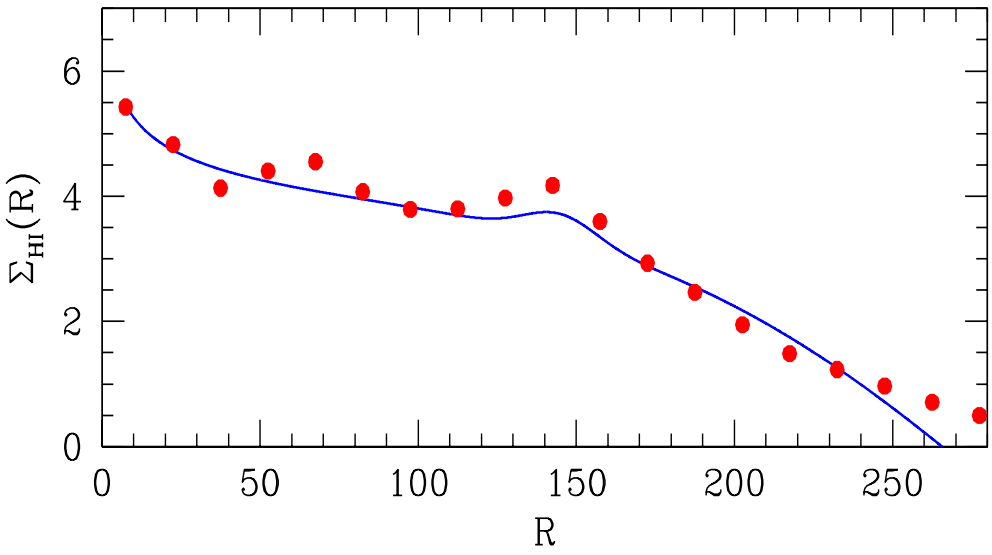

Figure 3.1: The HI surface density in DDO47

The high resolution VLA HI observations we use here are discussed in detail in Walter & Brinks (2001). In summary, VLA observations of DDO47 in the B, C, DnC, and D array yielded a resolution of $7.8'' \times 7.2''$ (velocity resolution: 2.6 km/s). The rotation curve presented here is based on a moment 1 map of HI data, which have been convoluted to $30''$ resolution; the rotation curve itself has been derived with the task ROTCUR in the GIPSY package. For our new analysis, we have checked the previously derived curve by also subjecting the data to the task INSPECTOR in GIPSY, which provides the same results. The best–fit results are summarized by: v_{sys} = 272 km/s; inclination i=35°; position angle PA=310°. The data points presented in Fig.3.1 are all independent measurements. DDO47 is assumed at a distance of 4 Mpc; anyway, our following results do not depend on this assumption.

3.2 Mass Modeling and Results

The DDO47 baryonic components are: 1) an exponential stellar thin disk of length scale $r_D = 28" \pm 2"$, whose contribution to the circular velocity $V(r)$ is:

$$V_D^2(x) = 1.28\ \beta\ V_{opt}^2\ x^2\ (I_0K_0 - I_1K_1)|_{1.6x} \tag{3.3}$$

where $x \equiv r/r_D$ and β is the disk mass fraction at $R_{opt} = 3.2\ r_D$, being $\simeq 0$ (see Persic, Salucci & Stel, 1996); 2) a HI disk (whose surface density is given in Fig.3.1) of mass $2 \times 10^7 M_\odot$, negligible with respect to the dynamical mass. In detail, under the assumption of spherical symmetry, the HI contribution to the circular velocity can be written as: $V_{\rm HI}^2(x) \simeq G\ M_{\rm HI}(r)/r \simeq 10^{-4} V^2(r)$ (the exact computation for a thin disk differs much lesser than a factor 2).

We plot in Fig.3.1 the HI surface density (data are in Walter & Brinks, 2001) and its fit. We realize that, for $r > 20$", it decreases faster than r^{-1}, implying that $V_{\rm HI}(r)$ significantly decreases in the region where the RC is steeply and steadily increasing. This is a further case (see Corbelli & Salucci, 2000) in which the HI disk, and any other component likewise distributed, cannot account for the gravitating matter, independently of the total mass. Notice that since the quantity $V_D^2(x) + V_{\rm HI}^2(x)$ decreases with radius at $r > 2\ r_D$, if we assume it equal to zero we favor the CDM scenario. Indeed, given that the gravitating matter is steeply increasing with radius, the more the baryonic contribution (which increases with r much more slowly) is different from zero, the steeper the halo mass profile is.

DDO47's rotation curve (see Fig.3.2) increases with radius almost *linearly*. It is straightforward to infer that it is dominated by a dark halo almost everywhere (e.g. Persic & Salucci, 1988), from the absence of the disk–halo transition point, which is clearly identifiable when the stellar gravitational potential is important (Salucci & Frenk, 1989). Velocity data are available out to 9.1 r_D and, being basically free from baryonic contributions, they directly measure the gravitational potential of the dark halo, at least for $r > 2\ r_D$, along 6 disk length scales.

The increase of the circular velocity is remarkable: from 27 km/s at 2.7 r_D, it reaches a value of 68 km/s at 9.1 r_D, the farthest radius with data. The circular

velocity local slope $d\log V/d\log r$ is always > 0.75. Since $V(r) \simeq V_h(r)$, i.e. the baryonic contribution is small, we can obtain a rough estimate of the "core" halo density:

$$\rho_h(< 1 \text{ kpc}) \simeq \frac{1}{4\pi\ G\ r^2}\ \frac{d(V^2 r)}{dr}\ \simeq \left(1 + 2\ \frac{d\log V}{d\log r}\right)\Bigg|_{1\text{kpc}} \sim 2 \times 10^{-24}\ \text{g/cm}^3 \qquad (3.4)$$

This pair density–radius is well off those of the ΛCDM Universal Profile that, at the kpc scale, has much higher halo densities (e.g. Bullock et al., 2001). Considering $d\log\rho_h/d\log r$ as the slope of the dark matter halo density, we estimate:

$$\frac{d\log\rho_h}{d\log r} \gtrsim\ -0.5 \qquad\qquad 2.7\ r_D < r < 9.1\ r_D \qquad (3.5)$$

at variance with CDM, which predicts in the same region (Moore et al., 1999, Bullock et al., 2001): $d\log\rho_h/d\log r < -1$ and, more likely, ~ -2. Over the above radial range, there is an *increase* in V^2 of 600%, confronting a *decrease* of $\sim 20\% \pm 20\%$ associated with ΛCDM (Bullock et al., 2001).

We model the mass distribution by three mass components (stellar disk + HI disk + dark halo); the baryonic components are taken as shown above, whereas the dark matter density is described by a Burkert profile:

$$\rho_B(r) = \frac{\rho_0\ r_0^3}{(r + r_0)(r^2 + r_0^2)} \qquad (3.6)$$

where ρ_0 and r_0 are, respectively, the central density and the size of the region of (almost) constant density. Then, the dark mass distribution is given by:

$$M_B(r) = 4\ M_0\ \{\ln(1 + r/r_0) - \arctan(r/r_0) + 0.5\ln[1 + (r/r_0)^2]\} \qquad (3.7)$$

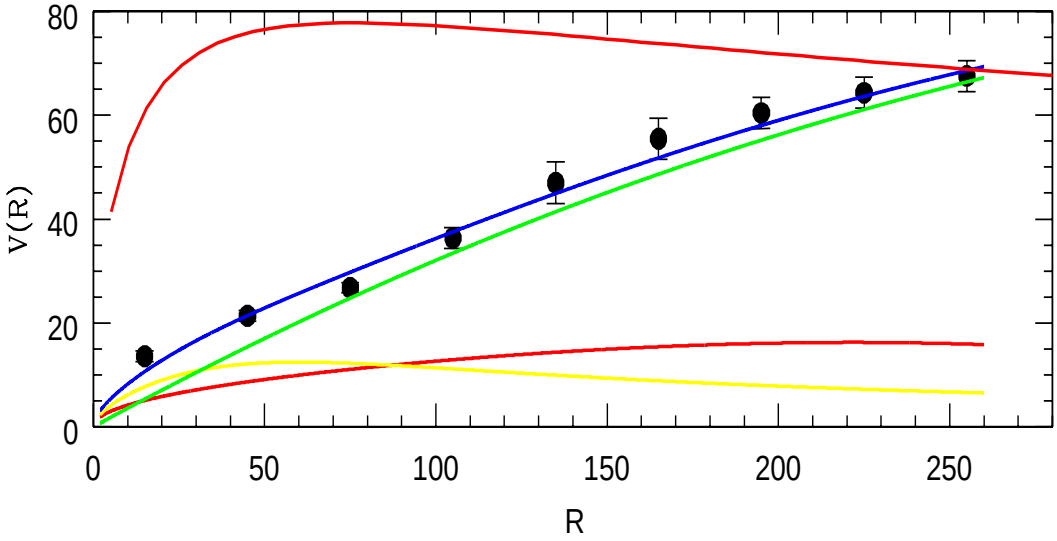

Figure 3.2: DDO47 rotation curve fitted by NFW and CDR models

where $M_0 = 1.6\ \rho_0 r_0^3$ is the halo mass within r_0 and the halo contribution to the circular velocity is: $V_B^2(r) = G\ M_B(r)/r$. We obtain the dark matter parameters: $\rho_0 = 1.1 \times 10^{-24}$ g/cm^3, $r_0 = 7.1$ kpc and the disk mass $M_D \sim 5.3 \times 10^7 M_\odot$, by the χ^2–minimization procedure of the quantity $V^2(r) - V_D^2(r) - V_B^2(r)$. The resulting mass model is shown in Fig.3.2: it fits the data in excellent way. Moreover, the values of r_0 and ρ_0 agree with the scaling law $\rho \propto r_0^{-2/3}$, found both for dwarfs (Burkert, 1995) and for normal spirals (§2; Salucci & Burkert, 2000).

As a comparison, we show the ΛCDM case, once V_{NFW} has been normalized to data at 9.1 r_D and the baryonic contribution set to zero. These are of advantage to CDM: we use ρ_s as a free parameter, independent of r_s and tunable to improve the fit. Furthermore we neglect the "baryonic" steepening of $V(r)$. As a result, in the region under study, the halo circular velocity would be *decreasing* with radius, leading to a discrepancy with the ever–rising velocity data (see Fig.3.2) that needs not commenting. Instead, it is instructive to show in which way CDM goes wrong. Let us plot, for cored and CDM models, the DM *density* at a radius r, measured in critical density units, *vs.* the mass enclosed in r (Fig.3.3). The two mass–density distributions are globally in radical and definitive disagreement, well beyond a local inconsistency.

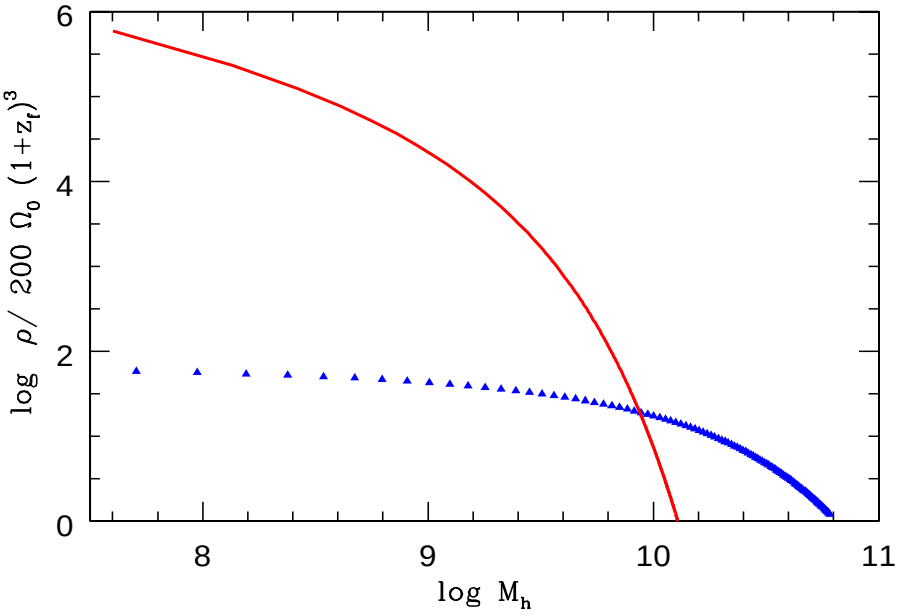

Figure 3.3: DM density at a radius r, measured in critical density units, *vs.* the mass enclosed in r, for cored and CDM models.

3.3 Conclusions

The DM halo density of DDO47, out to 9 r_D, is fully and uniquely determined by two parameters: its central density and core radius. These are quantities that are *missing* in the gravitational instability/hierarchical clustering Cold Dark Matter scenario.

Then, in order to reconcile this theory with observations one should conclude that current CDM simulations are not applicable for the innermost 10% of the halo mass distribution, in that the physics of the collapse is too complex for them. Or, alternatively, one may postulate that a yet unknown physical process, occurring in the innermost 10^{-3}% of the dark halo volume, cuts down the post–collapse DM density by $1-2$ orders of magnitudes, and, moreover, it is fine–tuned with its original *local* value (Salucci & Burkert, 2000).

Chapter 4

Properties of Dark Halos from Large Samples of Spirals

4.1 Introduction

Until mid 90's, it has been difficult to investigate the internal structure of dark matter (DM) halos, due to both a poor knowledge of the exact amount of luminous matter present in the innermost regions of spirals and the limited number of suitable rotation curves (RC's). The situation is more favorable for low surface brightness (LSB) and dwarf galaxies, which are strongly dark matter dominated even at small radii. The kinematics of these systems shows an universality of the dark halo density profiles, but it results in disagreement with that predicted by Cold Dark Matter (CDM) theories, in particular because of the existence of dark halo density cores (e.g. Moore 1994; Burkert 1995). The origin of these features is not yet understood; likely, it involves more physics than a simple hierarchical assembly of cold structures.

To cope with this observational evidence, Burkert (1995) proposed an empirical profile that successfully fitted the halo rotation curves of four DM–dominated dwarf galaxies:

$$\rho_B(r) = \frac{\rho_0 r_0^3}{(r + r_0)(r^2 + r_0^2)} \tag{4.1}$$

where ρ_0 and r_0 are free parameters, representing the central dark matter density and the scale radius. This sample has been later extended to 17 dwarf irregular and LSB galaxies (Kravtsov et al., 1998) which all are found to confirm eq.(4.1). Adopting spherical symmetry, the mass distribution of the Burkert halos is given by:

$$M_B(r) = 4\ M_0 \left\{ \ln\left(1 + \frac{r}{r_0}\right) - \arctan\left(\frac{r}{r_0}\right) + 0.5\ \ln\left[1 + \left(\frac{r}{r_0}\right)^2\right] \right\} \tag{4.2}$$

with M_0, the dark mass within the core, given by:

$$M_0 \simeq 1.6\ \rho_0\ r_0^3 \tag{4.3}$$

The halo contribution to the circular velocity is then: $V_B^2(r) = GM_B(r)/r$. Although the dark matter core parameters r_0, ρ_0 and M_0 are in principle independent, the observations reveal a clear correlation (Burkert, 1995):

$$M_0 = 4.3 \times 10^7 \left(\frac{r_0}{kpc}\right)^{7/3} M_\odot \tag{4.4}$$

which indicates that dark halos represent a 1–parameter family, completely specified, e.g. by the core mass.

The analysis of a large sample of $\sim$ 1000 RC's (Persic, Salucci & Stel, 1996; hereafter PSS96) has provided a suitable framework to investigate the dark halo density distribution in spirals. In Fig.4.1 we plot the synthetic, coadded rotation curves of spirals, sorted per luminosity bins: $V_{syn}(r/R_{opt};\ L_I/L_*)$, with L_I the I–band luminosity and $L_I/L_* = 10^{-(M_I+21.9)/5}$). Remarkably, *individual* RC's have a very small variance with respect to the corresponding synthetic curves (PSS96; Rhee, 1996; Rhee & van Albada, 1996; Roscoe, 1999; Swaters, 1999): spirals sweep a very narrow locus in the RC–profile/amplitude/luminosity space.

The whole set of synthetic RC's can be quite well reproduced by the Universal Rotation Curve (URC): $V_{URC}(x)^2 = V_D(x)^2 + V_h(x)^2$, where $x \equiv r/R_{opt}$,

$$V_D^2(x) = 1.28\ \beta V_{opt}^2\ x^2\ (I_0K_0 - I_1K_1)|_{1.6\ x} \tag{4.5}$$

is the contribution to the circular velocity of the luminous exponential thin disk and

$$V_h^2(x) = V_{opt}^2\ (1-\beta)\ (1+a^2)\frac{x^2}{(x^2+a^2)} \tag{4.6}$$

is the circular velocity term of the spherical DM halo. The free parameters in the mass model are: $\beta \equiv (V_D(R_{opt})/V_{opt})^2$ and a, the halo core radius in units of R_{opt}. At

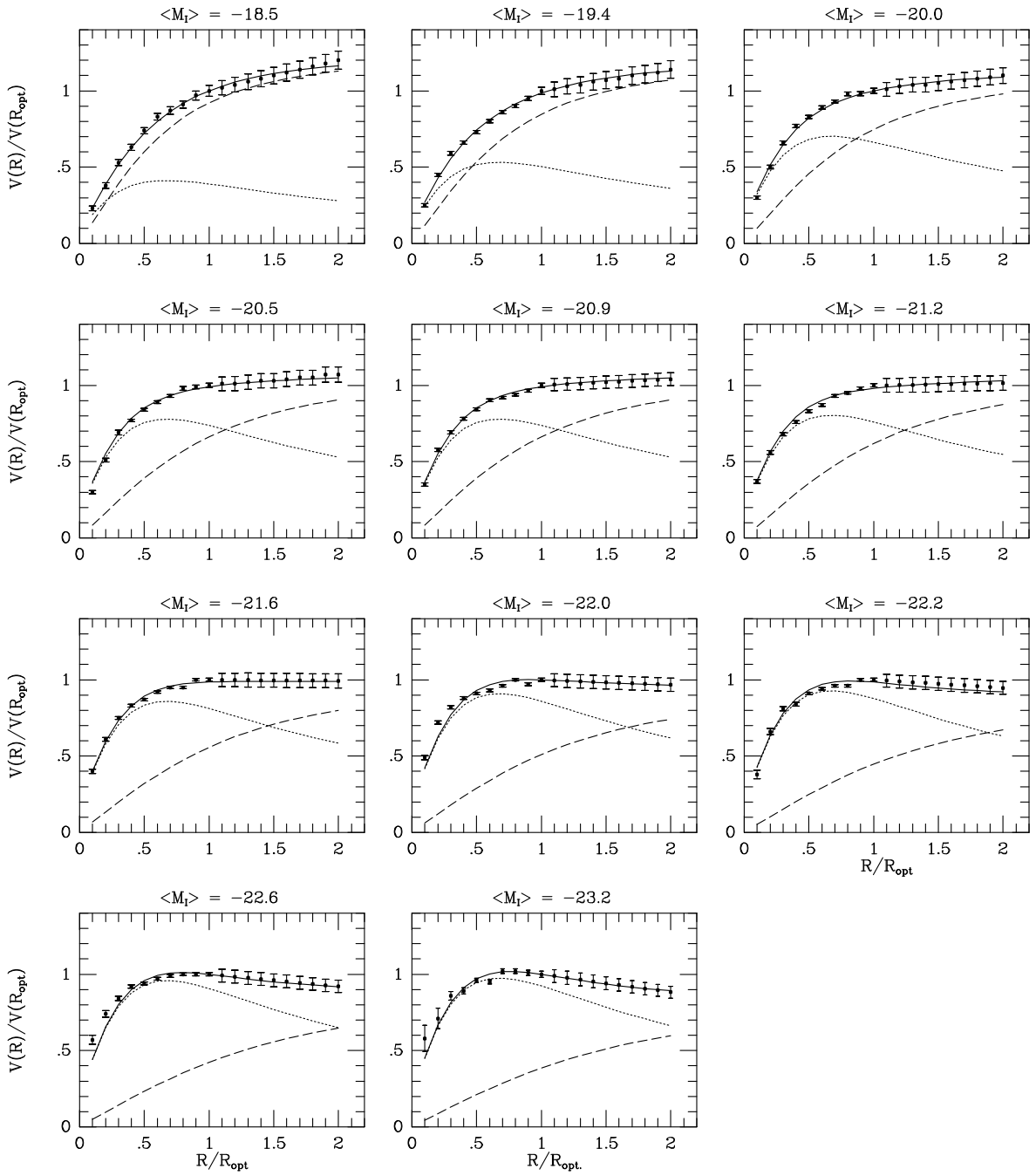

Figure 4.1: Synthetic rotation curves (points with errorbars) sorted per luminosity bin. The solid line are the URC fits; also shown the separate dark/luminous contributes (dotted line: disk; dashed line: halo).

high luminosities the contribution from a bulge component has been also considered (Salucci & Persic, 1999b). The procedure of fitting the URC to the synthetic curves yields (PSS96):

$$\beta \simeq 0.72 + 0.44 \log(L_I/L_*) \tag{4.7}$$

$$a \simeq 1.5(L_I/L_*)^{1/5} \tag{4.8}$$

More in detail, at any luminosity and radius, $|V_{URC} - V_{syn}| < 2\%$ and the 1σ fitting uncertainties on a and β are about 20% (Fig.4.1). These results unveil that crucial structural properties of spirals, like the disk contribution to the RC at the optical edge and the DM halo core radius, do significantly depend on the sole galaxy luminosity.

Within this scenario, the main aim of our work is to expand the above findings on spirals and to relate them to the Burkert profile. We take $H_0 = 75$ km/s/Mpc and $\Omega_m = 0.3$; anyway, no result depends on these choices.

4.2 Halo Density Profiles and Scaling Laws

We compare the dark halo velocities, obtained from eq.(4.6), (4.7) and (4.8), to the Burkert velocities $V_B(r)$ derived from eq.(4.2). We leave ρ_0 and r_0 as free parameters, i.e. we do not impose the relationship of eq.(4.4). The results are shown in Fig.4.2: the Burkert density profile reproduces, for the whole spiral luminosity sequence, the DM halos mass distribution, out to the outermost radii ($\sim 6\ r_D$), where $V_B(r)$ and $V_h(r)$ are indistinguishable. However, for $r \gg 6\ r_D$, i.e. beyond the region described by the URC, the two velocity profiles progressively differ.

The values obtained for r_0 and ρ_0 from the synthetic RC's fit agree with the extrapolation at high masses of the scaling law $\rho \propto r_0^{-2/3}$ (Burkert, 1995) established for objects with core radii ten times smaller (see Fig.4.3). Let us notice that the core

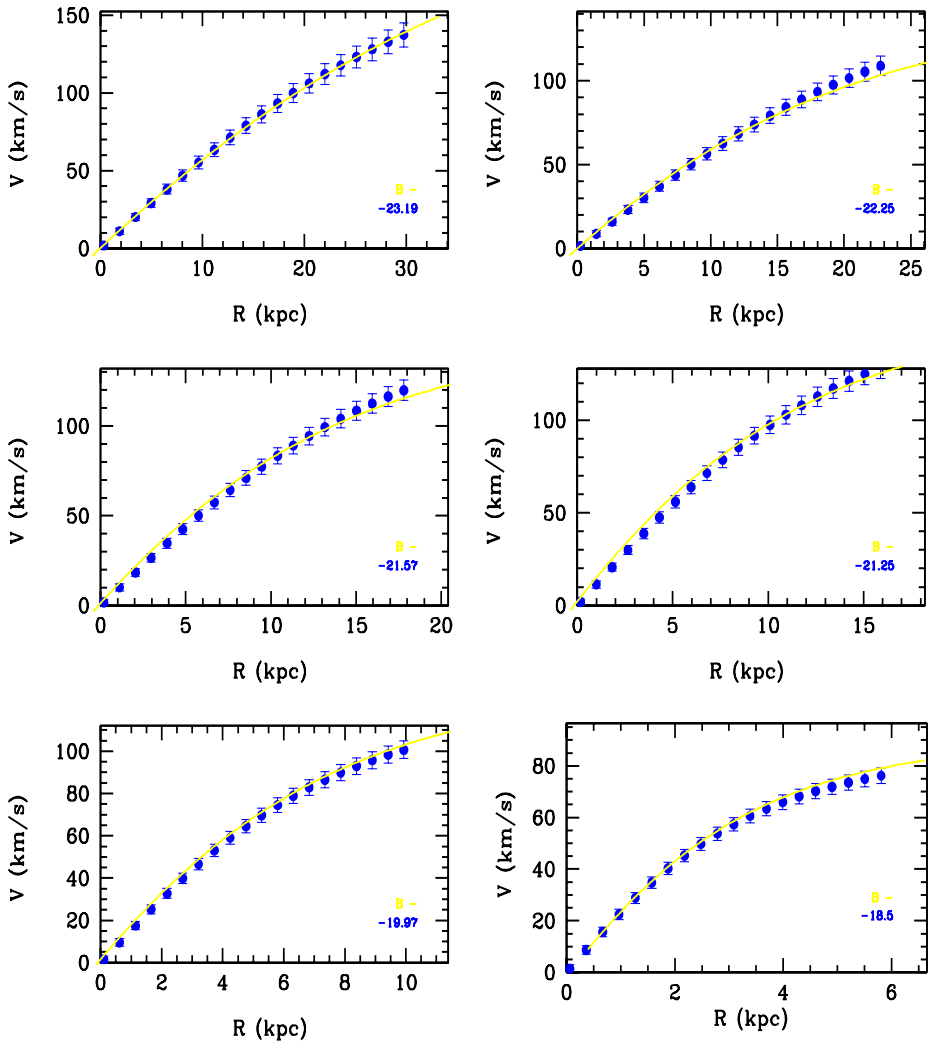

Figure 4.2: Comparison of the halo velocity profiles obtained, respectively, from the URC fit to the RC's (points with errorbars) and from the Burkert model fit (solid lines). The bin magnitudes are also indicated.

radii are very large: $r_0 \gg r_D$ so that an ever–rising halo RC cannot be excluded by the data. Moreover, the central halo density *vs.* disk mass relationship, $\rho_0 \propto M_d^{-1/3}$, found for dwarf galaxies (Burkert, 1995), holds also for disk systems of stellar mass up to $10^{11} M_\odot$ (see Fig.4.3): the densest halos harbor the least massive disks.

The above relationship shows a curvature at the highest masses/lowest densities. It can be related to the existence of an upper limit in the dark halo virial mass M_{200} (defined as $M_{200} \equiv 200 \cdot 4/3\pi\rho_{bkg} R_{200}^3$), which is evident by the sudden decline of the baryonic *mass* function of disk galaxies at $M_D^{max} = 2 \times 10^{11} M_\odot$ (Salucci and Persic, 1999a) and implying a maximum halo mass of:

$$M_{200}^{max} \sim \frac{\Omega_m}{\Omega_b} \, M_D^{max} \sim 10 \, M_D^{max} \tag{4.9}$$

where $\Omega_m = 0.3$ and $\Omega_b \simeq 0.03$ (e.g. Burles and Tytler, 1998) are the matter and baryonic densities of the Universe in units of critical density. From the definition of M_{200}, by means of eq.(4.2), (4.3) and (4.4), we can write M_{200} in terms of the "observable" quantity M_0: $M_{200} \simeq 49 \, M_0^{0.95}$. Thus, from eq.(4.9), we obtain an upper limit to the core mass M_0, which implies a lack of objects with $\rho_0 \lesssim 1.2 \times 10^{-25}$ g/cm^3 and $r_0 \gtrsim 32$ kpc, as is evident in Fig.4.3. Turning the argument around, the deficit of such objects suggests that, at the mass scale $M_D \sim M_D^{max}$, the total–to–baryonic mass fraction may approach the cosmological value $\Omega_m/\Omega_b \sim 10$.

The Burkert density profile coincides, at very large radii, with the profile predicted by CDM theory ($\rho \propto r^{-3}$; e.g. Navarro, Frenk & White, 1997); however, it approaches a constant, finite density value at the center, in a way consistent with an isothermal distribution. This is in contradiction to cosmological models which predict that the velocity dispersion σ of the dark matter particles decreases towards the center to reach $\sigma \to 0$ for $r \to 0$. This work unequivocally shows that the dark halo inner regions cannot be considered as kinematically cold structures, but rather as "warm" regions of large size $r_0 \sim 4 - 7 \, r_D$, increasing with central density decreasing: $r_0 \propto \rho_0^{-3/2}$. Then,

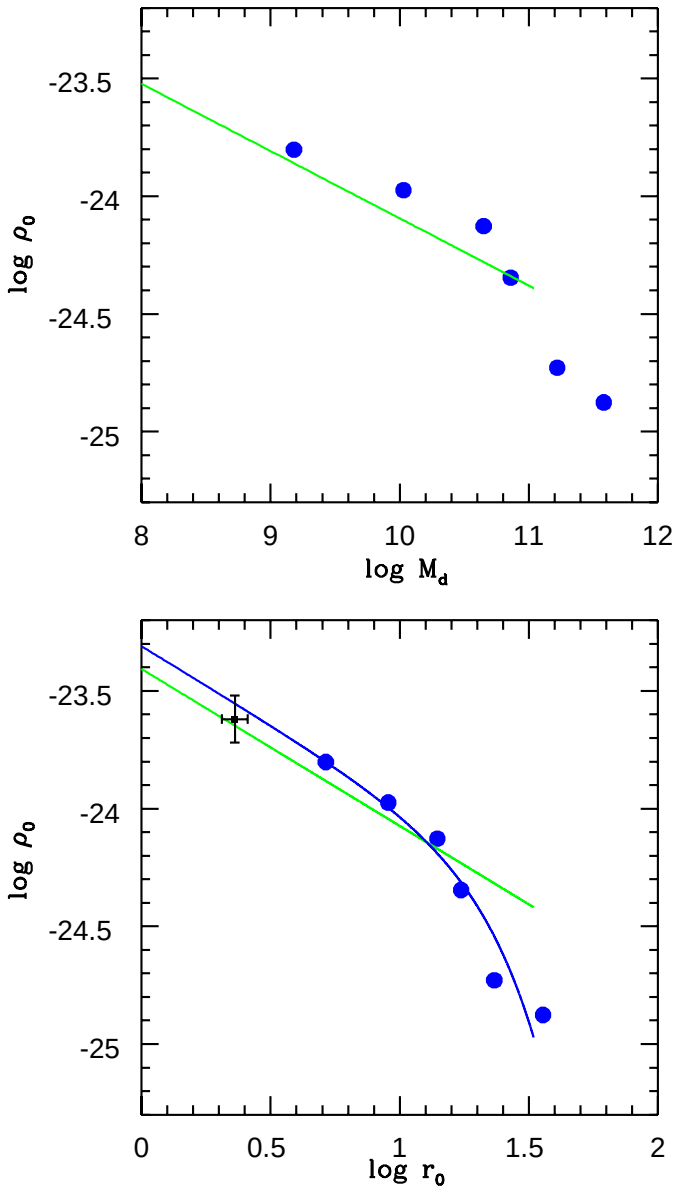

Figure 4.3: *Top:* Central halo density ρ_0 (in g/cm^3) *vs.* disk mass (in solar units), for normal spirals (*filled circles*). *Bottom:* central density *vs.* core radius (in kpc) for normal spirals (*filled circles*). The point with errorbar represents a typical dwarf galaxy from Burkert (1995) and the straight line (in both the plots) is the extrapolation to high luminosities of the dwarfs relation (Burkert, 1995). The curved line is the eye–ball fit: $\rho_0 = 5 \times 10^{-24} r_0^{-2/3} \exp -(r_0/27)^2$ g/cm^3.

the boundary of the core region is well beyond the region where the stars are located and, as in Corbelli & Salucci (2000), even at the outermost observed radius, there is not the slightest evidence that dark halos converge to a $\rho \sim r^{-1}$ (or steeper) regime.

4.3 Features of DM Halos at the Optical Edge

Our work, based on the mass modeling of DM–dominated rotation curves, is complementary to that of Salucci (2001), whose results are worth mentioning, as they completely support, by means of a different approach at the optical edge, the results of our previous works on *i)* a small sample of very high–quality spirals RC's (§2), *ii)* the remarkable case of a dwarf galaxy (§3) and *iii)* the spirals URC (this chapter, above sections), all of them obtained, however, over *the entire* stellar disk.

By means of a large sample of 140 RC's of different luminosity (131 spirals and 6 dwarfs) with a reliable profile out to R_{opt}, a crucial structural property of the corresponding dark halos has been derived: namely, the logarithmic gradient of the dark halo velocity at the disk edge:

$$\nabla_h(V_{opt}) \equiv \left.\frac{d\log V_h(r)}{d\log R}\right|_{R_{opt}} \tag{4.10}$$

where $V_h(r)$ is the contribution to the RC of the non–baryonic dark component. The ∇_h's have been obtained by means of a robust and straightforward procedure (Persic & Salucci, 1990b; Salucci, 2001), which ultimately exploits the fact that, at R_{opt}, the dark halo is always the main *density* component, even when it is a negligible *mass* component at about r_D. Moreover, even the bulge and gas contributions to the RC's have been taken into account. This method has been applied, with remarkably small errors, to RC's of galaxies of all luminosities, including the most luminous ones, for which the standard mass modeling is quite uncertain.

The most impressive result is shown in Fig.4.4, where the values of ∇_h are plotted

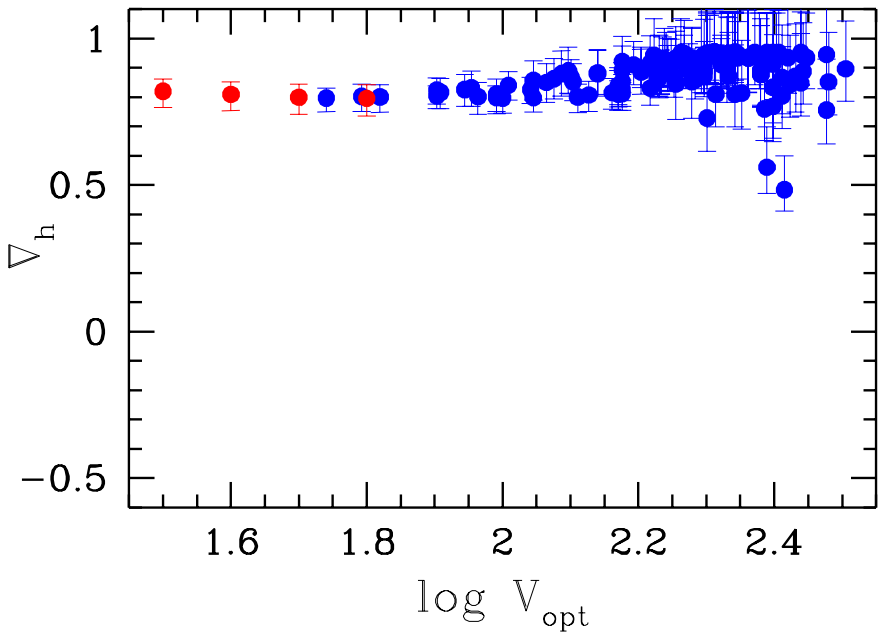

Figure 4.4: The dark halo slopes ∇_h at the optical radius as a function of V_{opt}, the measured circular velocity at R_{opt}. As a comparison, in CDM $-0.1 < \nabla_h \leq 0.5$.

as a function of $\log V_{opt}$: we immediately realize that ∇_h is roughly constant over the whole sample and it shows no systematic variations along the luminosity sequence. Such variations, if present, should have clearly appeared given the high–precision measurement of ∇_h: $\delta\nabla_h \simeq 0.1$ (for details, see Salucci, 2001)

Reminding that $\nabla_h = 0$ and $\nabla_h = 1$ mean, respectively, an isothermal and a solid–body regime, the average value for spirals, $< \nabla_h >= 0.8 \pm 0.06$, indicates that, at R_{opt}, the halo RC is steeply increasing, marginally compatible with a solid body law: $V_h \propto r$. By assuming a pseudo–isothermal density distribution: $\rho_h(r) \propto (r^2 + a^2)^{-1}$, it follows that $a > 1.3\ R_{opt}$, i.e. the core radius is significantly larger than r_D, the size of region where the bulk of the stellar component is located.

These clear and reliable findings on dark matter distribution, though relevant on their own, are also important as they are, once again, at strong variance with the structural properties of *standard* CDM halos. Indeed, the highest possible value for ∇_h^{CDM} is ~ 0.5, that, besides, is achieved on the ~ 10 kpc scale very rarely (see Bullock

et al., 2001). The average value found for dark halos from high–resolution N–body simulations converges to $\nabla_h^{CDM} \lesssim 1/4$ (e.g. Moore et al., 1998).

Of crucial importance is also the absence of a significant scatter in the ∇_h *vs.* $\log V_{opt}$ relationship. In fact, the CDM theory predicts that, in a very wide region centered at ~ 10 kpc and certainly including R_{opt}, galactic halos with the same mass do not follow a unique velocity curve but a family of them (according to different formation redshifts and merging histories). These can be described by a set of straight lines with slopes varying between -0.1 and $+0.5$ (e.g. Fig.6 in Bullock et al., 2001). According to CDM the $\nabla_h - \log V_{opt}$ plane should be filled below and well beyond the tiny strip of Fig.4.4. A possibility for this may be that the disk size R_{opt}, in units of virial radius, is *strongly* coupled with the structure of the dark matter halo (e.g. Dalcanton et al., 1997; Mo et al., 1998; van den Bosch et al., 2000; but see also Bullock et al., 2001).

Let us notice that CDM halos are tested, by this way, at R_{opt}, where the baryon infall has not significantly altered the original DM halo *velocity profile*: R_{opt} is external to the region into which most of the baryons have collapsed (Blumenthal et al., 1986). Violent dark halos–baryonic matter couplings, such as those proposed by Navarro et al. (1997) and Gelato and Sommer–Larsen (1999) might be able to modify the original halo distribution everywhere; however, given the very heuristic nature of these processes, it is best to first compare the standard–infall CDM halos to the galactic halo and, then, to consider the possibly emerging discrepancies in terms of new theoretical scenarios.

4.4 Conclusions

Two conclusive statements can be drawn: *a)* dark matter halos have an inner constant–density region, whose size exceeds the stellar disk length scale; *b)* there is no evidence that dark halos converge, at large radii, to a $\rho \sim r^{-2}$ (or steeper) profile. The existence of such density cores in DM halos is hardly explained within current theories of galaxy formation. Moreover, the evidence of a smooth halo profile is growing more

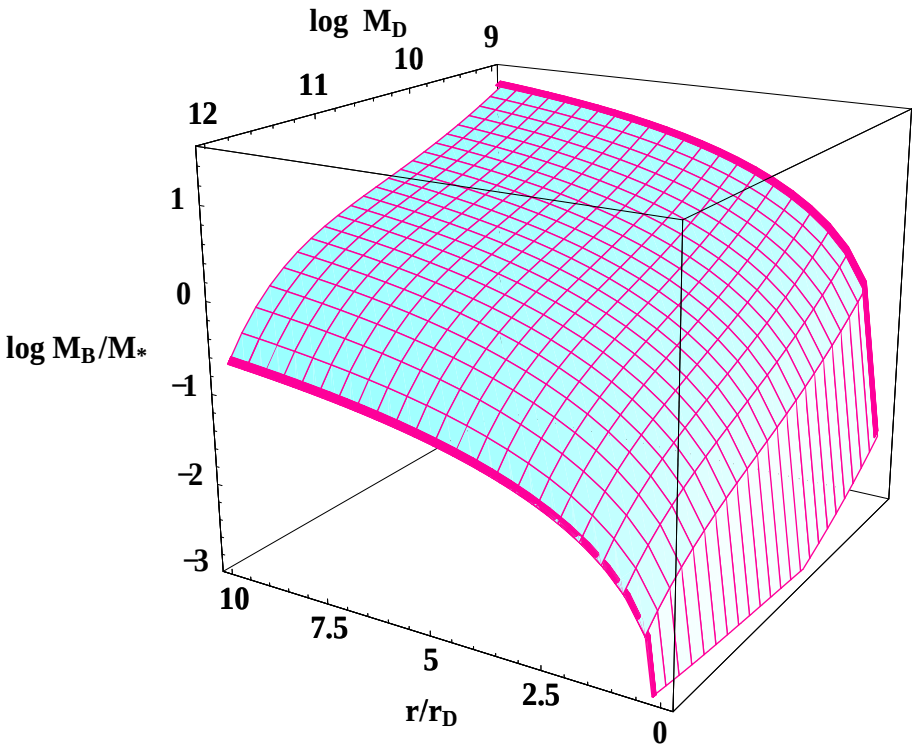

Figure 4.5: The dark–to–luminous mass ratio for spirals, as function of the normalized radius and the total disk mass.

an more in recent literature (e.g. de Blok et al., 2001; Trott & Webster, 2002; Matthews & Gallagher, 2002; Marchesini et al., 2002; Blais–Ouellette et al., 2002) and a number of different solutions have been proposed to solve this problem (e.g. White & Croft, 2000; Peebles, 2000; Firmani et al., 2000; El–Zant et al., 2001). Let us stress, however, that they should incorporate all the intriguing halo properties described above.

The dark halos around spirals emerge as an one–parameter family; it is relevant that the order parameter (either the central density or the core radius) correlates with the luminous mass. However, we do not know how it is related to the global structural properties of the dark halo, like the virial radius or the virial mass, unless we extrapolate out over the disk+Burkert halo profile. That is because the halo RC, out to the outermost data ($6r_D$), is completely determined by physical parameters,

the core density and radius, which are not defined in present gravitational instability/ hierarchical clustering scenario.

Caveat the above extrapolation, the location of spiral galaxies in the parameter space of virial mass/halo central density/stellar mass, that, on theorethical basis, should be roughly 3–D random determined by several different and non–linear physical processes, is remarkably found to degenerate and to lie on a curve. Indeed, in Fig.4.5 we show the dark–to–luminous mass ratio as function of the normalized radius and the total disk mass. The surface has been obtained by adopting the correlations between the halo and the disk parameters of Fig.4.3:

$$\log r_0 = 9.10 + 0.28\ \log \rho_0 - 3.49 \times 10^{10}\ \rho_0^{0.43} \tag{4.11}$$

$$\log \rho_0 = -23.0 - 0.077\ \log M_D - 9.98 \times 10^{-6}\ M_D^{0.43} \tag{4.12}$$

and:

$$\log r_D = 4.96 - 1.17\ \log M_D + 0.070\ (\log M_D)^2 \tag{4.13}$$

from data in PSS96. The dark–to–luminous mass ratio at fixed ratio increases as the total disk mass decreases; for example at $r = 10\ r_D$ it raises from 20% for massive disks ($M_D = 10^{12} M_\odot$) to 220% for smaller disks ($M_D = 10^9 M_\odot$).

We conclude by stressing that the above analysis is based on statistical methods; these have the drawback that, although *revealing* the discrepancy of DM observed properties with CDM predictions, cannot give a *quantitative measure* of the discrepancy itself.

Part III

ELLIPTICAL GALAXIES

Chapter 5

The Fundamental Plane of Ellipticals: the DM Connection

5.1 Introduction

From the hierarchical scenario of galaxies formation (White & Rees, 1978; Davis et al., 1985; Frenk et al., 1988), we expect that DM halos exist within and surrounding any galaxy, regardless of its luminosity and morphological type. This prediction had overwhelming confirms in disk galaxies, due to the existence of good dynamical tracers and their intrinsic simple geometry (see Salucci & Persic, 1997). Elliptical galaxies (E's), however, are much more complicated objects, due to their 3–dimensional shape, stellar orbital structure and velocity dispersion anisotropy. These factors have made ambiguous the interpretation of observational data.

A number of different mass tracers have been used to probe the gravitational potential in tenth of E's and derive their mass distribution: integrated stellar absorption spectra, X–ray emission from hot gas, rotating gas disks, motions of globular clusters or satellite galaxies and, in last years, weak gravitational lensing (see Danziger, 1997). As result, the presence of dark matter in E's, especially in the external regions ($\gtrsim 10$ kpc), is proven. On the other hand, modeling of the inner regions (i.e. within the half–luminosity "effective" radius r_e), based on E's kinematics, has been performed for a small number of galaxies (van der Marel, 1991; Saglia et al., 1992–1993; Bertin et al., 1994; Kronawitter et al., 2000; Gerhard et al., 2001, among the others); the results point to a small to moderate dark matter fraction inside the effective radius.

Since its discovery, the "Fundamental Plane" (Djorgovski & Davis, 1987; Dressler et al., 1987) has been one of the main tools to investigate E's properties: effective radius r_e, central velocity dispersion σ_0 and mean effective surface brightness I_e of spheroidal galaxies are linearly related in the logarithmic space, so that galaxies closely cluster on a plane, with a surprisingly low orthogonal scatter ($\sim 15\%$).

To explain this series of linear relations between photometric and dynamical quantities in log–space, most studies on the Fundamental Plane (FP) have considered models in which the mass is distributed parallel to light. However, in presence of non–baryonic dark matter, this hypothesis is an obvious oversimplification and, at least, unjustified.

Indeed, this would *a priori* require either: *i)* dark and luminous component are distributed according the same profile, thus revealing a similarity of properties and behavior which seems very unlikely or *ii)* the dark matter component is always negligible with respect to the luminous matter, even inside r_e.

Within the above framework, we will address the following issues:

- to derive the relation between the central velocity dispersion σ_0 and the mass distribution parameters, including the effect of a dark matter halo. In particular, we assume a spherical model, with a luminous component almost isotropic in the central region and a dark halo, more diffuse than the spheroid
- to reproduce the observed Fundamental Plane with a reliable mass model and therefore to constraint the mass distribution in E's, in the light of the very existence of the FP
- to put the results in the frame of theoretical mass–to–light ratios and in that of Λ Cold Dark Matter (CDM) predictions.

Considering elliptical galaxies as two–components systems, two complementary strategies are possible. The first chooses a distribution function (DF) for both the components and, then, imposes specific constraints from the observations. The second embeds the ordinary baryonic component, traced by light, in a frozen spherical halo. The former approach is helpful in exploring the self–consistency of the dynamical configuration (e.g. Ciotti, 1999). The latter, we will adopt in our work, has instead the advantage of better specify the connection between observational quantities and the mass model parameters.

In §5.2 we describe two–components models, whose mass distributions are presented in §5.3. In §5.4 we derive and discuss the velocity dispersion (line–of–sight profile and central value), predicted by the models. In §5.5, we introduce the data and fit the models to the Fundamental Plane. Finally, conclusions are presented in §5.6.

Throughout the following work, we assume, where needed, a flat ΛCDM Universe, with $\Omega_m = 0.3$, $\Omega_\Lambda = 0.7$, $h = 0.7$ and $\sigma_8 = 1.0$.

5.2 A General Two–Components Model

The calculus of the observed velocity dispersion and, in particular, of the central velocity dispersion σ_0 must take into account the gravitational potential of both the dark halo and the luminous component. Assuming a spherical and non–rotating stellar system, the strongest assumption which can be made is that the stellar velocity dispersion is the same in all directions perpendicular to a given radial vector. If $\sigma_r^2(r)$ denotes the stellar velocity dispersion along the radial vector and $\sigma_\theta^2(r)$ the dispersion in the perpendicular directions, the Jeans hydrodynamic equation for the luminous mass density $\rho_{sph}(r)$ in the radial direction writes (Binney & Tremaine, 1987):

$$\frac{d\rho_{sph}(r)\sigma_r^2(r)}{dr} + \frac{2\ \beta(r)\rho_{sph}(r)\sigma_r^2(r)}{r} = -\frac{GM(r)}{r^2}\rho_{sph}(r) \tag{5.1}$$

with the boundary condition $\rho_{sph}(r)\sigma_r^2(r) \to 0$ for $r \to \infty$. In eq.(5.1), the parameter $\beta(r) \equiv 1 - \sigma_\theta^2(r)/\sigma_r^2(r)$ describes the anisotropy degree of the velocity dispersion at each point, with $\beta = 1, 0, -\infty$ for completely radial, isotropic and circular orbit distributions, respectively.

Results from dynamical analysis of ellipticals exclude substantial amount of tangential anisotropy and find $\beta(\lesssim r_e) \simeq 0.1 - 0.2$ (e.g. Matthias & Gerhard, 1999; Gerhard et al., 2001; Koopmans & Treu, 2002), with no dependence on circular velocity (or luminosity). Therefore, in calculating the central velocity dispersion for statistical studies over a large sample of galaxies, we can safely assume an isotropic velocity dispersion tensor: $\beta = 0$.

Eq.(5.1) connects the spatial velocity dispersion of the luminous component to its density profile and to the *total* matter distribution $M(r) = M_{sph}(r) + M_h(r)$. Under

the hypothesis of isotropy, the above equation assumes the integral form:

$$\begin{aligned}
\sigma_r^2(r) &= \frac{G}{\rho_{sph}(r)} \int_r^\infty \frac{\rho_{sph}(r')M(r')}{r'^2}\, dr' \\
&= \frac{G}{\rho_{sph}(r)} \int_r^\infty \frac{\rho_{sph}(r')M_{sph}(r')}{r'^2}\, dr' + \frac{G}{\rho_{sph}(r)} \int_r^\infty \frac{\rho_{sph}(r')M_h(r')}{r'^2}\, dr' \\
&\equiv \sigma_{r;sph}^2(r) + \sigma_{r;h}^2(r) \qquad (5.2)
\end{aligned}$$

As external observers of galaxies we measure only projected quantities. Let R be the projected radius and $\Sigma(R)$ the surface stellar mass density. Simple geometry shows that the mass density and the spatial velocity dispersion are related to the surface mass density $\Sigma(R)$ and to the projected velocity dispersion $\sigma_P(R)$ by the two Abel integral equations for the quantity ρ_{sph} and $\rho_{sph}\sigma_r^2$; thus, the second step consists in performing a further integration along the line of sight to obtain the observed velocity dispersion profile $\sigma_P(r)$:

$$\begin{aligned}
\sigma_P^2(R) &= \frac{2}{\Sigma(R)} \int_R^\infty \frac{\rho_{sph}(r)\ \sigma_r^2(r)\ r}{\sqrt{r^2 - R^2}}\, dr \\
&= \frac{2}{\Sigma(R)} \int_R^\infty \frac{\rho_{sph}(r)\ \sigma_{r;sph}^2(r)\ r}{\sqrt{r^2 - R^2}}\, dr + \frac{2}{\Sigma(R)} \int_R^\infty \frac{\rho_{sph}(r)\ \sigma_{r;h}^2(r)\ r}{\sqrt{r^2 - R^2}}\, dr \\
&\equiv \sigma_{P;sph}^2(R) + \sigma_{P;h}^2(R) \qquad (5.3)
\end{aligned}$$

where $\Sigma(R) = \int_R^\infty [2\ r\ \rho_{sph}(r)/(r^2 - R^2)^{1/2}]\ dr$.

As spectro–photometric observations are performed through an aperture, let us define $\sigma_A(R_A)$ as the luminosity–weighted average of σ_P within a circular aperture of radius R_A:

$$\begin{aligned}
\sigma_A^2(R_A) &= \frac{2\pi}{L(R_A)} \int_0^{R_A} \sigma_P^2(R)\ I(R)\ R\ dR \\
&= \frac{2\pi}{L(R_A)} \left(\int_0^{R_A} \sigma_{P;sph}^2(R)\ I(R)\ R\ dR + \int_0^{R_A} \sigma_{P;h}^2(R)\ I(R)\ R\ dR \right)
\end{aligned}$$

$$\equiv \quad \sigma^2_{A;sph}(R_A) + \sigma^2_{A;h}(R_A) \tag{5.4}$$

where $I(R)$ is the surface brightness profile $I(R) = \Sigma(R)/\Upsilon$ (assuming the stellar mass–to–light ratio Υ constant with radius) and $L(R_A) = 2\ \pi\ \int_0^{R_A} I(R)\ R\ dR$ is the aperture luminosity.

The dynamical quantity in the Fundamental Plane is the "central" velocity dispersion σ_0, not corresponding to the central value of the projected profile $\sigma_P(0)$. It is, in fact, *the projected velocity dispersion, luminosity–weighted within the aperture of the observations*. Since it depends on the aperture size of the observations, on the galaxy distance and on the dark and stellar density distributions, it is required that the velocity dispersion data are brought to a common system, independent of the telescope and galaxy distance: this is done by correcting them to the same aperture of $r_e/8$ (Jørgensen et al., 1996), which is typical of measurements on nearby galaxies. Therefore, we compare model and observations by calculating σ_0 as the luminosity–weighted $\sigma_P(R)$ within $R_A = 1/8\ r_e$.

Eventually, the resulting velocity dispersion profiles, $\sigma_r(r)$, $\sigma_P(R)$ and $\sigma_A(R_A)$, can be all expressed as the sum of two terms (eq.5.2, 5.3 and 5.4): the former is due to the self–potential of the stellar spheroid (labelled by *sph*), the later (labelled by h) is the effect of the luminous–dark matter gravitational interaction and, therefore, it charges relevance according the characteristics of the DM distribution. As a consequence, we stress that: *i) a priori*, σ_0^2 is not a measure of GM_{sph}/r_e and *ii)* to automatically link σ_0^2 to GM_h/r_{vir} is unjustified.

Table 5.1: **Summary of the used symbols**

Symbol	Definition
r_e	Half–luminosity ("effective") radius of the stellar spheroid
r_0	DM halo density core radius (Burkert profile)
r_s	DM halo density scale radius (NFW profile)
r_{vir}	DM halo virial radius
σ_r	Spatial velocity dispersion in the radial direction
σ_P	Line–of–sight velocity dispersion
σ_A	L.o.s. velocity dispersion, luminosity weighted within an aperture
σ_0	"Central" velocity dispersion: $\sigma_A(r_e/8)$
Γ_{vir}	Dark–to–luminous mass ratio at virial radius
Γ_e	Dark–to–luminous mass ratio at r_e

5.3 The Mass Distribution

5.3.1 The stellar distribution

We describe the stellar component by means of the Hernquist (1990) spherical density distribution, which is a good approximation to the de Vaucouleur $R^{1/4}$ law (de Vaucouleur, 1948) when projected and, at the same time, allows analytical calculations:

$$\rho_{sph}(r) = \frac{M_{sph}}{2\pi} \frac{k\ r_e}{r\ (r + k\ r_e)^3} \tag{5.5}$$

where M_{sph} is the total stellar mass and $k \simeq 0.55$. The mass profile derived from eq.(5.5) is:

$$M_{sph}(r) = M_{sph} \frac{(r/r_e)^2}{(r/r_e + k)^2} \tag{5.6}$$

The Hernquist functional form, of course, cannot reproduce the fine features of the surface brightness profile (e.g. boxy isophotes, small variations in slope), but it is good enough for our aims, since we will just consider large scale properties in the mass distribution of objects belonging to a large E's sample.

5.3.2 The DM distribution: ΛCDM halos

N–body simulations of hierarchical collapse and merging of CDM halos have shown that gravity, starting from scale–free initial conditions, produces an universal density profile that, for $r \to 0$, varies with radius as $r^{-\alpha}$, with $\alpha \sim 1-2$ (e.g. Navarro, Frenk & White, 1997, hereafter NFW; Fukushige & Makino, 1997; Moore et al., 1998; Ghigna et al., 2000), weakly dependent on the cosmological model.

We adopt the well–known NFW halo density profile:

$$\rho_{NFW}(r) = \frac{\rho_s}{(r/r_s)(1+r/r_s)^2} \tag{5.7}$$

where r_s is the inner characteristic length scale, corresponding to the radius where the effective logarithmic slope of the profile is -2, and $\rho_s = 4\ \rho_{NFW}(r_s)$. It results convenient to write the NFW mass profile as:

$$M_{NFW}(r) = M_{vir}\ \frac{A(r, r_s)}{A(c_{vir}, r_s/r_e)} \tag{5.8}$$

where $A(x_1, x_2) \equiv \ln(1+x_1/x_2) - (1+x_2/x_1)^{-1}$, for any pair of variables (x_1, x_2). The concentration parameter is defined as $c_{vir} \equiv r_{vir}/r_s$; r_{vir} and M_{vir} are, respectively, the halo virial radius and mass. The definition of the virial radius is strictly within the framework of the standard dissipationless spherical collapse model (SCM); however, also in more realistic hierarchical models, it provides a measure of the boundary of virialized region of halos (Cole & Lacey, 1996).

Considering a dark halo at redshift z, the virialized region is the sphere within which the mean density is $\Delta_{vir}(z)$ times the background universal density at that redshift ($\rho_{bkg} = \rho_c\ (1+z)^3$, with ρ_c the critical density for closure at $z = 0$). The virial mass is defined as: $M_{vir} \equiv \frac{4}{3}\ \pi\ \Delta_{vir}(z)\ \rho_{bkg}\ r_{vir}^3$, with the virial overdensity Δ_{vir} being a function both of the cosmological model and the redshift. For the family of flat cosmologies ($\Omega_{\rm m} + \Omega_\Lambda = 1$), it can be approximated by (Bryan & Norman, 1998): $\Delta_{vir}(z) \simeq 18\pi^2 + 82(\Omega(z) - 1) - 39(\Omega(z) - 1)^2/\Omega(z)$. From the above equations, we derive:

$$r_{vir} = 0.142\ \Delta_{vir}(z)^{-1/3}(1+z)^{-1} \left(\frac{M_{vir}}{M_\odot}\right)^{1/3}\ h^{-2/3}\ \mathrm{kpc} \tag{5.9}$$

A fundamental result of CDM theory is that the halo concentration c_{vir} well correlates with the virial mass M_{vir}: low–mass halos are denser and more concentrated than high–mass halos (Bullock et al., 2001; Cheng & Wu, 2001; Wechsler et al., 2002), in that, in average, they collapsed when the Universe was denser. In detail, we follow Wechsler et al. (2002) for a population of halos identified at $z = 0$, extrapolating their $c_{vir} - M_{vir}$ correlation to low mass halos $M_{vir} \lesssim 10^{11-12} M_\odot$:

$$c_{vir}(M_{vir}) \simeq 20.8\ \left(\frac{M_{vir}}{10^{11}\ M_\odot}\right)^{-0.13} \tag{5.10}$$

Summarizing, our first mass model is composed by a stellar bulge with a Hernquist profile embedded in a spherical dark NFW halo (hereafter H+NFW model). It is worth noticing that we neglect the effects of a possible adiabatic coupling between baryons and dark matter. However, this coupling would have the effect (if any) of slightly increasing the DM density inside r_e and to strengthen the results we find for the H+NFW model (see §5.5.3).

The "total" dark–to–luminous mass ratio, defined as $\Gamma_{vir} \equiv M_{vir}/M_{sph}$ is a crucial parameter of this mass model. Of course, the value of Γ_{vir} is different from the BBN

DM–to–baryons ratio $\simeq 10$. Indeed, due to stellar feedback, central QSO activity and long cooling times for the outer gas (e.g. Granato et al., 2001), only a fraction of baryons can cool and collapse into stars. It has been computed that Γ_{vir} can reach values as high as ~ 70, especially in small objects (e.g. Romano et al., 2002).

5.3.3 The DM distribution: cored halos

In last years, studies of high resolution rotation curves of spiral galaxies have shown that the dark halos around them are not centrally cuspy and that very different density shapes characterize their luminous and dark components. The dark halo is more diffuse than the luminous component and its density flattens at small radii, whereas the stellar distribution peaks towards the centre (e.g. Moore, 1994; Flores & Primack, 1994; Burkert, 1995; de Battista & Sellwood, 1998; Salucci & Burkert, 2000; Borriello & Salucci, 2001; de Block et al., 2001a).

An useful analytic form for halos with soft cores has been proposed by Burkert (1995) for dwarf galaxies and then extended to the whole family of spirals (Salucci & Burkert, 2000; Borriello & Salucci, 2001):

$$\rho_B(r) = \frac{\rho_0}{(1 + r/r_0)[1 + (r/r_0)^2]} \tag{5.11}$$

The profile is characterized by a density–core of extension r_0 and value ρ_0, while it resembles the NFW profile at large radii. From eq.(5.11) the mass profile writes:

$$M_B(r) = M_e \, \frac{B(r, r_0)}{B(1, r_0/r_e)} \tag{5.12}$$

where $B(x_1, x_2) \equiv -2\arctan(x_1/x_2) + 2\ln(1 + x_1/x_2) + \ln[1 + (x_1/x_2)^2]$, for any pair of variables (x_1, x_2), and M_e is the dark mass within r_e.

In analogy of spiral galaxies, we propose a different mass model consisting of a Hernquist bulge plus a Burkert dark halo (hereafter H+B model). We characterize the

halo mass distribution by two free parameters: the dark–to–luminous mass ratio within the effective radius $\Gamma_e \equiv M_B/M_{sph}\,|_{r_e}$ and the halo core radius in units of the effective radius r_0/r_e. It is obvious that $r_0 \gtrsim r_e$, to ensure a constant DM density where the stars reside; as a matter of fact, models with $r_0 < r_e$ would essentially coincide with the NFW ones. It is worth noticing that the Burkert profile is purely empirical and featureless in the optical regions of galaxies; as a consequence, unless data at large radii are available, we can not determine the halo virial radius and mass, neither predict links between the local and the global properties of the dark halos.

5.4 Models Velocity Dispersions

The existence of a DM halo, of course, alters the shape of the predicted velocity dispersion profile, making it flatter, or in some case increasing, and making higher the absolute value of the velocity dispersion. We compute the models velocity dispersion profiles, including the effect of a spherical dark halo, for both H+NFW and H+B cases. We resolve the Jeans eq.(5.2), eq.(5.3) and eq.(5.4) by assuming the density/mass profiles of eq.(5.5), eq.(5.6) and eq.(5.8) in H+NFW case, and of eq.(5.5), eq.(5.6) and eq.(5.12) in the H+B case. In the following section we give an overview of the detailed calculus.

5.4.1 Velocity dispersion in detail

We will detail the procedure to compute velocity dispersions by means of Jeans hydrodynamic equations. Let us set all radii in units of the effective radius: $\tilde{r} \equiv r/r_e$, $\tilde{R} \equiv R/r_e$, $\tilde{r}_0 \equiv r_0/r_e$, $\tilde{r}_s \equiv r_s/r_e$ and $\tilde{r}_{vir} \equiv r_{vir}/r_e$.

Mass distributions

a) Stellar component – the radial profiles of mass density, mass and surface mass density write (Hernquist, 1990):

$$\rho_{sph}(\tilde{r}) = \frac{k}{2\pi} \frac{M_{sph}}{r_e^3} F_1(\tilde{r}) \tag{5.13}$$

$$M_{sph}(\tilde{r}) = M_{sph} F_2(\tilde{r}) \tag{5.14}$$

$$\Sigma(\tilde{R}) = \frac{1}{2\pi k^2} \frac{M_{sph}}{r_e^2} F_3(\tilde{R}) \tag{5.15}$$

where $k \simeq 0.55$ and:

$$F_1(\tilde{r}) = \frac{1}{\tilde{r} (\tilde{r}+k)^3} \tag{5.16}$$

$$F_2(\tilde{r}) = \frac{\tilde{r}^2}{(\tilde{r}+k)^2} \tag{5.17}$$

$$F_3(\tilde{R}) = \frac{\left[\left(2+\frac{\tilde{R}^2}{k^2}\right) X(\tilde{R}) - 3\right]}{(1-\frac{\tilde{R}^2}{k^2})^2} \tag{5.18}$$

with $X(\tilde{R}) = [1-(\tilde{R}/k)^2]^{-1/2}\mathrm{Sech}^{-1}(\tilde{R}/k)$ for $0 \leq \tilde{R} < k$ and $X(\tilde{R}) = [(\tilde{R}/k)^2 + - 1]^{-1/2}\ \mathrm{Sec}^{-1}(\tilde{R}/k)$ for $\tilde{R} \geq k$.

b) Dark matter halo – the NFW mass profile writes:

$$M_{NFW}(\tilde{r}) = M_{sph}\ \Gamma_{vir}\ \frac{A(\tilde{r},\tilde{r}_s)}{A(\tilde{r}_{vir},\tilde{r}_s)} \tag{5.19}$$

where, for any pair of variables (x_1, x_2), $A(x_1,x_2) \equiv \ln(1+x_1/x_2) - x + 1/(x_1+x_2)$. In particular, recalling that $c_{vir} \equiv r_{vir}/r_s$, we have $A(\tilde{r}_{vir},\tilde{r}_s) = \ln(1+c_{vir}) - c_{vir}/(1+c_{vir})$. The Burkert halo mass profile writes:

$$M_B(\tilde{r}) = 0.416\ M_{sph}\ \Gamma_e\ \frac{B(\tilde{r},\tilde{r}_0)}{B(1,\tilde{r}_0)} \tag{5.20}$$

where $B(x,y) \equiv -\arctan(x/y) + 2\ln(1+x/y) + \ln[1+(x/y)^2]$.
By inserting eq.(5.13), (5.14), (5.15), (5.19) and (5.20) in eq.(5.2), (5.3) and (5.4) (after variables substitutions), we will obtain the velocity dispersions profiles:

Spheroid self–interaction terms

Out of the stellar spheroid self–interaction terms, $\sigma^2_{r;sph}$, $\sigma^2_{P;sph}$ and $\sigma^2_{A;sph}$, the first two can be analitically obtained (Hernquist, 1990):

$$\sigma^2_{r;sph}(\tilde{r}) = \frac{1}{12\ k}\ \frac{GM_{sph}}{r_e}\ \left[\frac{12}{k^4}\ \tilde{r}\ (\tilde{r}+k)\ \ln\left(\frac{\tilde{r}+k}{\tilde{r}}\right) - \frac{\tilde{r}}{\tilde{r}+k}\cdot \right.$$
$$\left. \cdot\left(25 + \frac{52}{k}\ \tilde{r} + \frac{42}{k^2}\ \tilde{r}^2 + \frac{12}{k^3}\ \tilde{r}^3\right)\right] \tag{5.21}$$

$$\sigma^2_{P;sph}(\tilde{R}) = \frac{1}{6\ k}\ \frac{GM_{sph}}{r_e^3}\ \frac{F_4(\tilde{R})}{F_3(\tilde{R})} \tag{5.22}$$

where:

$$F_4(\tilde{R}) = \frac{1}{2}\ \left(1-\frac{\tilde{R}^2}{k^2}\right)^{-3}\ \left[-3\ \frac{\tilde{R}^2}{k^2}\ X(\tilde{R})\ \left(8\ \frac{\tilde{R}^6}{k^6} - 28\ \frac{\tilde{R}^4}{k^4} + 35\ \frac{\tilde{R}^2}{k^2} - 20\right) + \right.$$
$$\left. -24\ \frac{\tilde{R}^6}{k^6} + 68\ \frac{\tilde{R}^4}{k^4} - 65\ \frac{\tilde{R}^2}{k^2} + 6\right] - 6\ \pi\ \frac{\tilde{R}}{k} \tag{5.23}$$

We obtain the luminosity weighted velocity dispersion in the aperture $\tilde{R}_A \equiv R_A/r_e$, by integrating eq.(5.22):

$$\sigma^2_{A;sph}(\tilde{R}_A) = \frac{1}{6\ k}\ \frac{GM_{sph}}{r_e^3}\ \frac{\int_0^{\tilde{R}_A} F_4(\tilde{R})\ \tilde{R}\ d\tilde{R}}{\int_0^{\tilde{R}_A} F_3(\tilde{R})\tilde{R}\ d\tilde{R}} \tag{5.24}$$

where integrals must be numerically performed.

Spheroid–halo interaction terms

We apply the same procedure for calculating the luminous–dark matter interaction terms: $\sigma^2_{r;h}$, $\sigma^2_{P;h}$ and $\sigma^2_{A;h}$. In this case, however, the integrations are always numerical.

a) H+NFW model

$$\sigma^2_{r;NFW}(\tilde{r}) = \frac{GM_{sph}}{r_e}\ \frac{\Gamma_{vir}}{A(\tilde{r}_{vir},\tilde{r}_s)}\ \frac{\int_{\tilde{r}}^{\infty} \frac{F_1(\tilde{r}')\ A(\tilde{r}',\tilde{r}_s)}{\tilde{r}'^2}\ d\tilde{r}'}{F_1(\tilde{r})} \tag{5.25}$$

$$\sigma^2_{P;NFW}(\tilde{R}) = 2\ k^3\ \frac{GM_{sph}}{r_e}\ \frac{\Gamma_{vir}}{A(\tilde{r}_{vir},\tilde{r}_s)}\ \frac{\int_{\tilde{R}}^{\infty} \tilde{r}\ \frac{\int_{\tilde{r}}^{\infty} \frac{F_1(\tilde{r}')\ A(\tilde{r}',\tilde{r}_s)}{\tilde{r}'^2}\ d\tilde{r}'}{\sqrt{\tilde{r}^2-\tilde{R}^2}}\ d\tilde{r}}{F_3(\tilde{R})} \tag{5.26}$$

$$\sigma^2_{A;NFW}(\tilde{R}_A) = 2\ k^3\ \frac{GM_{sph}}{r_e}\ \frac{\Gamma_{vir}}{A(\tilde{r}_{vir},\tilde{r}_s)}\ \frac{\int_0^{\tilde{R}_A} \tilde{R}\ \frac{\int_{\tilde{R}}^{\infty} \tilde{r}\ \frac{\int_{\tilde{r}}^{\infty} \frac{F_1(\tilde{r}')\ A(\tilde{r}',\tilde{r}_s)}{\tilde{r}'^2}\ d\tilde{r}'}{\sqrt{\tilde{r}^2-\tilde{R}^2}}\ d\tilde{r}}{F_3(\tilde{R})}\ d\tilde{R}}{\int_0^{\tilde{R}_A} F_3(\tilde{R})\ \tilde{R}\ d\tilde{R}} \tag{5.27}$$

where we can reduce the free parameters to the only virial mass *i)* by using eq.(5.9) for the virial radius, with $\Delta_{vir}(z=0) \simeq 337$:

$$r_{vir} \simeq 2.59 \times 10^{-2} \left(\frac{M_{vir}}{M_\odot}\right)^{1/3}\ \text{kpc} \tag{5.28}$$

and *ii)* by assuming the ΛCDM correlation between c_{vir} and M_{vir} of eq.(5.10) (from Wechsler et al., 2002), which, together with eq.(5.28), gives:

$$r_s \equiv \frac{r_{vir}(M_{vir})}{c_{vir}(M_{vir})} \simeq 6.17 \left(\frac{M_{vir}}{10^{11}\ M_\odot}\right)^{0.48}\ \text{kpc} \tag{5.29}$$

b) H+B model

$$\sigma^2_{r;B}(\tilde{r}) = 0.416\ \frac{GM_{sph}}{r_e}\ \frac{\Gamma_e}{B(1,\tilde{r}_0)}\ \frac{\int_{\tilde{r}}^{\infty} \frac{F_1(\tilde{r}')\ B(\tilde{r}',\tilde{r}_0)}{\tilde{r}'^2}\ d\tilde{r}'}{F_1(\tilde{r})} \tag{5.30}$$

$$\sigma^2_{P;B}(\tilde{R}) = 0.831\ k^3\ \frac{GM_{sph}}{r_e}\ \frac{\Gamma_e}{B(1,\tilde{r}_0)}\ \frac{\int_{\tilde{R}}^{\infty} \tilde{r}\ \frac{\int_{\tilde{r}}^{\infty} \frac{F_1(\tilde{r}')\ B(\tilde{r}',\tilde{r}_0)}{\tilde{r}'^2}\ d\tilde{r}'}{\sqrt{\tilde{r}^2-\tilde{R}^2}}\ d\tilde{r}}{F_3(\tilde{R})} \tag{5.31}$$

$$\sigma^2_{A;B}(\tilde{R}_A) = 0.831\ k^3\ \frac{GM_{sph}}{r_e}\ \frac{\Gamma_e}{B(1,\tilde{r}_0)}\ \frac{\int_0^{\tilde{R}_A} \tilde{R}\ \frac{\int_{\tilde{R}}^{\infty} \tilde{r}\ \frac{\int_{\tilde{r}}^{\infty} \frac{F_1(\tilde{r}')\ B(\tilde{r}',\tilde{r}_0)}{\tilde{r}'^2}\ d\tilde{r}'}{\sqrt{\tilde{r}^2-\tilde{R}^2}}\ d\tilde{r}}{F_3(\tilde{R})}\ d\tilde{R}}{\int_0^{\tilde{R}_A} F_3(\tilde{R})\ \tilde{R}\ d\tilde{R}} \tag{5.32}$$

5.4.2 Velocity dispersion profiles

In Fig.5.1 (*top*) we show, for H+NFW models, the radial profile of the fraction $\sigma^2_{P;sph}/\sigma^2_P$, the line–of–sight velocity dispersion due to the only stellar component, in units of the total l.o.s. velocity dispersion. We take $M_{sph} = 2 \times 10^{11} M_\odot$; anyway, the mass dependence is very weak and the curves in Fig.5.1 are well representative of those with stellar masses in the range $\sim 5 \times 10^9 - 5 \times 10^{11} M_\odot$. We consider different plausible values for the total dark–to–luminous mass ratio Γ_{vir} and r_e. Let us notice that, once fixed the total halo mass $M_{vir} \equiv \Gamma_{vir} \cdot M_{sph}$, the halo characteristic radius r_s is completely determined via the $c_{vir} - M_{vir}$ correlation; therefore, different curves in Fig.5.1 (*top*) correspond to $2 \lesssim r_s/r_e \lesssim 30$. We can see that the contribution of a CDM halo to the velocity dispersion can be strong ($\sim 50\%$) even at small radii $R \lesssim r_e/2$, in galaxies with large effective radii and/or small values of r_s/r_e, regardless of Γ_{vir}.

In Fig.5.1 (*bottom*) we plot the stellar–to–total l.o.s. velocity dispersion ratio for H+B models, for different values of the parameters r_0/r_e and Γ_e. As the profiles just depend on these parameters, it is not necessary to assume specific values both for M_{sph}

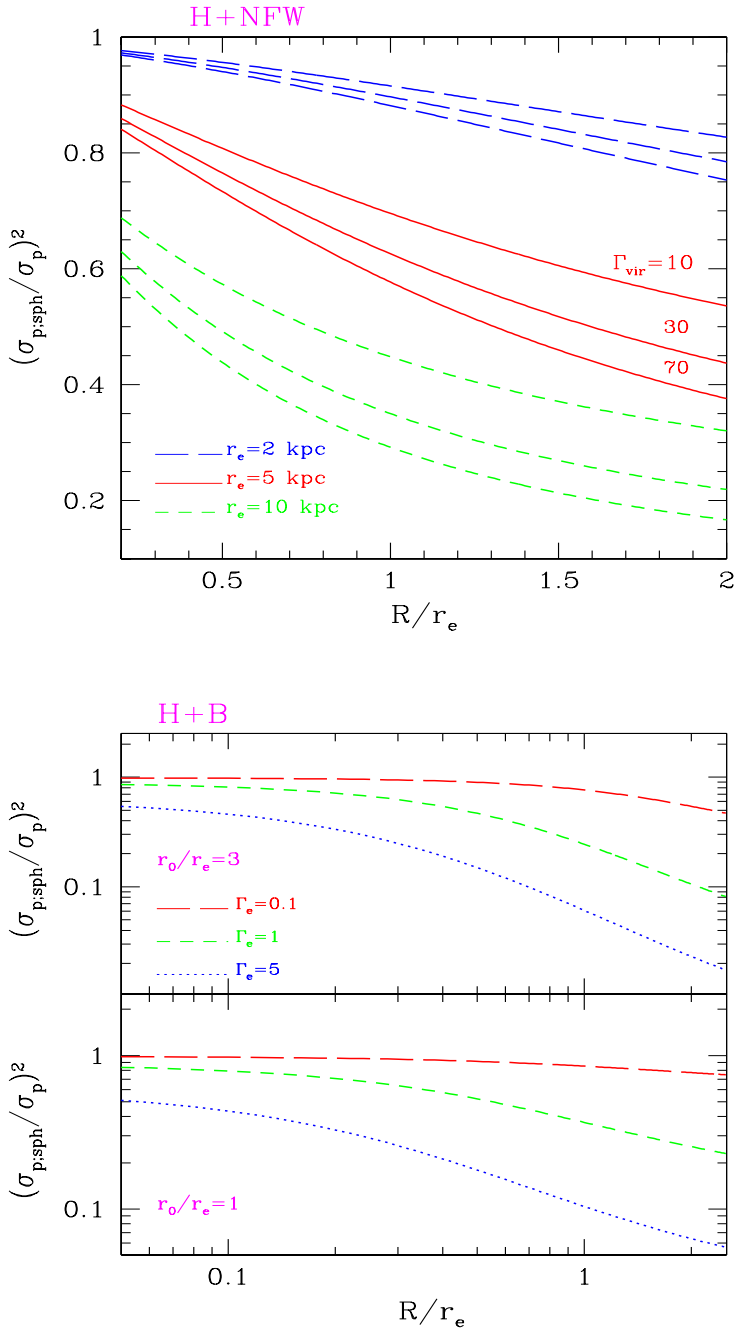

Figure 5.1: Ratio of line–of–sight velocity dispersion due to the spheroid ($\sigma_{P;sph}$) to the total one (σ_P) as function of radius: *top)* H+NFW case, for different values of r_e and Γ_{vir}; *bottom)* H+B case, for different values of r_0/r_e and Γ_e.

and r_e. The main consequence of the smooth halo profile in the H+B model is that the halo contribution to $\sigma_P(R)$ is still low at small R, even for models with a relevant amount of DM in the central region (e.g. $\sigma^2_{P;sph}/\sigma^2_P \sim 80\%$ at $r_e/3$ when $\Gamma_e = 1$). The velocity dispersion in the central regions is more directly connected to the properties of the stellar distribution.

5.4.3 Central velocity dispersion

The "central velocity" dispersion σ_0 is considered a good indicator of the total bulge mass when we neglect the dark halo contribution. Anyway, a linear correlation of σ_0^2 with the quantity GM_{sph}/r_e is in principle altered by the existence of a dark halo. From eq.(5.24), by setting the aperture $\tilde{R}_A = 1/8$, we obtain the stellar self–interaction contribution to the "central" velocity dispersion:

$$\begin{aligned} \sigma^2_{0;sph} &= \frac{1}{6\ k}\ \frac{GM_{sph}}{r_e^3}\ \frac{\int_0^{1/8} F_4(\tilde{R})\ \tilde{R}\ d\tilde{R}}{\int_0^{1/8} F_3(\tilde{R})\ \tilde{R}\ d\tilde{R}} \\ &\simeq 0.174\ \frac{GM_{sph}}{r_e} \end{aligned} \tag{5.33}$$

Likewise, from eq.(5.27) and (5.32), for $\tilde{R}_A = 1/8$, we obtain the halo contribution to the central velocity dispersion. Finally, the "total" central velocity dispersion, predicted by both the mass models, writes:

$$\sigma_0^2 = (0.174 + \Gamma_{vir}\ F_{NFW})\ \frac{G\ M_{sph}}{r_e} \qquad \text{H} + \text{NFW} \tag{5.34}$$

$$\sigma_0^2 = (0.174 + \Gamma_e\ F_B)\ \frac{G\ M_{sph}}{r_e} \qquad \text{H} + \text{B} \tag{5.35}$$

where F_{NFW} and F_B are defined as:

$$F_{NFW} \simeq 2\ \frac{k^3}{\int_0^{1/8} F_3(\tilde{R})\ \tilde{R}\ d\tilde{R}}\ \frac{1}{A(\tilde{r}_{vir}(M_{vir}), \tilde{r}_s(M_{vir}))}\ .$$

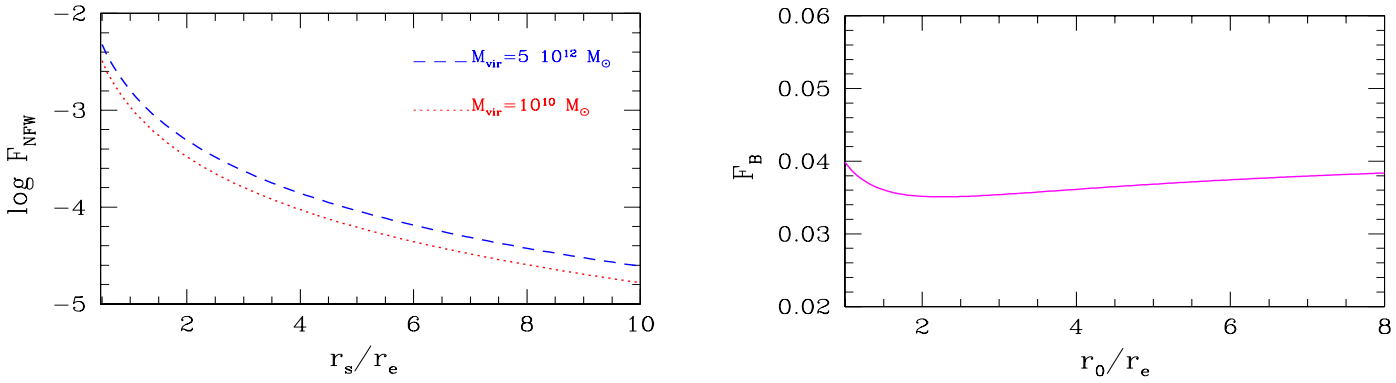

Figure 5.2: The functions F_{NFW} and F_B, entering the expression of the central velocity dispersion σ_0, for H+NFW (*left*) and H+B (*right*) models.

$$\cdot \int_0^{1/8} \tilde{R}\, \frac{\int_{\tilde{R}}^{\infty} \tilde{r}\, \frac{\int_{\tilde{r}}^{\infty} \frac{F_1(\tilde{r}')\ A(\tilde{r}', \tilde{r}_s(M_{vir}))}{\tilde{r}'^2}\, d\tilde{r}'}{\sqrt{\tilde{r}^2 - \tilde{R}^2}}\, d\tilde{r}}{F_3(\tilde{R})}\, d\tilde{R} \tag{5.36}$$

$$F_B \simeq 0.83\, \frac{k^3}{\int_0^{1/8} F_3(\tilde{R})\ \tilde{R}\, d\tilde{R}}\, \frac{1}{B(1, \tilde{r}_0)} \int_0^{1/8} \tilde{R}\, \frac{\int_{\tilde{R}}^{\infty} \tilde{r}\, \frac{\int_{\tilde{r}}^{\infty} \frac{F_1(\tilde{r}')\ B(\tilde{r}', \tilde{r}_0)}{\tilde{r}'^2}\, d\tilde{r}'}{\sqrt{\tilde{r}^2 - \tilde{R}^2}}\, d\tilde{r}}{F_3(\tilde{R})} d\tilde{R} \tag{5.37}$$

with the constant of proportionality: $k^3 / \int_0^{1/8} F_3(\tilde{R})\ \tilde{R}\, d\tilde{R} \simeq 8.31$.

We show the functions F_{NFW} and F_B in Fig.5.2. The former depends on $r_s(M_{vir})/r_e$ and, very weakly, on $M_{vir} \equiv \Gamma_{vir} \cdot M_{sph}$. As a consequence, a linear correlation between σ_0^2 and GM_{sph}/r_e is lost and, according to the values of the model parameters, σ_0 can be strongly affected by the DM gravitational potential, then it is a poor indicator of the bulge mass. This is shown in (Fig.5.3, *top*), where we plot the stellar–to–total σ_0^2, assuming $M_{sph} = 2 \times 10^{11} M_\odot$ and different model parameters: the stellar contribution to σ_0^2 is under dominant also at small r_s/r_e and becomes almost negligible for $r_s/r_e \lesssim 1$ and $\Gamma_{vir} \gtrsim 30$.

On the other hand, F_B just weakly depends on r_0/r_e, so that we can safely assume $F_B \simeq 3.6 \times 10^{-2}$. Therefore, the stellar contribution to σ_0^2 (Fig.5.3, *bottom*) stays

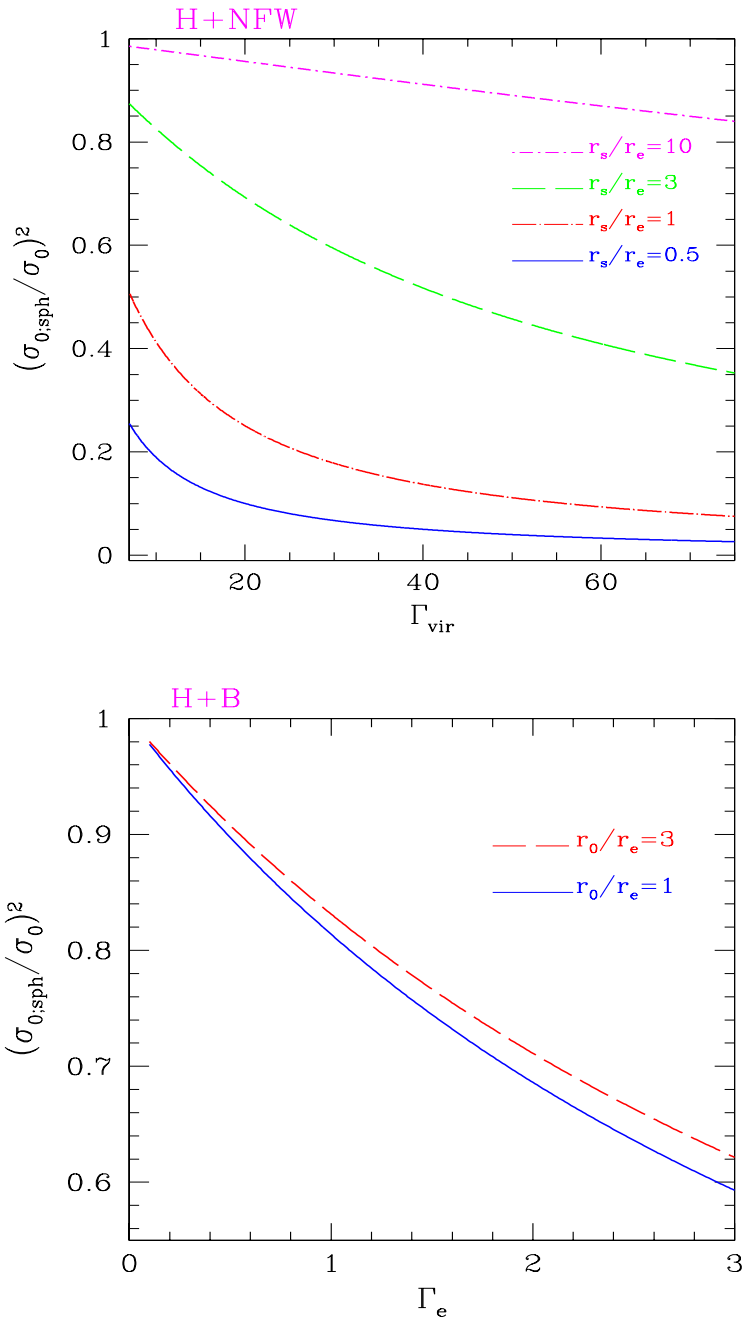

Figure 5.3: The stellar contribution to σ_0 for different models parameters: *top*) H+NFW predictions for $M_{sph} = 2 \times 10^{11} M_\odot$, as function of Γ_{vir} and for different r_s/r_e.; *bottom*) H+B predictions, as function of the parameters Γ_e and r_0/r_e.

dominant, even for an amount of DM within r_e comparable to the luminous one. Finally, for cored configurations ($r_0 > r_e$) σ_0 is weakly dependent on the DM internal amount: it just increases of $\sim 30\%$ when Γ_e varies of a factor 3. This is a natural consequence of the smoothness of the dark matter distribution with respect to the more concentrated distribution of the luminous spheroid.

5.5 Fitting models to the Fundamental Plane

5.5.1 The sample

We build the data sample from several works by Jørgensen, Franx & Kjaergaard (hereafter JFK). They provide spectroscopy and multicolour CCD surface photometry of E/S0 galaxies in nearby clusters. The photometric data are from JFK (1992) and (1995a) in Gunn–r, the passband with the largest quantity of data. The spectroscopic measurements are taken from JFK (1995b) and references therein. Typical measurement errors are: $\Delta \log r_e = \pm 0.045$, $\Delta \log I_e = \pm 0.064$, $\Delta \log L_r = \pm 0.036$ and $\Delta \log \sigma_0 = \pm 0.036$ Out of the whole JFK sample, we selected a homogeneous subsample of 221 E/S0 galaxies in 9 clusters, including Coma, whose properties are shown in Tab.5.2, at the end of this chapter. In particular, we rejected spiral, interacting, peculiar and field galaxies (the last ones, due to the greater uncertainty of their distance). For each cluster, we adopt the distance derived in JFK (1996), through an analysis of the different clusters FP's. The FP scatter of 0.084 in $\log r_e$ is equivalent to a $\sim 17\%$ uncertainty in distances to single galaxies.

To better characterize the selected galaxies, we show in Fig.5.4 their statistical distributions: effective radius, ellipticity at r_e, observed central velocity dispersion and Gunn-r luminosity. Notice that sample galaxies are distributed around $L_* = 2.7 \times 10^{10} L_{\odot;r}$, the characteristic luminosity of the ellipticals luminosity function in r–band (Blanton et al., 2001) and that most of the objects have little/moderate ellipticity ($< \epsilon >= 0.29 \pm 0.17$) and then, a reasonably spherical stellar distribution (see §5.5.3).

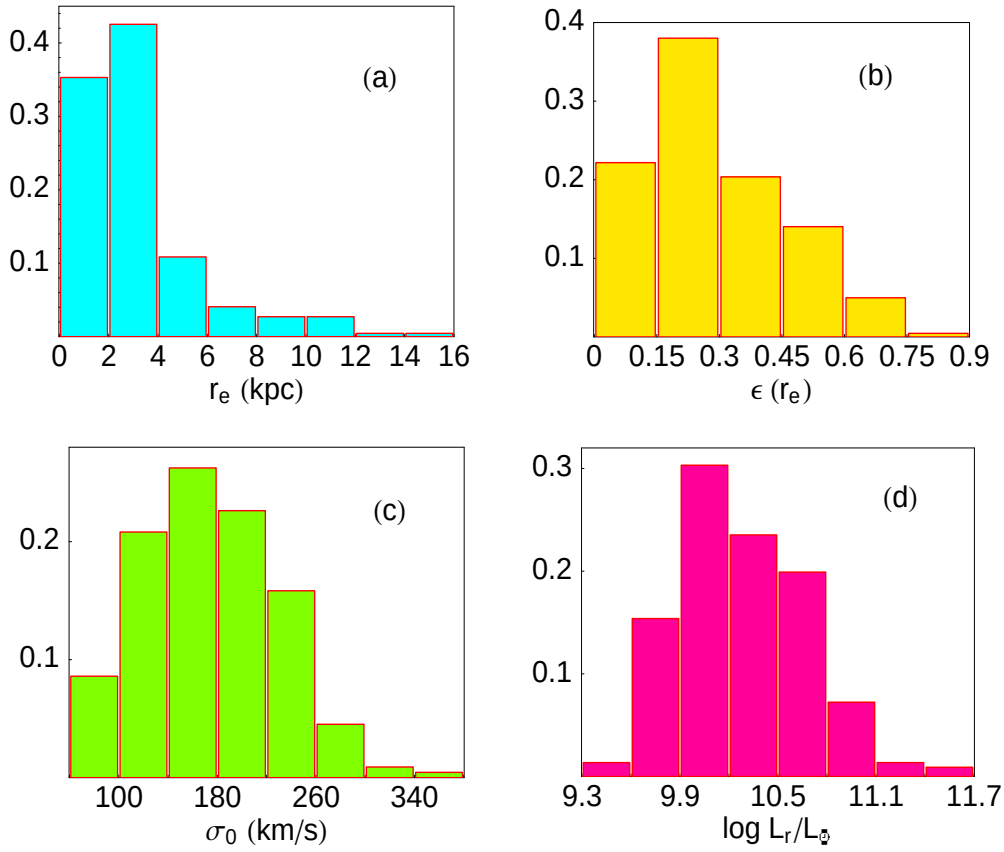

Figure 5.4: Histograms of some remarkable properties of the sample galaxies: (a) effective radius r_e, (b) ellipticity ϵ at r_e, (c) central velocity dispersion σ_0 and (d) luminosity L_r in r-Gunn band .

5.5.2 Forcing models to the FP

The physical interpretation of the Fundamental Plane assumes the virial theorem to be the main constraint to the structure of ellipticals. If the luminosity profiles, as well as the dynamical structure of the ellipticals, are similar (i.e. if elliptical galaxies are 1–component and homologous systems), the virial theorem and the existence of the FP imply a slow but systematic variation of the mass–to–light ratio M/L with the luminosity, whose physical origin is debated. This homology also determines a quasi–linearity of the relations connecting the gravitational and kinetic energies of the galaxies to the observables σ_0 and r_e. However, by adding a second dark mass component, this property will be lost, in such a way that the gravitational and photometric scales are not anymore connected in a simple, log–linear way.

We adjust the mass models parameters to fit the observations in the coordinates space: effective radius r_e, central velocity dispersion $\sigma_0 \equiv \sigma_A(r_e/8)$ and total luminosity in Gunn-r band, defined as $L = 2\pi\ r_e^2\ I_e$. The effective surface brightness I_e in $\mathrm{L}_\odot/\mathrm{pc}^2$ is calculated from μ_e in mag arsec^{-2}: $\log I_e = -0.4\mu_e - 26.4$, for Gunn–$r$ band (JFK, 1995a). In fitting the surface $\sigma_0(r_e,\ L_r)$ to the observations, we leave free the stellar mass–to–light ratio M_{sph}/L_r and, respectively, Γ_{vir} in the H+NFW case and Γ_e in the H+B case. In the latter, we assign a constant value to the parameter $r_0/r_e = 2$, suggested by our results for spirals (see Part II), as the fit depends quite weakly on it.

We characterize the stellar mass–to–light ratio as $\Upsilon_r \equiv M_{sph}/L_r = \Upsilon_{r*}\ (L_r/L_*)^\alpha$, with Υ_{r*} and α free parameters. Here, we neglect a possible weak dependence of Υ_r on r_e; anyway, we will discuss this point later.

5.5.3 Results and discussion

H+NFW mass model

This model is unable to provide a plane surface in the log–space (σ_0, r_e, L_r), for plausible values of the free parameters. For example, in Fig.5.5 we show the effect

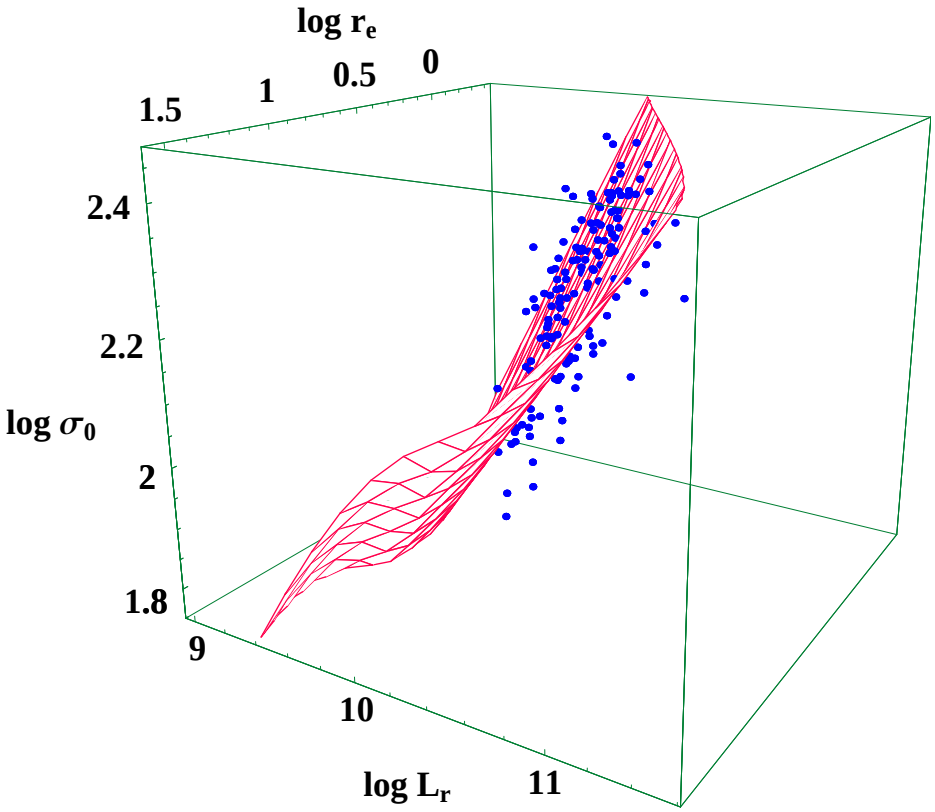

Figure 5.5: The surface $\sigma_0 = \sigma_0(r_e,\ L_r)$ where we expect objects according to the H+NFW model, with $\Gamma_{vir} = 30$, compared with the position of observational data. The units are: r_e in kpc, L_r in $L_{r\odot}$ and σ_0 in km/s.

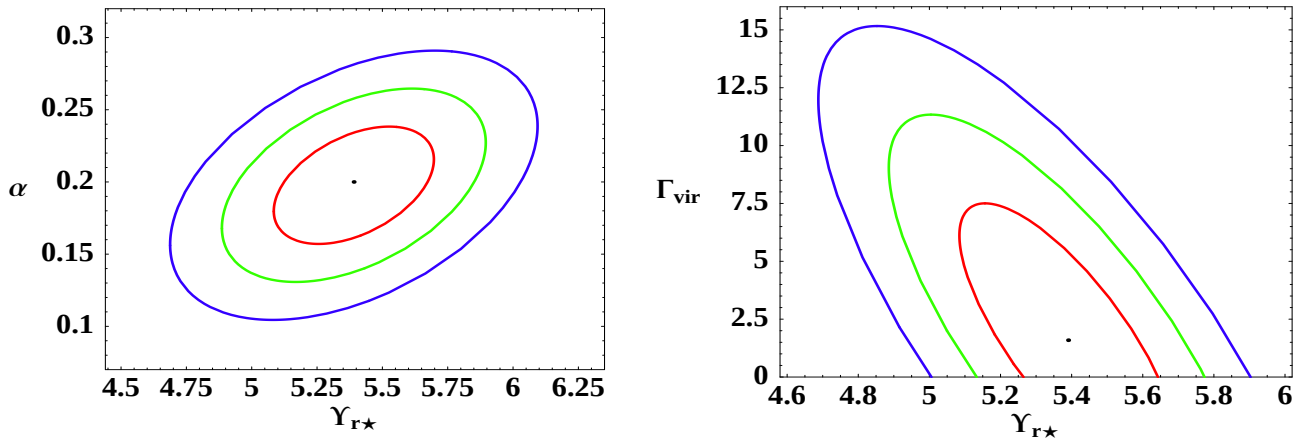

Figure 5.6: The best–parameters from fitting to the FP the surface $\sigma_0(r_e,\ L_r)$, predicted in the H+NFW case (68%, 95% and 99% CL). The value found $\Gamma_{vir} \simeq 2.5$ is obviously senseless.

on the surface by adding to the stellar spheroid a dark NFW component with the reasonable dark–to–luminous mass ratio of $\Gamma_{vir} = 30$. The surface curvature prevents us from properly fitting the data, especially in the region occupied by galaxies with large effective radius and low luminosity, for which the DM contribution to σ_0 is unacceptably high.

The results of the fitting procedure is shown in Fig.5.6, with contours representing 68%, 95% and 99% CL. The best–fit model is consistent even with the no–DM model ($\Gamma_{vir} = 2 \pm 4$ at 1σ) and values of $\Gamma_{vir} \gtrsim 10$ are excluded at $> 95\%$ CL. Solutions marginally excluded ($\Gamma_{vir} \simeq 10 - 15$) will still require very high efficiency of collapse of baryons in stars ($\sim 90\%$).

This would be at strong variance with our ideas about the galaxy formation: indeed, feedback mechanisms, such as SN explosions and central QSO activity, transfers thermal energy into the ISM, thus inhibiting a very efficient star formation (e.g. Dekel & Silk, 1986; Granato et al., 2001; Romano et al., 2002) transferring the whole initial baryonic content into stars. This is also confirmed by the chemical properties of giant E's stellar populations (e.g. Bower et al., 1992; Bernardi et al., 1998; Thomas &

Kauffmann, 1999), which reveal a sole and short initial star formation phase. As result, we expect a value of Γ_{vir} much higher than the original value of ~ 10.

H+B mass model

In this case, the presence of dark matter, distributed in a way independent of the stellar profile, does not alter the FP surface shape, which still remains a plane. Of course, the greater DM amount in the bulge region, the lower the stellar mass–to–light ratio derived from the fit. The best–fit mass model is obtained for (see Fig.5.7):

$$\Upsilon_r = (5.3 \pm 0.1) \left(\frac{L_r}{L_*}\right)^{0.21\pm0.03} \tag{5.38}$$

$$\Gamma_e = 0.29 \pm 0.06 \tag{5.39}$$

(at 68% CL). In Fig.5.8 (*left*) we show the 68%, 95% and 99% confidence contours for the parameters Υ_{r*} and α. In the fit, the parameter Γ_e results strongly correlated to Υ_{r*}. In Fig.5.8 (*right*) we show this correlation with indicated the range of Γ_e corresponding to 99% CL in Υ_{r*}.

Finally, to check the reliability of the fit against our assumption of spherical stellar distribution, we perform the model fit to galaxies with small ellipticity $\epsilon < 0.4$; the resulting best–fit parameters are consistent with the previous ones, with a difference in the mean values of $\sim 5\%$.

Although the data do not allow for a deeper investigation, we point out that keeping Γ_e constant in the fit is not the most general possibility and, in principle, the DM contribution within r_e could vary with luminosity. However, our choice is in agreement with results from the most recent dynamical and photometric studies of mass distribution in ellipticals (Kronawitter et al., 2000; Gerhard et al., 2001), which show that the luminosity dependence in the FP (i.e. its "tilt") is a stellar population

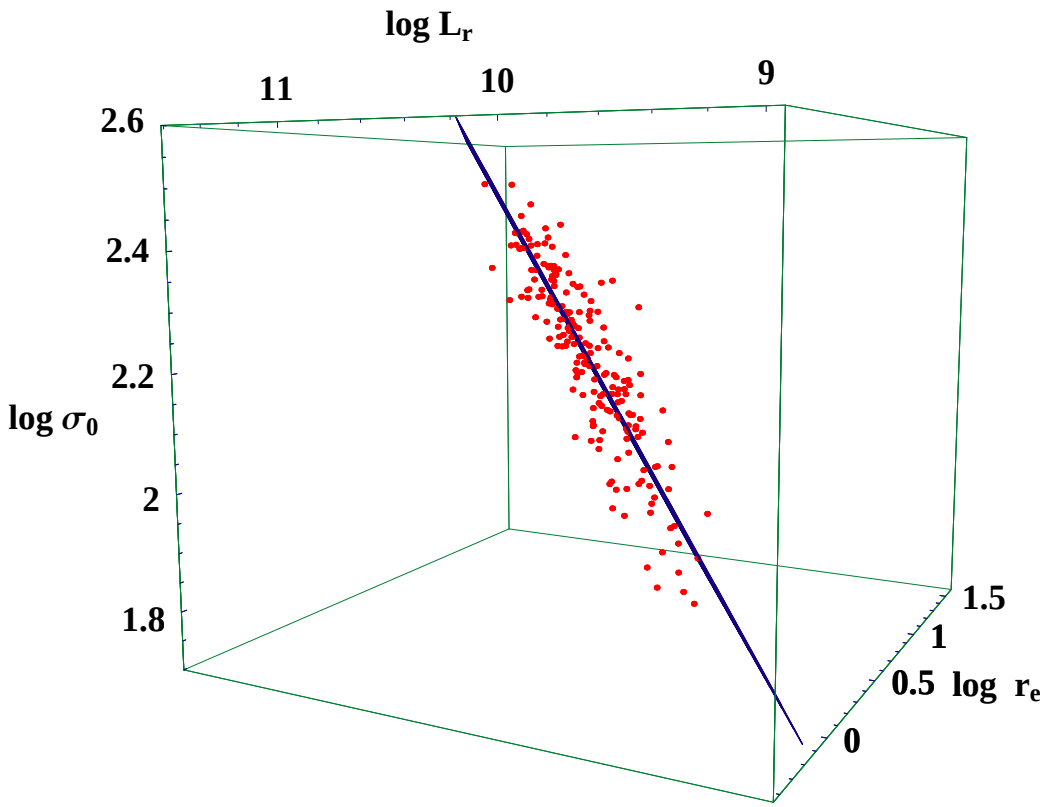

Figure 5.7: The H+B plane (edge–on), best fitting the observational data.

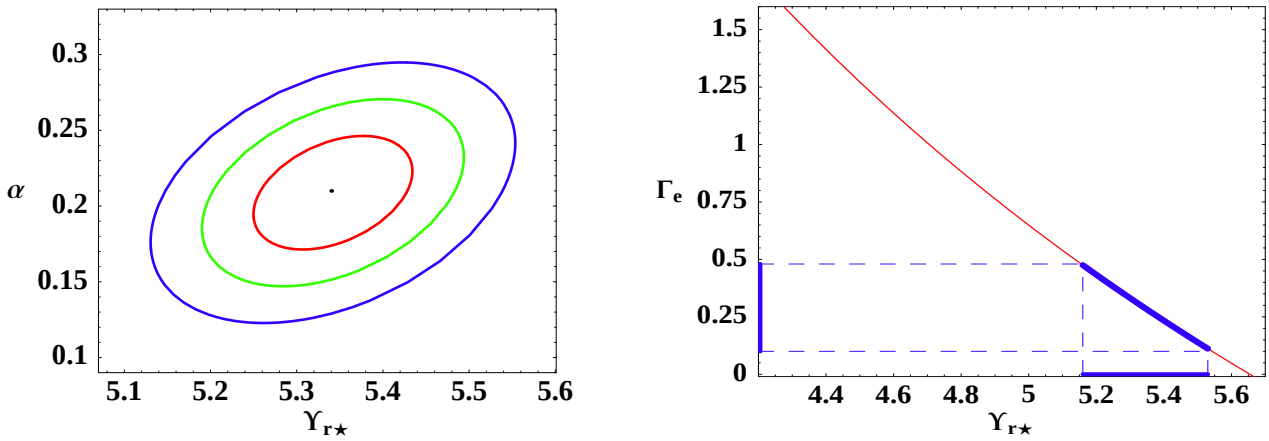

Figure 5.8: Best–fit H+B mass model: *left*) 68%, 95% and 99% CL for the stellar mass–to–light parameters; *right*) the correlation between Υ_{r*} and Γ_e, the dark–to–stellar mass ratio within r_e. Dashed lines mark the 99% C.L. in Υ_{r*} and Γ_e.

effect. Notice that they find $M_{DM}/M_{tot}|_{r_e} \sim 10 - 40\%$; in comparison, from eq.(5.39) we find $M_{DM}/M_{tot}|_{r_e} \sim 20\%$.

From eq.(5.35), we derive the relation between the "virial quantity" $\sigma_0^2 r_e/G$ and the spheroid mass:

$$M_{sph} \simeq (0.17 + 3.6 \times 10^{-2}\ \Gamma_e)^{-1} \cdot \frac{\sigma_0^2\ r_e}{G} \tag{5.40}$$

Assuming the best–fit value $\Gamma_e = 0.3$, eq.(5.40) is in good agreement with results by Ciotti et al. (1996); indeed, they find for their HP model (a mass configuration similar to our H+B model) $M_{sph} = c_M\ \frac{\sigma_0^2\ r_e}{G}$ with $c_M \simeq 3 - 6$, according to the value of the total dark–to–luminous mass ratio (in the range $10 - 70$). Moreover, for dark–to–luminous mass ratio within r_e of ~ 0.3, the *total* mass within the effective radius, $M_e \simeq (1 + \Gamma_e)\ 0.42\ M_{sph}$, writes:

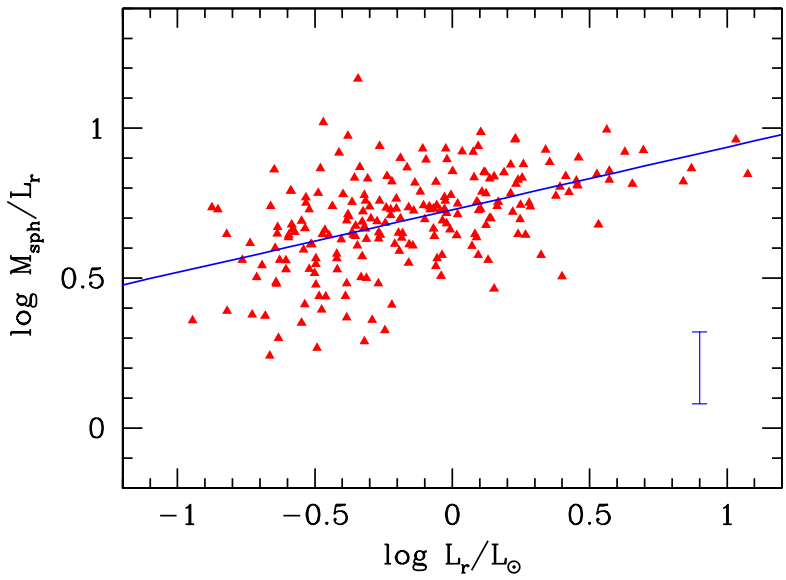

Figure 5.9: The distribution of the stellar mass–to–light ratio in Gunn-r band. Continous line is the mean correlation of the FP. The typical data error at 1 σ is also shown.

$$M_e \equiv M_{sph}(r_e) + M_h(r_e) \simeq \ 2.9 \ \cdot \frac{\sigma_0^2 \ r_e}{G} \tag{5.41}$$

which is to be compared with the "gravitational" mass at r_e: $2\ \sigma_0^2\ r_e/G$, introduced by Burstein et al. (1997), taking the standard Keplerian formula $M_e = r_e V_{rot}^2/G$ and assuming $V_{rot}^2 = 3\sigma_0^2$.

In Fig.5.9 we show the distribution of the stellar mass–to–light ratio in Gunn-r band for single objects, obtained by inserting in eq.(5.40) the observed σ_0, r_e and L_r. Continous line is the "mean" correlation provided by the FP fit : $\Upsilon_r = 5.3\ (L_r/L_*)^{0.21}$. By testing the residuals of the stellar mass–to–light ratio in Gunn-r band as function of the effective radius r_e, we find, within the statistical errors, no correlation: $\Upsilon_r \propto (R/r_e)^{0.00\pm0.05}$. A possible weak dependence on the effective radius, therefore, seems not sufficient to justify the scatter observed in the luminosity dependence of M_{sph}/L.

Since part of the galaxy sample has also been observed in different photometric bands (JFK, 1992; JFK, 1995a; see Tab.5.2), we investigated the M_{sph}/L variations

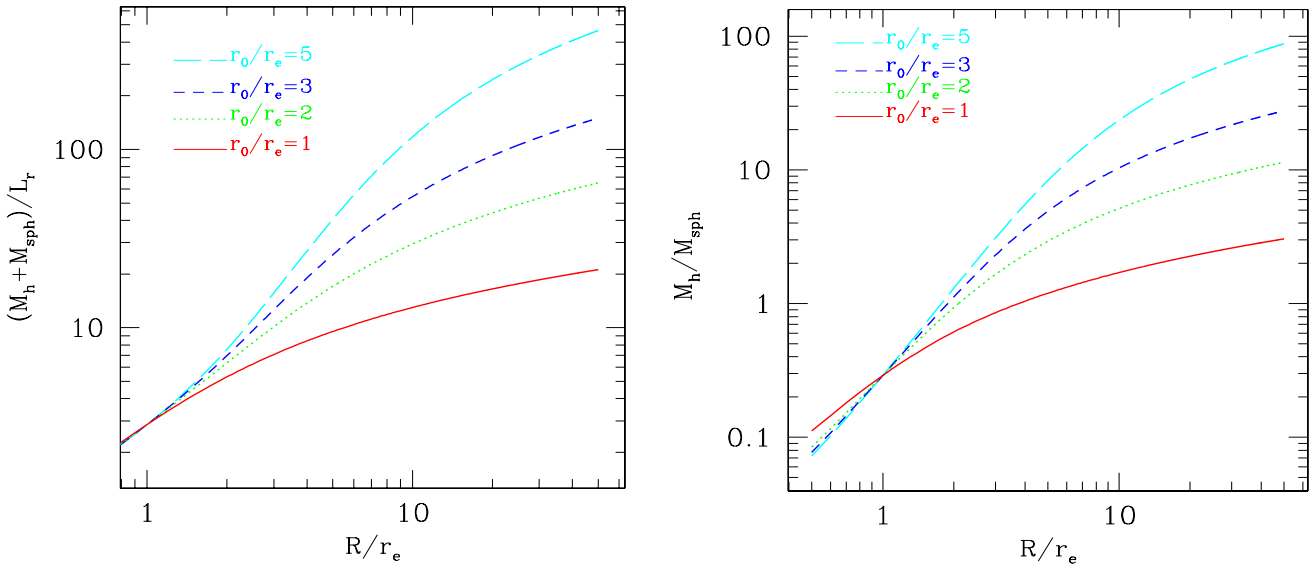

Figure 5.10: Properties of H+B mass model for a L_* galaxy ($\Upsilon_r = 5.3$, $\Gamma_e = 0.3$): *left)* total (dark+luminous) mass–to–light ratio in r–band *vs.* radius, for different values of halo core radius; *right)* dark–to–luminous mass ratio as function of the radius for different values of r_0/r_e.

with luminosity (for a smaller number of galaxies) in Johnson U and B and Gunn–v band, obtaining, respectively, the slopes 0.25 ± 0.06, 0.27 ± 0.03 and 0.34 ± 0.05, with similar large scatter, thus independent of the photometric band. The slope of the relation $M_{sph}/L_B \propto L_B^{0.25\pm0.04}$ seems to be not consistent with the value of $\sim 0.6 \pm 0.1$, obtained from velocity dispersion profiles analysis (Gerhard et al., 2001). Moreover, assuming the dark–to–luminous mass ratio Γ_e weakly decreasing with luminosity (as we would expect), this slope tends to decrease further on.

Recent improvements in the observations has made galaxy–galaxy (weak) lensing a powerful tool to probe the DM halo around galaxies at large radii, where kinematic tracers are useless. Studies of weak lensing by SDSS collaborations (McKay et al., 2002; Guzik & Seljak, 2002) find $M_{260}/L_r \simeq 110$ for a L_{r*} elliptical galaxy, where M_{260} is the mass projected within an aperture of radius 260 h^{-1} kpc. Albeit their results are obtained by assuming a NFW halo, rather than a cored profile, SDSS g–g lensing

is not sensitive to small scales (where NFW and Burkert profiles actually differ), since the first data bin is at $R = 75\ h^{-1}$ kpc: therefore, comparisons to our findings, when extrapolated to large radii, are still useful.

We estimate at large radii the dark–to–luminous mass ratios and the total mass–to–light ratio of the H+B mass model, testing the consistency with SDSS results. In Fig.5.10 (*left*) we show the (dark+luminous) cumulative mass–to–light ratio for a L_{r*} elliptical galaxy. Assuming $r_e \simeq 5 - 10$ kpc for $L = L_*$, the 260 h^{-1} kpc aperture corresponds to $\sim (35 - 70) r_e$, for $h = 0.7$. We obtain the value $M/L_r \simeq 110$ at this aperture for halo core radii in the range $\sim (2.4 - 2.8)\ r_e$. This result for the halo core extension is in agreement with the results of studies in spirals (see Part II), which indicate a constant halo–to–stellar length scales ratio $\gtrsim 1.5 - 2$. Both suggest a form of DM–baryons interplay as the origin of the soft density cores in halos.

In Fig.5.10 (*right*) we show the cumulative dark–to–luminous mass ratio M_h/M_{sph}. The above range of values for the halo core radius $r_0 \simeq (2.4 - 2.8)\ r_e$ corresponds to a mass ratio at very large radius of $M_h/M_{sph} \simeq 15 - 30$. Remarkably, this is in very good agreement with estimates of M_h/M_{sph} from spectro–photometric models of E's formation, which include both chimical evolution and feedback (Romano et al., 2002; their Fig.10), in the spheroid mass range $3 \times 10^9 \lesssim M_{sph} \lesssim 2 \times 10^{11}$.

5.6 Conclusions

With the help of a large sample of elliptical galaxies with suitable data, we used the empirical relation known as the Fundamental Plane as a tool to investigate the DM properties within these objects. We have found a number of results that re–vitalize the field of dark and luminous matter in spheroids:

• the observed "central velocity dispersion" σ_0, as defined in the Fundamental Plane and in others relations, is a hybrid quantity which is not *a priori* related to a single quantity of a single mass component. In fact, σ_0 is linked in a complex way to photometric, dynamical and geometrical quantities of both luminous and dark

matter. In this paper, we present the relations found for an isotropic and spherical two–components mass model, where DM density profile is, alternatively, the NFW profile, predicted by ΛCDM theory, and a cored density profile, suggested by spiral galaxies observations

• the very existence of the Fundamental Plane constraints the acceptable mass model for elliptical galaxies: in particular, it severely challenges the ΛCDM theory predictions. In such a theory the structural properties of dark and luminous matter are so interwoven that in the space (σ_0, r_e , L) they produce a curved surface, rather than a plane, for plausible values of the total dark–to–luminous mass ratio

• considering a cored DM density distribution, we find a dark–to–luminous mass fraction within the effective radius of $\sim$ 30% and a luminosity dependence of the stellar mass–to–light ratio in Gunn–r band: $M_{sph}/L_r \propto L_r^{0.21\pm0.03}$. The inferred stellar mass–to–light ratios for the single galaxies, obtained with a good accuracy by properly correcting for the small effect of the dark matter, will become, in a future work, a benchmark for following the cosmological evolution of spheroids, once we correlate them to galaxy color and metallicity and we compare them with predictions of stellar population models

• to overlap the luminous component of galaxies with a DM halo of low mass density, roughly constant within $2-3r_e$ and increasing as r^{-3} at larger radii, is successful to explain the structure of dwarf, spiral and elliptical galaxies, pointing to an intriguing homogeneous scenario.

Within this framework, we argue that constraints on dark matter in Ellipticals can be significatively improved by increasing the number of galaxies with measures of l.o.s. velocity dispersion at larger radii, greater than $\sim 1-2r_e$. Although, so far, such observations have been severely hampered by the steep decreasing of the surface brigthness with radius, higher and higher sensitivity reached by recent surveys offers a good view to obtain a better resolution of the two mass components in the whole region where baryons reside.

Table 5.2: Elliptical galaxies selected for the Fundamental Plane fit

Galaxy	$\log r_e$ (kpc)	$<\mu>_e$ (Gunn-r)	$\log \sigma_{r_e/8}$ (km/s)	Type	$U-r$	$B-r$	$v-r$	$g-r$
COMA:								
D24	0.28	19.06	2.366	E				
D27	0.31	20.17	2.015	E				
D31	1.12	21.18	2.416	ES0		1.22	1.40	
D46	0.46	19.35	2.383	ES0				
D49	0.69	19.79	2.418	E		1.22	1.28	
D57	0.59	20.05	2.232	S0a				
D58	0.8	21.13	2.263	S0				
D65	0.47	20.55	2.091	S0				
D67	0.03	18.81	2.215	S0				
D68	0.54	20.58	2.138	S0				
D69	0.38	19.42	2.299	E		1.17		
D70	0.28	19.51	2.199	E		1.21		
D72	0.17	19.	2.165	E				
D78	0.58	19.88	2.293	E				
D81	0.47	20.7	2.183	E				
D87	0.13	19.79	1.925	E				
D88	0.12	18.58	2.443	S0				
D98	0.37	19.78	2.2	S0a				
D101	0.21	19.42	2.14	S0				
D103	0.29	19.06	2.356	S0a				
D104	0.17	18.96	2.301	S0				
D105	0.53	19.74	2.323	E		1.21	1.24	
D106	0.04	18.99	2.247	S0		0.88	1.14	
D107	0.4	20.55	1.852	E		1.05	0.98	
D108	0.16	19.61	2.105	S0				
D109	0.38	19.77	2.276	S0				
D116	0.5	20.62	2.143	SB0				
D118	0.52	20.09	2.237	E		1.15	1.17	
D119	0.27	19.87	2.223	S0				
D122	0.33	19.93	1.992	S0				

Table 5.2: *continued*

Galaxy	$\log r_e$ (kpc)	$< \mu >_e$ (Gunn-r)	$\log \sigma_{r_e/8}$ (km/s)	Type	$U-r$	$B-r$	$v-r$	$g-r$
COMA: (*continued*)								
D124	0.36	19.47	2.277	E		1.12		
D125	-0.17	18.06	2.267	E		1.04		
D128	0.05	19.3	2.065	S0		1.11		
D129	1.5	22.13	2.376	D		1.20	1.42	
D130	0.13	18.53	2.352	ES0		1.28	1.22	
D131	0.57	20.24	2.251	S0		1.10	1.18	
D132	0.26	20.24	2.142	S0				
D133	0.14	18.53	2.375	E		1.20	1.13	
D135	0.28	20.5	1.92	E		0.96	1.19	
D136	-0.18	17.99	2.221	E		1.06	1.31	
D137	0.32	19.07	2.245	ES0				
D143	0.91	21.02	2.344	E		1.25	1.24	
D144	0.51	19.96	2.238	S0a				
D145	0.52	20.52	2.152	S0				
D146	0.7	21.31	2.042	SB0				
D148	1.18	20.64	2.572	D		1.22		
D150	0.34	19.98	2.044	E		1.02		
D151	0.62	20.38	2.184	E		1.16		
D152	0.6	20.73	2.217	SB0		1.35		
D153	0.22	19.58	2.153	E		1.06		
D155	0.52	20.09	2.203	S0				
D156	0.16	19.96	2.025	ES0				
D157	0.14	19.48	2.142	S0				
D159	0.54	19.78	2.306	E		1.16	1.24	
D160	0.56	20.36	2.284	SB0				
D161	0.56	20.07	2.251	E				
D167	0.5	19.6	2.336	S0E				
D168	0.29	18.79	2.347	E		1.12		
D170	0.51	20.38	2.174	SB0				
D172	0.16	19.02	2.227	E				

Table 5.2: *continued*

Galaxy	log r_e (kpc)	$< \mu >_e$ (Gunn-r)	log $\sigma_{r_e/8}$ (km/s)	Type	$U-r$	$B-r$	$v-r$	$g-r$
COMA: (*continued*)								
D173	0.18	19.52	2.179	S0				
D174	-0.02	18.23	2.287	E				
D175	0.49	19.91	2.263	S0				
D176	0.14	18.98	2.249	S0				
D177	0.21	19.98	2.038	S0				
D179	0.36	18.77	2.404	S0				
D181	0.16	19.45	2.194	S0				
D191	0.01	18.95	1.994	S0				
D192	0.42	20.15	1.989	S0				
D193	0.27	20.04	2.101	E				
D194	0.58	19.64	2.398	E				
D204	0.43	20.42	2.116	E				
D206	0.65	19.86	2.351	S0				
D207	0.25	19.66	2.192	E				
D210	0.24	19.26	2.246	Ep				
D217	0.69	20.24	2.317	E		1.15		
D238	0.05	18.94	2.041	E				
D239	0.58	19.88	2.359	E		1.08		
D240	0.9	20.39	2.415	E		1.13		
A194:								
N0538	0.618	20.47	2.31	Sa				
ZH05	0.268	19.88	2.179	S0a	1.63	1.13		
ZH08	0.338	19.79	2.09	S0a	1.52	1.07		
ZH48	0.348	20.97	1.889	S0	1.51	1.07	0.98	0.39
D52	0.098	19.86	1.901	E	1.51	1.07	1.00	0.40
I0120	0.368	20.21	2.054	S0	1.65	1.17	1.14	0.45
I1696	0.308	19.53	2.203	E	1.67	1.15	1.14	0.45
N0533	1.078	21.14	2.4	E			1.28	0.46
N0535	0.558	20.47	2.118	Sa	1.60	1.15	1.06	0.48
N0541	0.798	20.61	2.281	D	1.65	1.14	1.23	0.45

Table 5.2: *continued*

Galaxy	log r_e (kpc)	$< \mu >_e$ (Gunn-r)	log $\sigma_{r_e/8}$ (km/s)	Type	$U-r$	$B-r$	$v-r$	$g-r$
A194: *continued*								
N0545	0.888	20.63	2.359	D	1.68	1.13	1.21	0.47
N0547	0.568	19.69	2.401	E	1.76	1.21	1.19	0.47
N0548	0.568	20.91	2.1	ES0	1.46	1.06	0.72	0.39
N0560	0.478	19.53	2.265	S0p	1.61	1.11	1.11	0.43
N0564	0.598	19.93	2.361	E	1.64	1.14	1.19	0.44
ZH07	0.168	18.98	2.203	S0	1.61	1.10	1.08	0.43
ZH09	0.218	19.69	2.106	S0	1.59	1.11	1.16	0.43
ZH10	0.118	18.8	2.345	S0	1.75	1.18	1.21	0.47
ZH12	0.228	19.28	2.231	S0	1.69	1.14	1.15	0.43
ZH19	0.388	19.81	2.066	S0			0.99	0.41
ZH31	0.198	19.97	1.854	S0a			1.00	0.41
ZH39	0.268	19.5	2.298	S0			1.06	0.46
ZH52	0.098	19.41	2.036	S0			1.15	0.45
ZH53	0.418	20.65	1.947	S0			0.92	0.38
ZH56	0.228	19.41	2.348	S0			1.22	0.47
A539:								
D16	0.627	19.65	2.301	S0				0.46
D31	0.817	20.81	2.199	S0				0.37
D38	0.797	20.69	2.238	Sab				0.49
D39	0.667	20.35	2.231	S0				0.43
D41	0.267	19.31	2.223	S0				0.47
D42	0.627	20.51	2.182	S0				0.45
D43	0.647	21.03	2.096	SB0				0.39
D44	0.437	19.3	2.311	S0				0.44
D45	0.517	19.71	2.364	E				0.46
D48	-0.103	17.99	2.303	E				0.56
D50	0.357	19.12	2.372	E				0.50
D51	0.437	19.67	2.234	S0				0.43
D52	0.187	19.38	2.168	S0				0.51

Table 5.2: *continued*

Galaxy	$\log r_e$ (kpc)	$< \mu >_e$ (Gunn-r)	$\log \sigma_{r_e/8}$ (km/s)	Type	$U-r$	$B-r$	$v-r$	$g-r$
A539: *continued*								
D53	0.457	19.19	2.397	S0				0.47
D54	0.527	20.62	2.148	S0				0.42
D57	0.527	20.43	2.257	S0				0.51
D59	0.767	20.75	2.233	S0				0.45
D60	0.697	20.24	2.411	S0a				0.52
D61	0.007	18.6	2.186	S0				0.51
D62	0.597	20.05	2.283	S0				0.44
D63	0.477	19.38	2.272	E				0.40
D64	0.717	20.97	2.173	S0				0.39
D68	0.867	20.25	2.51	E				0.44
D69	-0.113	17.75	2.413	S0				0.49
D75	0.097	19.16	2.143	E				
A3381:								
D21	0.55	20.34	2.302	S0				0.52
D25	0.94	20.69	2.3	ES0				0.48
D33	0.33	18.59	2.308	S0				0.48
D34	0.66	20.36	2.38	S0				0.44
D37	0.41	20.61	1.995	S0				0.55
D55	1.04	21.37	2.326	DS0				0.51
D56	0.59	20.18	2.349	S0				0.51
D64	0.34	19.8	2.154	S0				0.46
D67	0.07	18.86	2.089	ES0				0.56
D68	0.52	20.17	2.203	E				0.49
D73	0.51	20.33	2.135	S0				0.48
D75	0.61	20.07	2.346	E				0.51
D100	0.64	19.97	2.315	S0				0.55
D112	0.91	20.73	2.342	ESOp				0.65

Table 5.2: *continued*

Galaxy	log r_e (kpc)	$< \mu >_e$ (Gunn-r)	log $\sigma_{r_e/8}$ (km/s)	Type	$U-r$	$B-r$	$v-r$	$g-r$
A3574:								
W22	0.34	19.09	2.346	E		1.24	1.27	
W39	1.01	21.75	2.156	S0		1.16	1.46	
W47	1.04	20.88	2.38	S0		1.20	1.40	
W60	0.72	20.39	2.35	S0		1.20	1.07	
W69	0.4	20.12	1.949	S0		1.02		
W74	0.17	18.94	2.342	S0		1.17		
W81	0.54	19.97	2.279	S0		1.22	1.05	
S639:								
E264G23	0.79	20.62	2.339	S0				0.47
E264G24	0.52	18.92	2.357	ES0				0.38
E264G300	0.67	19.78	2.451	D				0.46
E264G301	0.23	18.92	2.284	S0				0.41
E264G302	0.15	18.75	2.298	S0				0.49
E264G31	0.82	20.28	2.388	ES0				0.42
J13	0.38	18.98	2.311	E				0.44
J14	0.51	19.97	2.143	S0				0.40
J15	0.02	18.63	2.132	E				0.40
J16	0.18	19.65	2.115	E				0.42
S753:								
W10	0.053	18.74	2.127	S0		1.09		
W12	0.233	19.29	2.222	S0		1.18	1.23	
W17	0.173	19.53	2.016	E		1.04		
W26	0.543	20.13	2.163	S0		1.12	1.23	
W29	0.503	19.6	2.431	E		1.27	1.34	
W37	0.123	18.85	2.247	S0		1.19	1.24	
W39	0.173	19.36	2.354	S0		1.35		
W47	0.203	19.31	2.089	S0		1.15		
W51	0.343	19.95	2.188	E		1.13		

Table 5.2: *continued*

Galaxy	$\log r_e$ (kpc)	$< \mu >_e$ (Gunn-r)	$\log \sigma_{r_e/8}$ (km/s)	Type	$U-r$	$B-r$	$v-r$	$g-r$
S753: *continued*								
W54	0.493	19.9	2.259	E		1.14	1.18	
W64	1.043	20.36	2.512	S0		1.19		
W73	0.483	19.79	2.271	S0		1.20		
W84	0.293	19.05	2.337	S0		1.18		
W95	0.343	19.9	2.125	E		1.13		
DC2345-28:								
D32	0.579	19.64	2.473	E	1.72	1.20	1.21	0.50
D33	0.399	20.83	1.927	S0	1.50	1.09		
D37	0.419	20.67	1.963	S0	1.35	0.98	0.90	0.37
D38	0.239	19.13	2.086	S0	1.61	1.12	1.15	0.44
D39	0.459	20.43	2.134	S0	1.46	1.06		
D40	0.429	20.98	1.927	S0	1.45	1.07		
D42	1.049	21.25	2.327	D	1.62	1.14	1.28	0.44
D43	0.689	20.46	2.273	S0	1.55	1.10	1.07	0.42
D44	-0.311	17.37	2.243	E	1.81	1.22	1.34	0.55
D45	0.399	20.2	2.109	E	1.45	1.08	0.87	0.35
D49	0.169	19.62	2.121	S0	1.47	1.01		
D50	0.679	20.43	2.31	SB0a	1.60	1.15		
D51	-0.011	18.92	2.21	S0	1.64	1.14	1.21	0.47
D52	0.379	20.92	1.822	E			0.97	0.40
D53	-0.001	19.68	1.872	S0			1.03	0.48
D55	0.249	19.05	2.239	E	1.68	1.14	1.26	0.49
D56	0.929	20.54	2.415	D	1.65	1.14	1.14	0.46
D58	0.559	19.52	2.419	E	1.68	1.16	1.15	0.48
D59	0.459	20.21	2.237	S0	1.57	1.11		
D60	0.329	19.64	2.107	E	1.52	1.08	1.18	0.37
D65	0.759	20.48	2.33	S0	1.64	1.13		
D66	0.239	20.11	2.051	S0	1.50	1.06		
D67	0.529	21.3	2.018	S0	1.41	1.04		
D68	-0.041	19.25	2.123	E	1.56	1.10		

Table 5.2: *continued*

Galaxy	log r_e (kpc)	$< \mu >_e$ (Gunn-r)	log $\sigma_{r_e/8}$ (km/s)	Type	$U-r$	$B-r$	$v-r$	$g-r$
DC2345-28: *continued*								
D69	0.919	22.44	1.908	S0a	1.26	0.97		
D70	-0.181	18.47	2.168	E			1.27	0.51
D76	0.349	20.01	2.155	S0	1.53	1.08		
D77	0.609	19.7	2.316	S0	1.65	1.14		
D83	0.559	20.51	2.113	S0	1.57	1.10		
HYDRA:								
E436G44	0.383	19.37	2.229	S0				0.48
E437G11	0.323	19.33	2.292	S0				0.56
E437G13	0.203	19.	2.246	S0				0.52
E437G21	0.463	19.84	2.261	SB0				0.53
E437G45	0.493	20.18	2.114	S0				0.48
E501G03	0.543	20.08	2.332	E3S0				0.49
E501G13	0.353	19.23	2.369	S0				0.50
I2597	0.763	20.07	2.389	E3S0				0.50
N3305	0.373	19.18	2.407	E1				0.52
N3308	0.913	20.94	2.284	SB0				0.51
N3309	0.743	20.	2.42	E1				0.51
N3311	1.463	22.53	2.265	S0				0.31
RMH26	0.293	20.27	2.043	E2				0.48
RMH28	0.193	19.75	2.17	S0				0.52
RMH29	0.013	18.43	2.213	S0				0.52
RMH30	0.563	20.99	2.294	E6				0.48
RMH35	0.203	19.62	2.112	E7S0				0.51
RMH50	0.223	20.62	1.984	S0				0.43

Table 5.2: Observational properties of the sample galaxies: (1) galaxy name; (2) effective radius in kpc; (3) mean surface brightness within the effective radius in Gunn–r band; (4) central velocity dispersion corrected to an aperture of radius $r_e/8$; (5) morphological type; (6) $U-r$ color; (7) $B-r$; (8) $v-r$; (9) $g-r$. Data are from Jørgensen, Franx & Kjaergaard (1992, 1995a, 1995b) and referencies therein.

Part IV

CONCLUSIONS

Chapter 6

Conclusions and Perspectives

6.1 The Core Radius Phenomenon: Summary of Results

Much work has been done in 80's and 90's about the "first order" properties of dark matter (DM) in galaxies: its very presence, its amount and variations with galaxies type and luminosity. Our work addressed to DM "second order " properties, namely the features of its *distribution* within and around galaxies, an issue strictly connected to cosmological arguments (e.g. galaxies formation, DM nature), that has turned crucial also for Fundamental Physics. This has been the guideline of present research on DM; we approached this issue, both in case of disk and spheroidal galaxies, by means of different strategies, according to the galaxies characteristics, in order to test the DM gravitational effects in galaxies against the Cold Dark Matter (CDM) theories predictions. To our aims, high quality kinematical data have been essential. Let us summarize our results.

As regards **disk galaxies**:

• we derived the fine structure of dark matter halos from the kinematics of a number of *suitably selected* individual RC's of low–luminosity galaxies. Indeed, in case of high–quality RC's, it is possible to decompose the galaxy mass structure into its dark and luminous component and to obtain, with good reliability, the DM halo distribution.
The analysis unveils that the halo component of the observed circular velocity increases *linearly* with radius out to the edge of the stellar disk, implying a constant dark halo density over the entire disk region. A good description of DM density distribution around galaxies is provided by the Burkert (1995) functional form (see also Salucci & Burkert, 2000): $\rho_B(r) \propto (r + r_0)^{-1}(r^{-2} + r_0^{-2})$, proposed in the analysis of individual dwarfs RC's (Burkert, 1995) and tested by means of the Universal Rotation Curve (Salucci & Burkert, 2000).
We found that typical DM halo central densities are in the range of $\rho_0 \sim 1 - 4 \times 10^{-24}$ g cm^{-3}, and scale with the core radius as $\rho_0 \propto r_0^{-2/3}$. DM cores extension, with respect

to the disk length scale, turns out to be remarkably large, at least $3-4\ r_D$, and roughly independent of galaxy luminosity and dark mass fraction.

• we study the remarkable test–case of a dwarf DM–dominated galaxy, DDO47, whose HI RC is known up to large radius ($\sim 9\ r_D$), with very high precision (velocity resolution: 2.6 km/s). We present most convincing evidence for a core in the density distribution of the dark halo around this dwarf galaxy. DDO47 has a rotation curve that increases linearly from 700 pc out to 6 kpc, which cannot be reproduced unless we consider a dark halo with a flat density core. The core region has a size $\gtrsim 3$ kpc, about twice the stellar disk size ($\sim 6\ r_D$).

• we performed a specific investigation of the Universal Rotation Curve, derived by analyzing a large and complete sample of 1000 spirals RC's. This statistical sample allowed us *1)* to verify the robustness of our results on individual galaxies and *2)* to derive the variations of DM halos properties, along the spirals luminosity sequence. In detail, a correlation holds between the halo central density and core extension:

$$\log r_0 = 9.1 + 0.28\ \log \rho_0 - 3.5 \times 10^{10}\ \rho_0^{0.43} \tag{6.1}$$

and between the DM core density and the disk mass:

$$\log \rho_0 = -23.0 - 0.077\ \log M_D - 10^{-5}\ M_D^{0.43} \tag{6.2}$$

pointing to a *physical* connection between halo and disk structures.

As regards DM in **spheroidal galaxies**, as a first step in our analysis, we considered a large sample of luminous (nearly spherical) elliptical galaxies, to derive the implications of the Fundamental Plane to the DM content and properties in these objects. We find that the "central velocity dispersion" σ_0, appearing in (e.g.) the Fundamental Plane, is linked, in a complex, but predictable way, to photometric, dynamical and geometrical quantities of both luminous and dark matter. Then, we find

that the very existence of the Fundamental Plane strongly constraints the mass models. In particular, it implies *i)* an average value for the dark–to–luminous mass ratio (inside the galaxy effective radius) of about 0.3 *ii)* a stellar mass–to–light increasing with spheroid luminosity: $M_{sph}/L_r \propto L_r^{0.2}$ in Gunn-r band, with a value of ~ 5.3 at L_{*r} and *iii)* the presence of *cored* dark matter halos around ellipticals, as found for both dwarf and spiral galaxies.

The properties of the halo mass structure we find in our study are on the line of claims for a small number of dwarf and low surface brightness (LSB) galaxies in mid 90's, providing, however, for more substantial evidence of a discrepancy between the halo mass distribution predicted in the Cold Dark Matter scenario and that actually detected around galaxies. In fact, our results definitely confirm this discrepancy and point toward an intriguing halo length scale, emerging out of the scale–free process of its formation. Moreover, in case of E's, we find that *the very existence* of the Fundamental Plane contradicts ΛCDM predictions: this theory, indeed, has structural properties of dark and luminous matter so interwoven that, in the space (σ_0, r_e, L) it predicts a curved surface, rather than a plane.

Crucially, the robust results we find in this thesis (due to the methods employed) level off to zero the criticisms (e.g. van den Bosch et al., 2000; van den Bosch & Swaters, 2001) raised to previous claims for DM cores in galaxies. We conclude by stressing that, for *any* theory of galaxy formation, time is come to seriously consider that the luminous component of galaxies lays down in dark halos whose density stays constant (and low) at least up to the optical radius, and, probably, farther.

6.2 Abandoning Collisionless Cold Dark Matter

After this work, the "core" problem affecting CDM theories is dramatically confirmed. Moreover, it also emerges the evidence that the DM distribution in the optical regions of galaxies is featureless and unrelated to global properties (e.g. virial mass and radius) of the dark halo, differently from what is naturally expected in a pure hierarchical clustering scenario. We are forced to consider the possibility that cosmological and/or astrophysical processes have cut the link between the initial conditions and the present–day galaxies properties: this connection, indeed, appears to be just missing in Nature.

The failure of *collisionless* CDM theories on galaxies scale has motivated, in last years, the raise of many hypotheses, which modify the DM properties on small scales, while preserving the success of CDM on large scales. These new scenarios are required to originate dark density cores in halo central regions and, even, to face a number of other observed discrepancies with theory, such as the excess of the observed disk angular momentum with respect to predictions and the lack of the predicted amount of halo substructure (the so–called "satellite question", i.e. the predicted number of subhalos on scales of the Local Group is at least a factor of ten higher than the observed number of dwarf galaxies (Klypin et al., 1999; Moore et al., 1999a)). It is quite difficult, anyway, to conceive new scenarios, without claiming "ad hoc" DM requisites.

Collisionless CDM has the non–negligible advantage of allowing to neglect dark–baryonic matter interactions, during the galaxy collapse and evolution; indeed, dissipationless simulations do not take into account the effect of baryonic infall and disk formation on the final halo density distribution. This led to the claim of an universal halo profile which is, however, at variance with actual halos.

A possible solution consists in coupling the luminous and dark components in galaxies, mostly by means of energetic mechanisms, such as feedback from evolving stars and heating by ionizing UV background, which are more efficient in low mass systems, due to the less deep potential well (e.g. Gelato & Sommer–Larsen, 1999;

Bullock et al., 2000); let us recall that since redshift $z < 10$, radiation processes and chemical evolution take place together with gravitational clustering, making the involved physics much complex. Although it cannot be excluded that this scenario, given its complexity, needs much more refined numerical simulations, combining gravity and hydrodynamics, it is worth stressing that these mechanisms seems unlikely to be able to solve the collisionless CDM crisis even for high mass galaxies.

An alternative solution regards the *nature* of DM, considering some form of interacting particles. For instance, Spergel & Steinhardt (2000) proposed self–interacting DM (SIDM) particles, with a finite cross–section for non–dissipative collision, such that their mean free path is on scales of kpc to Mpc for typical galactic densities. These collision thermalize the inner regions of the dark halos: indeed, the heat flux to the core smooth out the density cusp and reduces the amount of substructure by evaporating orbiting subhalos. Several works have explored this model numerically and analytically (e.g. Yoshida et al., 2000a; Firmani et al., 2001a; Colín et al., 2002), finding that SIDM halos present shallow cores, with *constant* cross section per unit mass σ_{DM} being ~ 5 cm^2 g^{-1} (Davé et al., 2001), in order to be in agreement with observations of galaxies, and even smaller, to account for clusters data (Yoshida et al., 2000b). On the other hand, when σ_{DM} is inversely proportional to the relative velocity of colliding particles, all halos will have central density approximately constant with mass, $\rho_c \sim 0.02$ M$_\odot$ pc^{-3} (Firmani et al., 2001b). Such a result is strongly different from CDM predictions. Anyway, important problems still affect SIDM; for example, the prediction of a fast core collapse in time scales of the order of the halo dynamical time (e.g. Burkert, 2000). Moreover, SI cross–sections large enough to modify the halo central profiles, would make the center of clusters more spherical (Yoshida et al., 2000b) and less dense (Meneghetti et al., 2001), at variance with gravitational lensing observations (e.g. Arabadjis et al., 2002). Finally, recent quantitative semi–analytical arguments proved that SIDM is unable to solve both the soft core and the satellite problems, *simultaneously* (D'Onghia & Burkert, 2002).

Other explored hypotheses, regarding, for example, warm dark matter (WDM) or

a finite annihilation cross section for DM particles, do not solve all the problems they are invoked to solve and create sometimes new problems (see Primack, 2002).

6.3 New Search for DM Particles

Particle physics have provided a number of possible candidates to cold DM; many of them fall under the general category of weakly interacting massive particles (WIMPs), out of which, the most discussed are axions and neutralinos. The idea of detecting galactic DM particles directly, by observing their elastic scattering on target nuclei through nuclear recoils in underground laboratory, has motivated a number of experiments, which have been carried out with controversial results (e.g. Bernabei et al., 2000; Abusaidi et al., 2000). Others are underway and/or planned in next future (e.g. Klapdor–Kleingrothaus et al., 2001).

Brand new DM candidates, with completely different properties, are probably needed to account for ever increasing observational data favouring collisional DM. A still unknown dark/baryons interaction mechanism may be operating, whose relic particles could be even undetectable, today. Future work will have to face the big challenge of describing, with enough detail, the dark mass distribution and characteristics on both galaxy and cluster scales. Indeed, the process of galaxies formation at $z \lesssim 10$ is strongly tighted to the issue of DM particles properties. Only then, it will be possible to progress in cosmological theories and to increase the chance of a direct DM particles detection in laboratory.

Bibliography

[1] Abusaidi, R. et al., (2000) Phys.Rev.Lett, **84**, 5699 CDMS

[2] Arabadjis, J.S., Bautz, M.W. & Garmire, G.P., (2002) ApJ, **572**, 66

[3] Armandroff, T.E., Olszewski, E. W. & Pryor, C. , (1995) AJ, **110**, 2131

[4] Bahcall, J.N. & Casertano, S., (1985) ApJ, **293**, 7

[5] Bahcall, J.N., (1997) AAS, **191**, 6101

[6] Bahcall, N. A., Ostriker, J. P., Perlmutter, S. & Steinhardt, P. J., (1999) Science, **284**, 1481

[7] Bergström, L., (2000) Rep. Prog. Phys., **63**, 793

[8] Bernabei, R. et al., (2000) Phys.Lett., **B480**, 23

[9] Bernardi, M., Renzini, A., da Costa, L.N., Wegner, G., Alonso, M.V., Pellegrini, P.S., Rite, C. & Willmer, C.N.A., (1998) ApJ, **508**, 143L

[10] Bertin, G., Bertola, F., Buson, L. M., Danziger, J., Dejonghe, H., Sadler, E. M., Saglia, R.P., Vietri, M., de Zeeuw, T. & Zeilinger, W. W., (1991) IAUS, **146**, 93

[11] Bertin, G., Pignatelli, E. & Saglia, R. P., (1993) A&A, **271**, 381

[12] Bertin, G., Bertola, F., Buson, L.M., et al., (1994) A&A, **292**, 381

[13] Bertola, F., Pizzella, A., Persic, M. & Salucci, P., (1993) ApJ, **416**, 45

[14] Bertola, F., Persic, M., Pizzella, A. & Salucci, P., (1993) ApJ, **416**, L45

[15] Bevington, P.R. & Robinson, D.K., (1992) *Data reduction and error analysis*; Boston: McGraw–Hill

[16] Binney, J., (1978) MNRAS, **183**, 501

[17] Binney, J. & Tremaine, S., (1987) *Galactic Dynamics*; Princeton: Univ. Press

[18] S. Blais-Ouellette, C. Carignan, P. Amram: astro-ph/0203146 to be published in: *Galaxies: the Third Dimension*, ASP Conf. Ser. (2002)

[19] Blanton, M.R. *et al.*, (2001) AJ, **121**, 2358

[20] Blumenthal, G. R., Pagels, H. & Primack, J. R. , (1982) Nature, **299**, 37

[21] Blumenthal. J.J., Faber, S.M., Flores, R. & Primack, J.R., (1986) ApJ, **301**, 27

[22] Bond, R. & Szalay, A., (1983) ApJ, **274**, 443

[23] Borriello, A. & Salucci, P., (2001) MNRAS, **323**, 285 (BS01)

[24] Bosma, A., (1978), PhD thesis, Groningen Univ.

[25] Bosma, A. & van der Kruit, P.C., (1979) A&A, **79**, 281

[26] Bosma, A., (1981) AJ, **86**, 1825

[27] Bower, R.G., Lucey, J.R. & Ellis, R.S., (1992) MNRAS, **254**, 589

[28] Broeils, A.H., (1992), Ph.D. Thesis, University of Groningen

[29] Broeils, A.H. & Courteau, S. (1997) in *Dark and Visible Matter in Galaxies.* ASP Conf. Ser., Vol. **117**, p.74; ed. Persic and Salucci

[30] Bryan, G.L. & Norman, M.L., (1998) ApJ, **495**, 80

[31] Bullock, J.S., Kravtsov, A.V. & Weinberg, D.H., (2000) ApJ, **539** 517

[32] Bullock, J.S., Kolatt, T.S., Sigad, Y., Somerville, R.S., Kravtsov, A.V., Klypin, A.A, Primack, J.R. & Dekel, A., (2001) MNRAS, **321**, 559

[33] Burkert, A., (1995) ApJ, **447**, L25

[34] Burkert, A. & Silk, J., (1997) ApJ, **488**, L55

[35] Burkert, A., (2000) ApJ, **534**, L143

[36] Burles, S. & Tytler, D., (1998) Space Sci. rev., **84**, 65

[37] Burles, S., Hui, L., Weinberg, D. H., Stebbins, A., Schlegel, D. J., Bernardi, M., Frieman, J. A., SubbaRao, M., & York, D. G., SDSS Collaboration, (2001) AAS, **198**, 2604

[38] Burstein, D., Bender, R., Faber, S.M. & Nolthenius, R., (1997) AJ, **114**, 1365

[39] Carignan, C. & Freeman, K.C., (1985) ApJ, **294**, 494

[40] Carignan, C. & Freeman, K.C., (1988) ApJ, **332**, 33

[41] Cheng, L. & Wu, X., (2001) A&A, **372**, 381

[42] Chengalur, J.N., Salpeter, E.E. & Terzian, Y., (1993) ApJ, **419**, 30C

[43] Ciotti, L., (1999) ApJ, **520**, 574

[44] Ciotti, L., (2000), in *Dynamics of Galaxies: from the Early Universe to the Present*. ASP Conf. Ser., Vol. **197**, p.95

[45] Ciotti, L. & Pellegrini, S., (1992) MNRAS, **255**, 561

[46] Ciotti, L., Lanzoni, B. & Renzini, A., (1996) MNRAS, **282**, 1

[47] Cole, S. & Lacey, C., (1996) MNRAS, **281**, 716

[48] Colín, P., Avila-Rees, V., Valenzuela, O. & Firmani, C., (2002) ApJ submitted, astro–ph/0205322

[49] Corbelli, E. & Salucci, P., (2000) MNRAS, **311**, 411C

[50] Coté, S. & Carignan, C., (1991) AJ, **102**, 904

[51] Côté, S., Freeman, K. & Carignan, C., (1997), in *Dark and visible matter in Galaxies*. ASP. Conf. Ser., Vol.**117**, ed. Persic and Salucci

[52] Coté, S. & Carignan, C., (1991) AJ, **102**, 904

[53] D'Onghia, E. & Burkert, A. (2002), ApJ submitted, astro–ph/0206125

[54] Dalcanton, J., Summers, F. & Spergel, D., (1997) ApJ, **482**, 659

[55] Danziger, I.J., (1997), in *Dark Matter in Early–type Galaxies*. ASP Conf. Ser., Vol.**117**, ed. Persic and Salucci

[56] Davé, R., Spergel, D.N., Steinhardt, P.J. & Wandelt, B.J., (2001) ApJ, **547**, 574

[57] Davies, R. L., Efstathiou, G., Fall, S.M., Illingworth, G., & Schechter, P.L., (1983) ApJ, **266**, 41

[58] Davies, J.I., Phillipps, S. & Disney, M.J., (1989) MNRAS, **239**, 703

[59] de Battista, V.P. & Sellwood, J.A., (1998) ApJ, **493**, L5

[60] de Bernardis, P. et al., (2000) Nature, **404**, 955

[61] de Blok, W.J.G., McGaugh, S.S. & van der Hulst, J. M., (1996) MNRAS, **283**, 18

[62] de Blok, W.J.G. & McGaugh, S.S., (1997) MNRAS, **290**, 533

[63] de Blok, W.J.G., McGaugh, S.S. & Rubin, V.C., (2001a) AJ, **122**, 2396

[64] de Blok, W.J.G., McGaugh, S.S., Bosma, A. & Rubin, V.C., (2001b) ApJ, **552**, 23

[65] de Blok, W.J.G & Bosma, A., (2002) A&A, **385**, 816

[66] de Jong, R.S., (1996) A&A, **313**, 377

[67] de Lapparent, V., Geller, M. J. & Huchra, J.P., (1986) ApJ, **302**, 1

[68] de Vaucouleur, G., (1948) Ann. d'Astroph., **11**, 247

[69] Davis, M., Efstathiou, G., Frenk, C.S. & White, S.D.M., (1985) ApJ, **292**, 371

[70] Dekel, A. & Silk, J., (1986) ApJ, **303**, 39

[71] Djorgovski, S. & Davis, M., (1987) ApJ, **313**, 59

[72] Dressler, A., Lynden-Bell, D., Burstein, D., Davies, R.L., Faber, S.M., Terlevich, R.J. & Wegner, G., (1987) ApJ, **313**, 42

[73] Driver, S.P., Phillipps, S., Davies, J. I.. Morgan, I. & Disney, M.J., (1994) MNRAS, **266**, 155

[74] Efstathiou, G., (1991) Physica Scripta, **T36**, 88

[75] Efstathiou, G., Bond, J. R. & White, S. D. M., (1992) MNRAS, **258**, 1

[76] Einasto, J., Einasto, M., Tago, E., Starobinsky, A. A., Atrio-Barandela, F., Mller, V., Knebe, A., Frisch, P., Cen, R., Andernach, H. & Tucker, D., (1999) ApJ, **519**, 441

[77] Einasto, J. & Einasto, M., (2000) Publ. Astron. Soc. Pac., **209**, 360

[78] El–Zant, A., Shlosman, I. & Hoffman, Y., (2001) ApJ, **560**, 636

[79] Evrard, A.E., 1997, MNRAS 292, 289

[80] Faber, S. M. & Lin, D.N., (1983) ApJ, **266**, 17

[81] Ferguson, H.C. & Binggeli, B., (1994) A&ARv, **6**, 67

[82] Firmani, C., D'Onghia, E., Avila–Reese, V., Chincarini, G. & Hernandez, X., (2000) MNRAS, **315**, 29

[83] Firmani, C., D'Onghia, E., Chincarini, G., Hernandez, X. & Avila–Reese, V., (2001a) MNRAS, **321**, 713

[84] Firmani, C., D'Onghia, E., Chincarini, G., (2001b) MmSAI, **72**, 805

[85] Flores, R. & Primack, J.R., (1994) ApJ, **427**, L1

[86] Freeman, K.C., (1970) ApJ, **160**, 811F

[87] Frenk, C.S., White, S.D.M., Davis, M. & Efstathiou, G., (1988) ApJ, **327**, 507

[88] Fukushige, T. & Makino, J., (1997) ApJ, **477**, L9

[89] Fukushige, T. & Makino, J., (2001) ApJ, **557**, 533

[90] Gelato, S. & Sommer-Larsen, J., (1999) MNRAS, **303**, 321

[91] Gerhard, O.E., (1993) MNRAS, **265**, 213

[92] Gerhard, O.E., Kronawitter, A., Saglia, R.P. & Bender, R., (2001) AJ, **121**, 1936

[93] Ghigna, S., Moore, B., Governato, F., Lake, G., Quinn, T., & Stadel, J., (2000) ApJ, **544**, 616

[94] Granato, G.L., Silva, L., Monaco, P., Panuzzo, P., Salucci, P., De Zotti, G. & Danese, L., (2001) MNRAS, **324**, 757

[95] Guzik, J. & Seljak, U., (2002), MNRAS in press, astro-ph/0201448

[96] Hanany, S. et al., (2000) ApJ, **545**, 5

[97] Hernquist, L., (1990) ApJ, **356**, 359

[98] Huchra, J. P., Geller, M. J., de Lapparent, V. & Burg, R. , (1988), in *Large Scale Structures of the Universe*; IAU Symp. **130**, p. 105, Kluwer Acad. Pub., Dordrecht

[99] Ibata, R.A., Wyse, R.F.G., Gilmore, G., Irwin, M.J. & Suntzeff, N.B., (1997) AJ, **113**, 634

[100] Impey, C.D., Sprayberry, D., Bothun, G.D. & Irwin, M.J., (1993) AAS, **183**, 304

[101] Jing, Y.P., (1999) ApJ, **515L**, 45J

[102] Jing, Y.P. & Suto, Y., (2000) ApJ, **529**, 69

[103] Jørgensen, I., Franx, M. & Kjaergaard, P., (1992) A&AS, **95**, 489

[104] Jørgensen, I., Franx, M. & Kjaergaard, P., (1995a) MNRAS, **273**, 1097

[105] Jørgensen, I., Franx, M. & Kjaergaard, P., (1995b) MNRAS, **276**, 1341

[106] Jørgensen, I., Franx, M.& Kjaergaard, P., (1996) MNRAS, **280**, 167

[107] Klapdor–Kleingrothaus, H.V., Majorovits, B., Baudis, L., Diets, A., Heusser, G., Krivosheina, I. & Strecker, H., (2001), in "Dark Matter in Astro and Particle Physics", ed. Springer; hep-ph/0103082

[108] Klypin, A. A., Kravtsov, A. V., Colin, P., Gottlober, S. & Khokhlov, A. M., (1998) AAS, **193**, 6101

[109] Klypin, A., Kravtsov, A,V., Valenzuela, O. & Prada, F., (1999) ApJ, **522**, 82

[110] Koopmans, L.V.E. & Treu, T., (2002) ApJ, **568**, 5

[111] Kormendy, J., (1988) ApJ, **325**, 128

[112] Krauss, L.M., (1998) ApJ, **501**, 461

[113] Krauss, L.M., (2001), in *Proceed. of the 3rd Intern. Workshop on the Identification of Dark Matter*, ed. Spooner and Kudryavtsev, Singapore

[114] Kravtsov, A.V., Klypin, A.A., Bullock, J.S., & Primack, J.R., (1998) ApJ, **502**, 48

[115] Kronawitter, A., Saglia, R.P., Gerhard, O.E. & Bender, R., (2000) A&AS, **144**, 53

[116] Makarova, L.N., Karachentsev, I. D., Grebel, E. K., & Barsunova, O.Y., (2002) A&A, **384**, 72

[117] Marchesini, D., D'Onghia, E., Chincarini, G., Firmani, C., Conconi, P., Molinari, E. & Zacchei, A., (2002) ApJ, **575**, 801

[118] Martin, C.L., (1999) ApJ, **513**, 142

[119] Mateo, M., (1994), in *ESO Conference and Workshop Proceedings*, ed. Meylan and Prugniel

[120] Mateo, M., (1997), in *The Nature of Elliptical Galaxies*. ASP Conf. Ser., Vol.**116**, p.259; ed. Arnaboldi, Da Costa; and Saha

[121] Mathewson, D.S., Ford, V.L. & Buchhorn, M.K.C., (1992) ApJS, **81**, 413

[122] Matthews, L.D. & Gallagher, J.S. III, (2002) ApJS, **141**, 429

[123] Matthias, M. & Gerhard, O.E., (1999) MNRAS, **310**, 879

[124] McGaugh, S. S. & Bothun, G. D., (1994) AJ, **107**, 530

[125] McGaugh, S.S., Schombert, J.M. & Bothun, G.D., (1995) AJ, **109**, 2019

[126] McGaugh, S.S.,& de Block, W.J.G., (1998) ApJ, **499**, 41

[127] McKay, T.A., Sheldon, E. S., Johnston, D., Grebel, E. K., Prada, F., Rix, H.-W., Bahcall, N. A., Brinkmann, J., Csabai, I., Fukugita, M., Lamb, D. Q. & York, D. G., (2002) ApJ, **571**, 85

[128] Meneghetti, M. et al., (2001) MNRAS, **325**, 435

[129] Merritt, D., (1993) Science, **259**, 1867

[130] Mo, H., Mao, S. & White, S.D.M., (1998) MNRAS, **295**, 319

[131] Moore, B., (1994) Nature, **370**, 629

[132] Moore, B., Governato, F., Quinn, T., Stadel, J.,& Lake, G., (1998) ApJ, **499**, L5

[133] Moore, B., Quinn, T., Governato, F., Stadel, J. & Lake, G., (1999) MNRAS, **310**, 1147

[134] Moore, B., (2001) AIP Conf. Proceed., **586**, p.73

[135] Morshidi, Z., Davies, J.I. & Smith, R., (1997), in *Dark and Visible Matter in Galaxies* ASP Conf. Ser., **117**, p.510

[136] Navarro, J.F., Frenk, C.S. & White, S.D.M., (1995) MNRAS, **275**, 56

[137] Navarro, J.F., Frenk, C.S. & White, S.D.M., (1996) ApJ, **462**, 563

[138] Navarro, J.F., Frenk, C.S. & White, S.D.M., (1997) ApJ, **490**, 493

[139] Nusser, A. & Sheth, R.K., (1999) MNRAS, **303**, 685

[140] Peebles, P.J.E., (1982) ApJ, **263**, 1

[141] Peebles, P.J.E., (2000) ApJ, **534**, 127

[142] Perlmutter, S. et al., (1999) ApJ, **517**, 565

[143] Persic, M. & Salucci, P., (1988) MNRAS, **234**, 131

[144] Persic, M. & Salucci, P., (1990b) MNRAS, **245**, 577

[145] Persic, M. & Salucci, P., (1990c) MNRAS, **247**, 349

[146] Persic, M. & Salucci, P., (1991) ApJ, **368**, 60

[147] Persic, M. & Salucci, P., (1992) ApL, **28**, 307

[148] Persic, M. & Salucci, P., (1995) ApJS, **99**, 501 (PS95)

[149] Persic, M. , Salucci, P. & Stel, F., (1996) MNRAS, **281**, 27P (PSS96)

[150] Primack, J.R., (2002) in *Proceed. 5th Int. UCLA Symposium*, astro–ph/0205391

[151] Pryke, C., Halverson, N. W., Leitch, E. M., Kovac, J., Carlstrom, J. E., Holzapfel, W. L. & Dragovan, M., (2002) ApJ, **568**, 46

[152] Pryor, C., (1992) in *Morphological and Physical Classification of Galaxies*, Astrophysics and Space Science Library, **178**, p.163

[153] Puche, D., Carignan, C. & Bosma, A., (1990) AJ, **100**, 1468

[154] Puche, D. & Carignan, C., (1991) ApJ, **378**, 487

[155] Ratnam, C. & Salucci, P., (2000) New Astron., **5**, 427

[156] Rhee, M.-H., (1996), PhD thesis, Groningen University

[157] Rhee, M.-H. & van Albada, T.S., (1996) A&AS, **115**, 407

[158] Richstone, D. O. & Tremaine, S., (1986) AJ, **92**, 72

[159] Riess, A.G. et al., (1998) AJ, **116**, 1009

[160] Romano, D., Silva, L., Matteucci, F. & Danese, L., (2002) MNRAS, **334**, 444

[161] Roscoe, D.F., (1999) A&A, **343**, 788

[162] Rubin, V.C., Ford, W.K. & Thonnard, N., (1980) ApJ, **238**, 471

[163] Saglia, R.P., Bertin, G. & Stiavelli, M., (1992) ApJ, **384**, 433

[164] Saglia, R.P., Bertin, G. & Bertola, F., et al., (1993) ApJ, **403**, 567

[165] Salucci, P., (2001) MNRAS, **320**, 1

[166] Salucci, P. & Frenk, C.S., (1989) MNRAS, **237**, 247

[167] Salucci, P. & Persic, M., (1997), in *Dark and visible matter in Galaxies.* ASP. Conf. Ser., Vol.**117**, ed. Persic and Salucci

[168] Salucci, P. & Persic, M., (1999a) MNRAS, **309**, 923

[169] Salucci, P. & Persic, M., (1999b) A&A, **351**, 442

[170] Salucci, P. & Burkert, A., (2000) ApJ, **537L**, 9

[171] Schindler, S., Guzzo, L., Ebeling, H., Boehringer, H., Chincarini, G., Collins, C. A., de Grandi, S., Neumann, D. M., Briel, U. G., Shaver, P. & Vettolani, G., (1995) A&A, **299L**, 9

[172] Schombert, J.M., Bothun, G.D., Schneider, S.E., & McGaugh, S.S., (1992) AJ, **103**, 1107

[173] Silva, L., Granato, G.L., Bressan, A., Lacey, C., Baugh, C.M., Cole, S. & Frenk, C.S., (2001) Ap&SS, **276**, 1073

[174] Spergel, D.N. & Steinhardt, P.J., (2000) Phys.Rev.Lett., **84**, 3760

[175] Stil, J., (1999), Ph.D. Thesis, Leiden University

[176] Swaters, R., (1997), in *Dark and Visible Matter in Galaxies.* ASP Conf. Ser., Vol.**117**, p.47, ed. Persic and Salucci

[177] Swaters, R., (1999), Ph.D. Thesis, Groningen University

[178] Swaters, R.A., Madore, B.F. & Trewhella, M., (2000) ApJ, **531**, 107

[179] Syer, D. & White, S.D.M., (1998) MNRAS, **293**, 337

[180] Tasitsiomi, A., (2002) astro-ph/0205464

[181] Thomas, D. & Kauffmann, G., (1999), in ASP Conf. Ser., Vol.**192**, p.261

[182] Tissera, P.B. & Dominguez-Tenreiro, R., (1998) MNRAS, **297**, 177

[183] Tormen, G., Bouchet, F.R. & White, S.D.M., (1997) MNRAS, **286**, 865

[184] Tremaine, S. & Gunn, J. E., (1979) Phys. Rev. Lett., **42**, 407

[185] Trott, C.M. & Webster, R.L., (2002) MNRAS, **334**, 621

[186] van Albada, T.S., Bahcall, J.S., Begeman, K. & Sancisi, R., (1985) ApJ, **295**, 305

[187] van den Bosch, F.C., Robertson, B.E., Dalcanton, J.J. & de Blok, W.J.G., (2000) AJ, **119**, 1579

[188] van den Bosch, F.C. & Swaters, R.A., (2001) MNRAS, **325**, 1017

[189] van der Marel, R.P., (1991) MNRAS, **253**, 710

[190] van der Hulst, J.M., Skillman, E.D., Smith, T.R., Bothun, G.D., McGaugh, S.S. & de Blok, W.J.G., (1993) AJ, **106**, 548

[191] Verheijen, M.A.W., (1997), Ph.D. Thesis (Cap. 6), Groningen University

[192] Walter, F. & Brinks, E., (2001) AJ, **121**, 3026

[193] Wechsler, R.H., Bullock, J.S., Primack, J.L., Kravtsov, A.V. & Dekel, A., (2002) ApJ, **568**, 52

[194] White, S.D.M. & Rees, M., (1978) MNRAS, **325**, 1017

[195] White, S. D. M., Efstathiou, G. & Frenk, C. S., (1993) MNRAS, **262**, 1023

[196] White, M. & Croft, R.A.C., (2000) AJ, **539**, 497

[197] Wilkinson, M.I. & Evans, N.W., (1999) MNRAS, **310**, 645

[198] Yoshida, N., Springel, V. & White, S.D.M., (2000a) ApJ, **535**, 103

[199] Yoshida, N., Springel, V., White, S.D.M. & Tormen, G., (2000b) ApJ, **544**, 87

[200] Zhao, H.S., (1996), MNRAS, **278**, 488

List of Publications

• **Salucci, P. & Borriello, A.**:

The Distribution of Dark Matter in Galaxies: Constant–Density Dark Halos Envelop the Stellar Disks.

Proceedings of the International Conference "DARK 2000"; Heidelberg (Germany), July 10–14, 2000. Edited by H.V. Klapdor–Kleingrothaus. Berlin Heidelberg: Springer–Verlag

2001dmap.conf...12S

• **Borriello, A. & Salucci, P.**:

The Dark Matter Distribution in Disk Galaxies

Monthly Notices of the Royal Astronomical Society, Vol.323, pp.285-292

2001MNRAS.323..285B

• **Gentile, G., Kalberla, P., Klein, U., Jozsa, G., Salucci, P. & Borriello, A.**:

The Dark Matter Distribution in Disk Galaxies.

Astronomische Gesellschaft Abstract Series, Vol.18. Abstracts of Contributed Talks and Posters, presented at the Annual Scientific meeting "JENAM 2001" of the European Astronomical Society and the Astronomische Gesellschaft; Munich (Germany), September 10–15, 2001

2001AGM...18S0537G

• **Salucci, P. & Borriello, A.**:
Cold Dark matter Halos Must Burn
to appear in the Proceedings of the MPA/ESO/MPE/USM Joint Conference: "Lighthouses of the Universe: The Most Luminous Celestial Objects and their use for Cosmology"; Garching (Germany), August 2001
2001astro.ph..6251S

• **Salucci, P. & Borriello, A.**:
The Intriguing Distribution of Dark Matter in Galaxies
Invited lecture to the 8th Adriatic Meeting: "Particle Physics in the New Millennium"; Dubrovnik (Croatia), September 4–14 2001. To be published in the series *Lecture Notes in Physics*, by Springer–Verlag
2002astro.ph..3457S

• **Salucci, P., Walter, F. & Borriello, A.**:
The Distribution of Dark Matter in Galaxies: the Constant–Density Halo around DDO47
A&A submitted
2002astro.ph..6340S

• **Borriello, A., Salucci, P. & Danese, L.**:
The Fundamental Plane of Ellipticals: I. The Dark Matter Connection
MNRAS submitted
2002astro.ph..8268B

Acknowledgements

I would like to express my gratitude to the International School of Advanced Studies, for giving me the great opportunity to do my Ph.D. research in such a prestigious and stimulating environment. It was quite a privilege.

I wish to thank Prof. Danese and Dott. Pignatelli, for their precious collaboration and stimulating discussions.

Finally, I am greatly indebted to Prof. Salucci, for his invaluable guidance, as well as for his support, encouragement, friendship and endless patience, the greatest gifts I have been given during these past years.

Per aspera ad astra